

Scientific Objectives of the *Hot Universe Baryon Surveyor (HUBS)* Mission

Joel Bregman¹, Renyue Cen², Yang Chen^{3,4}, Wei Cui^{5*}, Taotao Fang⁶, Fulai Guo^{7,8}, Edmund Hodges-Kluck⁹, Rui Huang⁵, Luis C. Ho^{10,11}, Li Ji¹², Suoqing Ji^{7,8*}, Xi Kang^{2,12}, Xiaoyu Lai¹³, Hui Li⁵, Jiangtao Li^{12,1}, Miao Li², Xiangdong Li^{3,4}, Yuan Li¹⁴, Zhaosheng Li¹⁵, Guiyun Liang¹⁶, Helei Liu¹⁷, Wenhao Liu¹², Fangjun Lu¹⁸, Junjie Mao⁵, Gabriele Ponti¹⁹, Zhijie Qu²⁰, Chenxi Shan²¹, Lijing Shao¹⁰, Fangzheng Shi⁷, Xinwen Shu²², Lei Sun^{3,4}, Mouyuan Sun⁶, Hao Tong²³, Junfeng Wang⁶, Junxian Wang²⁴, Q. Daniel Wang²⁵, Song Wang²⁶, Tinggui Wang²⁴, Weiyang Wang^{27,10}, Zhongxiang Wang²⁸, Dandan Xu^{5*}, Haiguang Xu^{21*}, Heng Xu²⁹, Renxin Xu^{27,10}, Xiaojie Xu^{3,4}, Yongquan Xue²⁴, Hang Yang¹², Feng Yuan^{7,8*}, Shuinai Zhang¹², Yuning Zhang⁵, Zhongli Zhang³⁰, Yuanyuan Zhao²¹, Enping Zhou³¹, and Ping Zhou^{3,4}

¹Department of Astronomy, University of Michigan, Ann Arbor, MI, 48109-1107, USA;

²Institute for Astronomy, School of Physics, Zhejiang University, Hangzhou 310027, China;

³School of Astronomy and Space Science, Nanjing University, Nanjing 210023, China;

⁴Key Laboratory of Modern Astronomy and Astrophysics, Nanjing University, Ministry of Education, Nanjing 210023, China;

⁵Department of Astronomy, Tsinghua University, Beijing 100084, China;

⁶Department of Astronomy, Xiamen University, Xiamen, Fujian 361005, China;

⁷Astrophysics Division, Shanghai Astronomical Observatory, Chinese Academy of Sciences, Shanghai 200030, China;

⁸Key Laboratory for Research in Galaxies and Cosmology, Shanghai Astronomical Observatory, Chinese Academy of Sciences, Shanghai 200030, China;

⁹NASA Goddard Space Flight Center, Greenbelt, MD 20771, USA;

¹⁰Kavli Institute for Astronomy and Astrophysics, Peking University, Beijing 100871, China;

¹¹Department of Astronomy, School of Physics, Peking University, Beijing 100871, China;

¹²Purple Mountain Observatory, Chinese Academy of Sciences, Nanjing 210023, China;

¹³Department of Physics and Astronomy, Hubei University of Education, Wuhan 430205, China;

¹⁴Department of Physics, University of North Texas, Denton, TX 76203, USA;

¹⁵Key Laboratory of Stars and Interstellar Medium, Xiangtan University, Xiangtan 411105, China;

¹⁶CAS Key Laboratory of Optical Astronomy, National Astronomical Observatories, Chinese Academy of Sciences, Beijing 100101, China;

¹⁷School of Physical Science and Technology, Xinjiang University, Urumuqi 830046, China;

¹⁸Key Laboratory for Particle Astrophysics, Institute of High Energy Physics, Chinese Academy of Sciences, Beijing 100049, China;

¹⁹INAF-Osservatorio Astronomico di Brera, I-23807 Merate (LC), Italy;

²⁰Department of Astronomy & Astrophysics, the University of Chicago, Chicago, IL 60637, USA;

²¹School of Physics and Astronomy, Shanghai Jiao Tong University, Shanghai 200240, China;

²²Department of Physics, Anhui Normal University, Wuhu 241002, China;

²³School of Physics and Materials Science, Guangzhou University, Guangzhou 510006, China;

²⁴Department of Astronomy, University of Science and Technology of China, Hefei 230026, China;

²⁵Department of Astronomy, University of Massachusetts, Amherst, MA 01003, USA;

²⁶Key Laboratory of Optical Astronomy, National Astronomical Observatories, Chinese Academy of Sciences, Beijing 100101, China;

²⁷School of Physics and State Key Laboratory of Nuclear Physics and Technology, Peking University, Beijing 100871, China;

²⁸Department of Astronomy, School of Physics and Astronomy, Yunnan University, Kunming 650091, China;

²⁹National Astronomical Observatories, Chinese Academy of Sciences, Beijing 100101, China;

³⁰Shanghai Astronomical Observatory, Key Laboratory of Radio Astronomy, Chinese Academy of Sciences, Shanghai 200030, China;

³¹Huazhong University of Science and Technology, Wuhan 430074, China

Received July 13, 2023; accepted January 00, 0000; published online July 13, 2023

The *Hot Universe Baryon Surveyor (HUBS)* is a proposed space-based X-ray telescope for detecting X-ray emissions from the hot gas content in our universe. With its unprecedented spatially-resolved high-resolution spectroscopy and large field of view, the *HUBS* mission will be uniquely qualified to measure the physical and chemical properties of the hot gas in the interstellar medium, the circumgalactic medium, the intergalactic medium, and the intracluster medium. These measurements will be valuable for two key scientific goals of *HUBS*, namely to unravel the AGN and stellar feedback physics that governs the formation and evolution of galaxies, and to probe the baryon budget and multi-phase states from galactic to cosmological scales. In addition to these two goals, the *HUBS* mission will also help us solve some problems in the fields of galaxy clusters, AGNs, diffuse X-ray backgrounds, supernova remnants, and compact objects. This paper discusses the perspective of advancing these fields using the *HUBS* telescope.

X-ray telescopes, Galactic halo, X-ray sources

PACS number(s): 95.55.Ka, 98.35.Gi, 98.70.Qy

Citation: J Bregman et al., Scientific Objectives of the *HUBS* Mission, *Sci. China-Phys. Mech. Astron.* **0**, 000000 (2023), <https://doi.org/??>

1 Introduction

Over 99% of the baryonic matter in the Universe is in the form of ionized plasma, among which diffuse gas is the most prevalent form that spans over a wide range of scales from the interstellar medium (ISM) to the circumgalactic medium (CGM), the intracluster medium (ICM), and the intergalactic medium (IGM). The diffuse gas is a key component in the cosmic baryon budget and cycle, as it is the main reservoir of mass, metals and energy, and thus regulates the formation of stars and galaxies (e.g., [1, 2]). In particular, galaxies may embrace pristine cosmological inflows as fuel for star formation, and, in the meanwhile, eject a significant fraction of mass and metals back to the surrounding diffuse gas via so-called feedback processes, e.g., supernova feedback and active galactic nucleus (AGN) feedback. The interplay between the inflow and outflow of baryons in galaxies is a key process in the formation and evolution of galaxies. Compared with dark matter which only interacts gravitationally, baryonic matter is more richly and sensitively imprinted with the history of galactic feedback and galaxy evolution, due to the more complicated and less understood baryonic physics, including gas (magneto) hydrodynamics, ionization, cooling and heating, and chemical enrichment. Therefore, understanding the physical and chemical properties of diffused gas residing in “galactic ecosystems” is a fundamental problem in modern astrophysics [3].

Unlike the ionized plasma in the form of stars which emit

photons powered by nuclear reactions and thus are easily observable, the ionized diffuse gas within and between galaxies is more difficult to probe. Fortunately, atomic physics enables the possible detection of diffuse gas via emission and absorption across a wide range of the electromagnetic spectrum, among which the X-ray band is highly prominent. X-rays are ubiquitous in astrophysical environments: at large (galaxy scale and above) scales, gas is usually virialized at the virial temperature that increases with the greater enclosed mass of the system, and thus hot diffuse gas is commonly expected especially in massive astrophysical systems. For instance, galaxy clusters are filled with hot ICM with temperatures up to $T \sim 10^8$ K. At smaller scales, the gas can be efficiently heated by the feedback processes from stars and AGNs. Due to the nature of the emission mechanism, the gas thermal properties, i.e., temperatures and densities of the X-ray-emitting gas, can be directly obtained from the X-ray spectra. In addition, through the detection of emission and absorption lines, the X-rays can also be used to determine the kinematic properties and chemical compositions of the hot gas, which contain a tremendous amount of important information for the physical processes such as AGN and stellar feedback and interaction between galaxies. The X-ray observation is thus a powerful tool to probe the thermal states and kinematics of the diffuse gas, and thus to understand the baryon budget and cycle in the Universe.

The *Hot Universe Baryon Surveyor (HUBS)* mission [4] is a timely effort to unravel the mystery of the baryon budget and cycle. The design of *HUBS* is highly optimized for detecting extended X-ray emission from the diffuse hot gas in and around galaxies [5]. Compared with other X-

*Corresponding authors (Wei Cui, email: cui@tsinghua.edu.cn; Suoqing Ji, email: suoqing@shao.ac.cn; Dandan Xu, email: dandanxu@mail.tsinghua.edu.cn; Haijuang Xu, email: hgxu@sjtu.edu.cn; Feng Yuan, email: fyuan@shao.ac.cn)

ray missions such as *XMM-Newton* and *Chandra*, two features of *HUBS* stand out: (1) large field-of-view (of 1° half-power diameter), and (2) high spectral resolution (of <1 eV for the central sub-array and 2 eV for the main array at 1 keV). The hybrid design of the detector is adopted to enhance absorption-line studies through observations of point-like background sources like active galactic nuclei (AGN) or gamma-ray bursts (GRBs), while staying within the capability of current readout technologies, which limit the number of pixels in the detector array. Other technical trade-offs have also been made. For instance, the spectral range is capped at 2 keV, to make it easier to realize high spectral resolution while maintaining good quantum efficiency of the detector. Because CGM and IGM are of very low density, the X-ray emission from them is expected to be extremely weak but, fortunately, be dominated by spectral lines. *HUBS* is designed to make full use of the unprecedented spectral capabilities of the transition edge sensor-based microcalorimeters in detecting hot CGM and IGM, through narrow-band imaging around strong emission lines, and in deriving their physical and chemical properties, through high-resolution X-ray spectroscopy. Moreover, for detecting very extended emissions, the larger the field of view, the more photons are let in, and the higher the signal-to-noise ratio. Furthermore, a large field of view provides high efficiency in covering nearby galaxies and galaxy groups or clusters. We refer the readers to Table 1 in [4] and Table 1 in [5] for detailed specifications of *HUBS*.

The high-resolution X-ray spectroscopic observations with *HUBS* are also expected to enable advancement in many other areas, including inflows and outflows in active galactic nuclei (AGN), elemental abundances and distribution in supernova remnants (SNRs), the origin of diffuse X-ray background, flaring activities, relativistic effects in compact objects, as well as lunar or planetary X-ray emission associated with solar wind charge exchange, which produces foreground X-ray emissions and bears high relevance to active research in the fields of laboratory astrophysics and atomic physics.

This paper discusses the scientific objectives of *HUBS*. As already mentioned, the design and optimization of the *HUBS* payload are driven by a set of core scientific objectives. Here, we present the core science at two levels, which cover two marginally overlapped spatial scales, with one focusing on feedback processes and baryon/metal cycling in the galactic ecosystem, and the other on the hot baryon budget and multi-phase status at larger scales. The former is discussed in §2 while the latter in §3, respectively. In §4, Galactic sciences of *HUBS* are discussed. In §5, we explore the capability of *HUBS* by reviewing adopted atomic models and analysis techniques. We finally report the current status of *HUBS* in §6 and conclude in §7.

2 Galactic ecosystem: feedback and baryon cycles

AGN and stellar feedback is a bottleneck in the study of galaxy formation and evolution, and it is also a cutting-edge topic in astrophysics in recent years. AGN feedback is believed to be dominant in relatively massive galaxies while stellar feedback is believed to be more important in less massive ones [6]. Both of them are closely related to star formation activity in galaxies and are responsible for the production of galaxy wind, generating an X-ray halo around galaxies, called circumgalactic medium [3, 7].

With the help of *HUBS*, we will be able to answer a few key questions driving our understanding of the feedback physics and its relationship to galaxy evolution, including:

- *How does AGN feedback suppress star formation and even quench the galaxy, and what are the respective roles of different feedback modes and different AGN outputs (radiation, wind, and jet) in these processes?*
- *How are different phases of the ISM/CGM regulated by the AGN and stellar feedback?*
- *How much energy is released, and how much matter is heated/accelerated during the interaction of feedback with the ISM/CGM?*
- *How can *HUBS* help to constrain important non-thermal physics in the CGM?*

The hot circumgalactic medium (CGM) may contain considerable mass and metals, and is crucial for us to understand the mechanism of feedback. High energy resolution imaging spectroscopy X-ray observations of galaxies and their surrounding CGM/IGM play an important role in our understanding of the role of the co-evolution and interplay between galaxies and their environments. As highlighted by the Decadal Survey on Astronomy and Astrophysics 2020 (Astro2020) [8], studying various forms of stellar and AGN feedback on the galaxy ecosystem over a large physical scale is critical in unveiling the hidden drivers of galaxy growth, including the connection between star formation and the ISM, the cycling of gas and metal in and out of the galactic disk and halo, as well as the ionizing sources of the Universe.

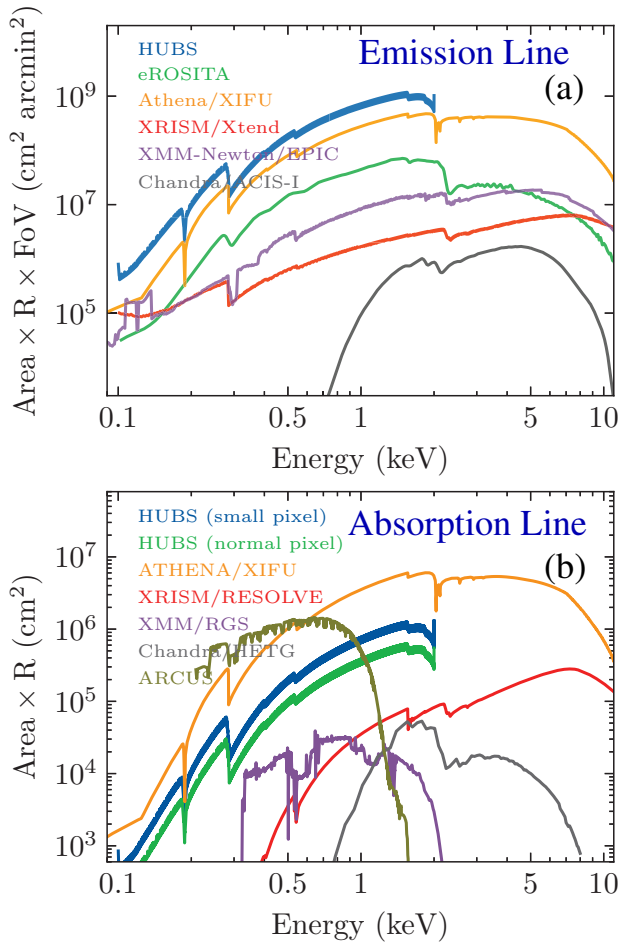


Figure 1 Comparison of the FoM of a few X-ray missions in the detection of emission lines from an extended source (a; FoM_{em}) and absorption lines from a point-like source (b; FoM_{ab}). The response files of the 60×60 normal array of *HUBS* are used in (a), while those of both the normal array and the 12×12 central sub-array are used in (b). For instruments with an X-ray grating (*XMM-Newton/RGS*, *Chandra/HETG*, and *ARCUS*), all available grating orders are combined together. *HUBS* has the highest FoM_{em} at $\lesssim 2$ keV among all the X-ray telescopes either currently in use or planned in the future, while it is also outstanding in FoM_{ab} , although not as powerful as some future X-ray missions with grating (*Athena* and *Arcus*).

With *HUBS*, the CGM and the associated physical processes can be probed through direct detection of emission lines, or absorption line studies with the observations of bright background sources, taking advantage of the superior spectral resolution of the central sub-array. In addition, observations of the CGM are also crucial to understand the baryon/metal cycling and budget. With its breakthrough technology of combining the high energy resolution microcalorimeter detector and a large-FOV X-ray telescope [5], *HUBS* has an unprecedented capability in resolving and detecting individual X-ray emission lines from the hot plasma either in thermal equilibrium or not (Fig. 1a). It is also outstanding in absorption line studies of X-ray bright background sources (Fig. 1b). The former is extremely impor-

tant in the study of how the stellar and AGN feedbacks affect the galactic ecosystem. Within ~ 5 years of science operation, *HUBS* will conduct milestone studies of stellar and AGN feedback mainly in two ways: either by moderately deep surveys of nearby objects with large angular sizes, resolving hot gas features with a physical size from star clusters to massive galaxy clusters ($\sim 10\text{--}10^6$ pc); or by deep enough observations of individual galaxy halos at moderate distances to measure the physical and chemical properties of the hot CGM.

2.1 AGN feedback

Active galactic nuclei (AGN) are the observational manifestation of matter inflow toward supermassive black holes, which can be found at the centers of almost all massive galaxies [9]. Compared to their host galaxies, AGNs are miniature in both size and mass. However, they are expected to provide substantial feedback (in the form of outflows) to their host galaxies and beyond [10–13].

Generally speaking, AGN-driven outflows have two forms: radio jets and ionized winds. Highly collimated relativistic jets, mainly observed in the radio band, can be found in some AGN accreting at relatively low efficiencies [12]. Radio jets are also known as the kinetic or maintenance mode of AGN outflow. Ionized winds with large solid angles are prevalent in AGN accreting at high efficiencies [14]. Ionized winds are often referred to as the radiative mode of AGN outflow. Presently, grating spectrometers in the X-ray and UV bands are the main working horses to probe these ionized winds via absorption spectroscopy since these winds are too small to be resolved via direct imaging.

In the X-ray band, there are mainly three types of ionized winds: warm absorbers, ultrafast outflows, and obscuring winds. The classical warm absorbers are identified with multiple narrow absorption lines with a typical outflow velocity of $\lesssim 10^3$ km s⁻¹ [15–21]. Ultrafast outflows are mainly inferred from the absorption features of highly ionized Fe xxvi and/or Fe xxv in the hard X-ray band [22–26]. The outflow velocity of ultrafast outflows can reach up to about a third of the speed of light ($\sim 10^4\text{--}5$ km s⁻¹). Ultrafast outflows occupy the high column density (N_H), ionization parameter (ξ), and outflow velocity (v_{out}) part of the parameter space, while warm absorbers occupy the other side of the parameter space. Transient obscuring winds are currently identified mainly in coordinated multi-wavelength observations [27–32]. In the $N_H - \xi - v_{out}$ parameter space, obscuring winds are in between warm absorbers and ultrafast outflows, overlapping more with the former.

To study weak absorption lines of AGN winds, two key instrument parameters are critical: energy resolution (R) and

effective area (A_{eff}). The larger the product $R \times A_{\text{eff}}$ (as the figure of merit), the better we can constrain weak absorption lines. As discussed at the beginning of §2, compared to existing grating spectrometers aboard *XMM-Newton* and *Chandra*, *HUBS* will greatly advance our knowledge of AGN winds.

Among the three types of AGN winds in the X-ray band, the classical warm absorbers are the most frequent to be detected [33-35]. Nonetheless, we still have gaps in our understanding of the warm absorber, e.g., its number density and distance to the black hole remain largely uncertain. These two parameters, linked with each other via the measurable ionization parameter, are essential to infer the origin of the warm absorber as well as its impact on the circumnuclear media and beyond.

The number density of ionized winds can be constrained with density-sensitive metastable absorption lines. In theory, such diagnostics can cover more than ten orders of magnitude in number density [18]. In practice, successful applications are rather scarce: NGC 4151 [36,37] and GRO J1655-40 [38, 39]. The latter is an X-ray binary. In addition, upper or lower limits were obtained for Mrk 279 [40] and NGC 5548 [18]. This is partly due to the insufficient figure of merit ($R \times A_{\text{eff}}$) of current instruments. The situation can be significantly improved with future missions like *HUBS*.

Figure 2 illustrates such diagnostics with *HUBS*. In this simulation, the 0.2 – 2 keV observed continuum flux is $\sim 7 \times 10^{-12} \text{ erg s}^{-1} \text{ cm}^{-2}$. This flux level is low when compared to those of the well-studied targets like NGC 5548 [18, 41] and NGC 3783 [20, 42]. Even for this low continuum flux, with 400 ks exposure, the central grid of *HUBS* (with the $< 1 \text{ eV}$ energy resolution) can well constrain the density of the wind with multiple key diagnostic lines. For targets with higher continuum flux, the required exposure time might be further reduced. In addition, the long exposure observations of *HUBS* can help us to better understand the wind density and in turn location via spectral timing analyses [43-46]. Moreover, potential eclipse events of the clumpy absorber could also provide useful constraints on its location and thus density [47].

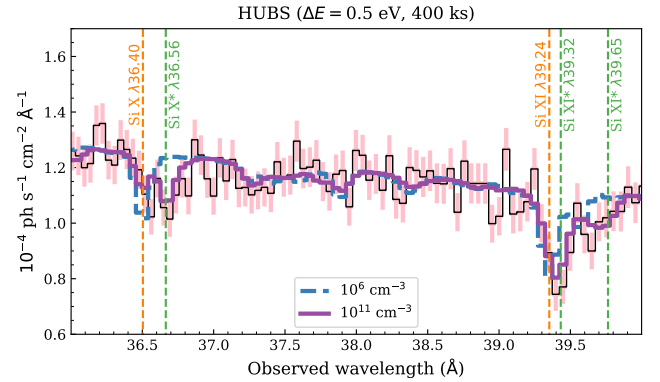


Figure 2 *HUBS* simulation of density diagnostics with metastable absorption lines. The central grid with 0.5 eV energy resolution is used for the simulation, which has an exposure time of 400 ks. The simulated data are shown in black with 1σ uncertainties shown in pink. The redshift of the AGN is 0.00386, while the warm absorber has a column density of 10^{21} cm^{-2} and an outflow velocity of -300 km s^{-1} . Warm absorber models with two different number densities are shown: 10^6 cm^{-3} (dashed curve in blue) and 10^{11} cm^{-3} (solid curve in purple). In the high-density model, absorption lines (in orange) from the ground level are weaker, while absorption lines (in green) from the metastable levels are stronger. This is mainly due to collisional excitation from the ground to the metastable level in a high-density wind.

Another fundamental parameter of the warm absorber that is not well constrained is its opening angle. This can be indirectly inferred from the warm absorber occurrence fraction in a sample of type 1 AGN. In the era of *ASCA*, the occurrence fraction of the warm absorber is $\sim 50\%$ [33]. The occurrence fraction was revised to $\sim 65\%$ in the era of *XMM-Newton* and *Chandra* [34, 35]. However, limited by the capability of current instruments, these sample studies are limited to bright targets. The largest sample size among the three studies is merely 26.

Such sample studies can be improved with *HUBS*. On one hand, its energy resolution and effective area are suitable for weak absorption line studies. On the other hand, its large field of view enables us to accumulate a large number of high-quality spectra in an efficient way. Figure 2 shows the *HUBS* simulation of warm absorber features of a serendipitous AGN when observing other core science or observatory science targets. If not filled with extended sources, the 1-square-degree field of view (with 3600 integral field units) might have a few serendipitous AGN with detectable warm absorber features [48, 49]. Even for a rather low continuum 0.2 – 2 keV flux of $1.0 \times 10^{-13} \text{ erg s}^{-1} \text{ cm}^{-2}$ (nearly two orders of magnitude lower than any of the sample targets in [33-35]), warm absorber features such as the Fe M-shell unresolved transition array (UTA) feature can be well detected with the 2 eV energy resolution of the normal grid. That is to say, without requesting dedicated observations, we can still accumulate a good sample of AGN warm absorbers.

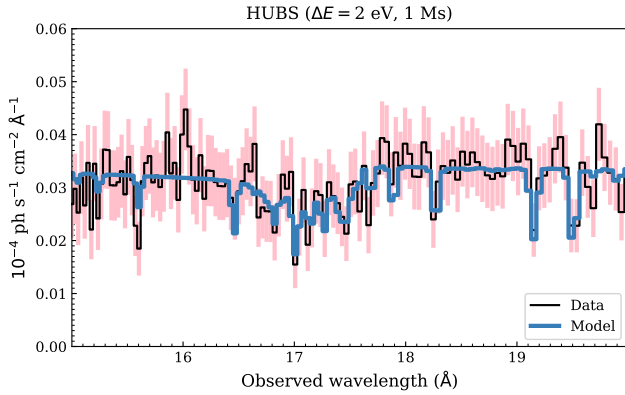


Figure 3 *HUBS* simulation of warm absorber features of a serendipitous AGN when observing other core science or observatory science targets. The normal grid with 2 eV energy resolution is used for the simulation, which has an exposure time of 1 Ms. The simulated data are shown in black with 1σ uncertainties shown in pink. The warm absorber model is shown in blue. The $0.2 - 2$ keV observed continuum flux of the AGN ($z = 0.03$) is 1.0×10^{-13} erg s $^{-1}$ cm $^{-2}$ and the warm absorber has a column density of 10^{21} cm $^{-2}$. The characteristic Fe M-shell unresolved transition array (UTA) feature around 17 \AA (in the observed frame) and other warm absorber lines are clearly detected.

By the same token, we can search for ultrafast outflows in the soft X-ray band in these serendipitous AGNs. The occurrence fraction of ultrafast outflows is at least 30 % in the sample studies by [23, 50, 51]. These fast winds are rarely detected in the soft X-ray band though [26, 52–56]. Moreover, ultrafast outflows can be quite variable [25, 26, 57, 58]. The long exposure observations of *HUBS* can also help us to better understand the evolution of these powerful winds.

Some AGN winds are probably powered by accretion disks. As a result, the disk winds may take a significant fraction of the accretion power away from the accretion disk, which significantly alters the disk temperature profiles [59], energy density distributions [60] and disk sizes [61, 62].

Transient accretion onto supermassive black holes (SMBH) in galactic centers can also lead to winds and outflows. The most interesting class is the stellar tidal disruption event (TDE). A TDE occurs when a star passes too close to a SMBH and gets tidally disrupted and accreted, producing a flare of radiation peaking in the UV and soft X-rays [63]. TDE provides a unique probe of quiescent SMBHs in normal galaxies, especially the physical processes associated with various accretion states on a practically observable timescale of several years. The super-Eddington fall-back rates and potentially super-Eddington accretion rates in TDEs have been predicted in several theoretical works [64, 65], which can lead to fast, radiation-driven outflows, as seen in MHD simulations of such systems [66, 67].

X-ray outflows in TDEs are crucial in constraining the super-Eddington accretion flows, yet observations are still

sparse [68]. This is possibly due to the X-ray faintness of most TDEs, particularly those discovered in the optical bands. An ionized X-ray outflow (from the blueshifted O VIII absorption trough) with a velocity of $0.2 c$ has been reported in a nearby TDE ASASSN-14li, but it disappeared in the late-time observations [69]. If a super-Eddington radiatively driven outflow were observed, it would have “turned off” only one year after the TDE luminosity peak. Interestingly, with dedicated *Chandra* grating spectroscopy observations, X-ray outflows with a much lower velocity (~ 300 km s $^{-1}$) in ASASSN-14li are detected, which are also variable in physical conditions [70]. Such a low-velocity outflow component would be common among TDEs, which could be interpreted as absorption through a super-Eddington wind or through a filament of stellar debris. Since TDEs are mainly peaking in the soft X-ray bands [71], with its superior sensitivity and spectral resolution, *HUBS* will allow for measuring precisely the soft X-ray outflow properties at different accretion states. For instance, *HUBS* is able to measure the evolution of ionized absorption features as a function of luminosity and/or accretion rate, especially in the rising and decaying phase of the TDE flares, establishing the connection between the outflows and the super-Eddington accretion process, which is still poorly constrained.

In the current model of galaxy formation and evolution, feedback is the most uncertain physical process. Almost all cosmological simulations adopt subgrid models of AGN feedback which are highly uncertain and distinctively different between one and another. In this sense, simulations of the evolution of a single galaxy have a significant advantage because a much higher resolution can be achieved and the inner boundary of the AGN accretion flow, which is the Bondi radius of black hole accretion, can even be resolved numerically. This ensures that by self-consistently evolving the gas flow from hundreds of kpc scales down to the inner Bondi radius, we can reliably trace the mass flux crossing the Bondi radius, i.e., the mass accretion rate of the AGN, which is crucial for the determination of the magnitude of AGN activity. Moreover, in this case, the state-of-the-art AGN physics [72] can be incorporated into the simulations (e.g., [73]). Fig. 6 shows such an example of simulation results, which describes the evolution of a single elliptical galaxy when the effects of AGN feedback are taken into account. Fig. 7 shows the mock spectra of an elliptical galaxy produced by the gas from 0.1–10 kpc using the response of *HUBS* telescope with four different models of AGN feedback, together with the fitting results of the one-temperature model. This result shows the ability of the high spectral resolution spectra obtained by *HUBS* to discriminate different feedback models. Next step, it is crucial to develop the model further by incorporating more physics into the model and to study in detail the roles of different

AGN outputs, such as radiation, wind, and jet in cold and hot feedback modes, in AGN feedback. Moreover, we also need to incorporate the simulation results into cosmological simulations.

2.2 Stellar feedback

Though there is no doubt that supernova feedback is crucial to the suppression of star formation and the launch of galactic winds, people now realize that early feedback from massive stars (e.g. fast OB winds and ionizing radiation) is equally important since the total energy output from them is comparable or even larger than that of the supernovae (SNe; e.g. [74-76]). More importantly, early feedback operates as soon as massive stars are formed, much earlier than the SN explosion at the death of the stars, which takes at least ten Myr. Given the fact that most star-forming regions are short-lived, early feedback processes determine the evolution and fate of individual star-forming regions. Modern galaxy formation simulations have already shown that early feedback disrupts local density concentrate, shuts off star formation (e.g. [77]), clears out material and enhances the effects of subsequent SN feedback, reduces the clustering of stars (e.g. [78]), enhances chemical enrichment in galactic environments [79, 80], and changes the mass and spatial distribution of GMCs (e.g. [81]).

However, there exists huge uncertainty regarding the intensity of these processes and the coupling to the ambient multi-phase turbulence-dominated medium. Diffuse X-ray observations of nearby star-forming regions, therefore, provide a direct laboratory to confront the theoretical expectation and observations on the effects of the feedback from the smallest scales. Previous observations have already demonstrated that diffuse X-ray emission is ubiquitous in star-forming regions (e.g. [82-84]). One famous example is the 30 Doradus, the most well-studied massive star-forming region in LMC.

Fig. 4 shows a composite image of X-ray, $H\alpha$, and UV bands. The complex exhibits many blisters and bubbles filled with hot plasma traced by soft X-rays. These bubbles are surrounded by warm gas traced by UV and $H\alpha$ emission, demonstrating the importance of the interface between gas of different phases. The 30 Doradus region has been investigated extensively in X-rays. Back in the 90s, Wang & Helfand 1991 ([85]) first revealed the diffuse X-ray emission using the Einstein Observatory and fitted the spectra with an isothermal plasma model of the temperature of 5×10^6 K. Most recently, using *Suzaku* observations of the 30 Doradus, Cheng et al. 2021 ([86]) showed that the spectra are better modeled with a log-normal temperature distribution, which leads to a higher estimate of the total thermal energy and gas pressure. However, due to the limited spectral resolution of

the existing X-ray telescopes, the detailed temperature distribution and total thermal energy of the hot gas are not well determined, therefore limiting our understanding of how feedback modulates hot gas around young star clusters. From a theoretical perspective, recently numerical simulations start to be able to model various key physical processes in massive star-forming regions. In Fig. 5, we show the results from a radiation-hydrodynamic that takes into account various stellar feedback processes such as fast stellar winds and ionizing radiation from massive stars (Li et al. in prep.). The combined effects of feedback disrupt the cloud very quickly in only a few Myr and generate a huge amount of hot gas with a complicated temperature distribution, which is a sensitive probe of the detailed feedback implementation.

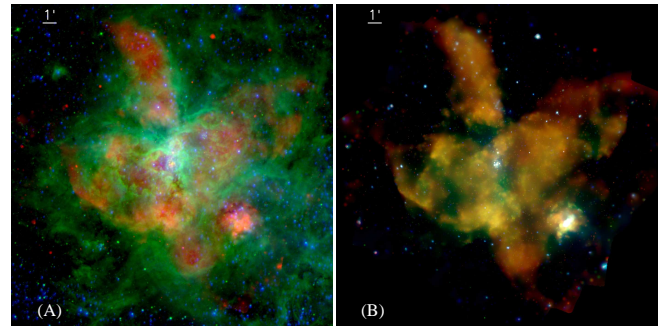


Figure 4 (A) Multi-wavelength image of 30 Doradus, one of the largest star-forming regions located in Large Magellanic Cloud. Million-degree hot gas emitting X-rays (red) is surrounded by warm ionized and neutral gas traced by UV (blue) and $H\alpha$ (green). (B) *Chandra* images in 0.5-1 keV (red), 1-2 keV (green), and 2-8 keV (blue) bands ([86]).

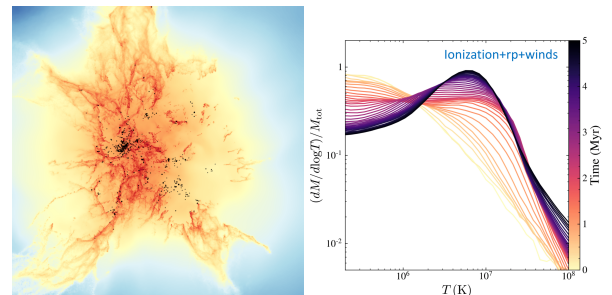


Figure 5 Left: Gas density projection plot of a simulated GMC in the late stage of its evolution. Fast stellar winds and ionizing radiation from massive stars disrupt the cloud and produce high-velocity high-temperature gas. The location of the massive stars formed in the cloud is shown as black dots. Right: Mass-weighted temperature distribution in the same simulation. The different color shows the distribution at different epoch. The exact shape of the distribution depends strongly on the stellar feedback processes included in the simulations (Li et al. in prep.).

HUBS will provide a major improvement on this matter, thanks to its large field of view and excellent spectral resolution. The 2 eV spectral resolution will reveal individual metal lines with different ionization states and determine the accu-

rate temperature and electron number density at each pixel of the observation. The high spectral resolution will also allow us to determine the shift of the line center and in turn the line-of-sight velocity of the hot gas. With *HUBS*'s huge field of view, with only a single pointing, we can obtain all the above key physical quantities in a spatially-resolved fashion across the whole star-forming region. These physical quantities together with the derived total energy budgets are powerful measures to directly constrain the dynamics of the regions caused by early stellar feedback processes from a single stellar population.

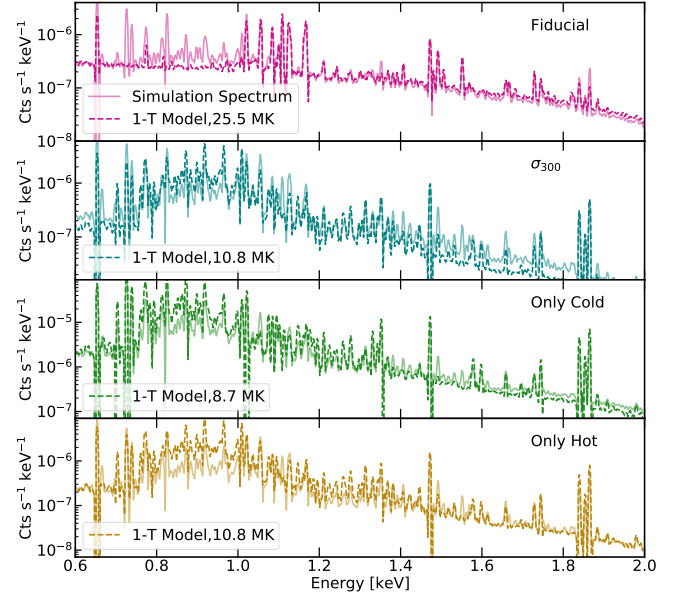


Figure 7 The simulated spectra of an elliptical galaxy emitted by the gas from 0.1-10 kpc with four different AGN feedback models. The *HUBS* response is used when producing the spectra. The best-fit spectra based on the one-temperature model are shown by the dashed lines. Taken from [87].

Star-forming regions are highly turbulent, multi-phase media. It has been demonstrated that wind feedback naturally creates fractal hot bubble surfaces, where cooling becomes extremely efficient in the interface between different phases of the gas ([88]). The interface is an ideal site to trigger charge exchange between ionized and neutral gas. The charge exchange (CX) X-ray emission is therefore a powerful tool to quantify the physical conditions between hot plasmas and cold neutral gas within the star-forming regions. Significantly different from collisional thermal emission, the X-ray spectra from CX present enhanced forbidden and intercombination lines relative to the resonance lines, such as the He α triplet of O VII, N VI, and Ne IX ([89]). However, clear signatures of CX in X-rays are extremely difficult to detect ([90]) because it requires high spectral resolutions and S/N ratios to resolve the triplets. *HUBS* will be a game changer for the detection of CX spectra signature due to its large effective area which enhances the S/N ratios, and will provide solid evidence and quantification of the fractal nature of the turbulent medium in star-forming regions.

Another advantage of the *HUBS* high spectral resolution is that the spectra can be used to determine the accurate abundance of many elements, such as O, Mg, Ne, and Fe. These measurements will provide stringent constraints on the metal yield from massive stars from the stellar population synthesis, which is still very uncertain due to the different models of binary evolution. Besides the total metal yields, the spatially-resolved metallicity distribution will also be used to study the time-dependent metal loading and the process of

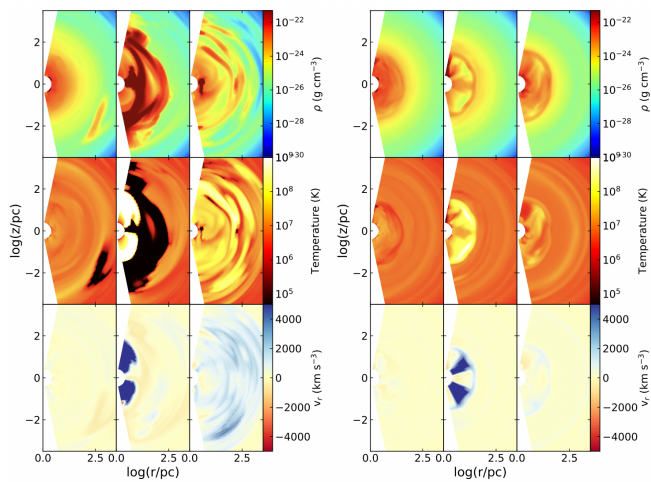


Figure 6 Spatial distribution of density, temperature, and radial velocity at three different times obtained from high-resolution simulations of the evolution of an elliptical galaxy when AGN feedback is taken into account. The figure is adapted from [73].

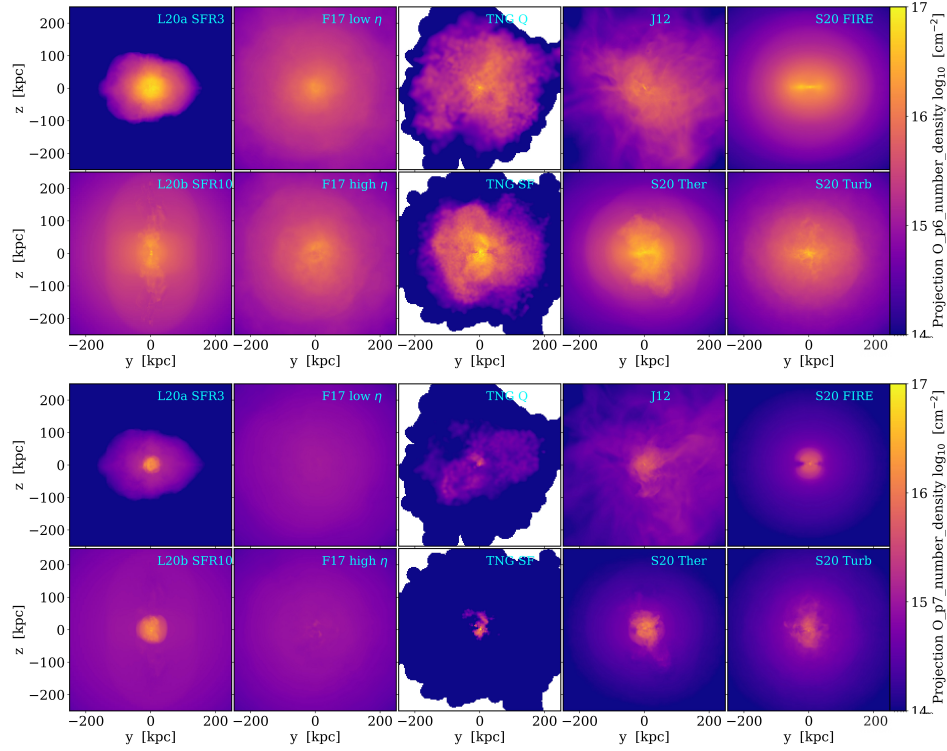


Figure 8 CGM O VII (top) and O VIII (bottom) column density projection. Different simulation uses different feedback models, resulting in different density distributions of these columns (Li et al., in prep).

metal diffusion, both of which are key physical ingredients of the large-scale galaxy formation models (e.g. [91]). Besides D30 Doradus, other interesting sources include Carina Nebula, NGC 3603, and M17. A compilation of star-forming regions of various evolutionary stages will provide us with a great opportunity to confront the theoretical understanding of the stellar feedback in different stellar populations.

2.3 CGM: constraining feedback physics and baryon cycle

At scales of a few hundred kpcs, the fraction of baryons in the universe contributing to the circumgalactic medium of galaxies is crucial to answering the question of “missing baryon”. Part of the missing baryons is likely to exist in the hot medium outside the galaxy [92], but the exact location is unclear: It may be mainly in the dark matter halo near the galaxy, or around a large-scale structure other than the dark matter halo [93]. The amount of baryons contained in the thermal medium is determined by the accretion driven by dark matter halos and the feedback of galaxies. It is now widely accepted that feedback in less massive and massive galaxies are dominated by supernovae and AGNs respectively [13, 94], while how they affect the baryon content of the circumgalactic medium remains under active investigation. Thankfully, since the density of the CGM is not forbiddingly

low, the emitted X-rays of the circumgalactic medium are still above the detection limit. Observations of the X-ray system of the galactic peripheral thermal medium can constrain the mass of the galactic medium, which will help us understand the distribution of baryons and feedback physics.

Because of its low density, CGM is very sensitive to the feedback effect, and the properties of CGM generated by different simulations are very different (e.g., [87]). Therefore, comparison with the observed CGM can be used to identify the credibility of the feedback model. Fig. 8 is a comparison of the distribution map of CGM O VII, O VIII column density (Li et al. in prep), including the mainstream cosmological simulation IllustrisTNG and zoom-in simulation [95], and the simulation of a single galaxy [96-98], each simulation adopts different feedback models. It can be seen that the O VII and O VIII in different simulations are very different. *HUBS*’s observations of CGM in neighboring galaxies can be compared with the results of numerical simulations to evaluate the reduction of CGM by different simulations and limit galaxy feedback models.

To better constrain the galaxy formation models, a large sample of the hot CGM is needed and systematically compared with the numerical simulations. At present, there are only dozens of disk galaxies that have detected halo, basically within 30 Mpc. Generally speaking, in less massive galaxies, the thermal CGM is fainter and less extended. *HUBS* can

use its large field of view to significantly improve observation efficiency and see fainter, farther and less massive galaxies, increasing the number of samples by at least an order of magnitude. In this way, there will be a statistically complete sample in various physical parameter intervals of galaxies, such as galaxy mass, stellar activity in the galaxy, and the large-scale environment in which the galaxy is located. This provides a comprehensive picture of how the properties of the hot CGM change with the physical parameters of the galaxy. Numerical simulations that have developed rapidly in recent years will also cover these physical parameters and systematically predict the outflow of these galaxies and the thermal medium around galaxies. Comparing the total luminosity, metal abundance, spectrum and other information of the observed X-rays with the results of numerical simulation, we can (1) constrain the feedback processes in galaxies under different conditions and give quantitative limits on the mass cycle of galaxies; (2) constrain the mass of hot baryons contained in the CGM from the statistical point of view, and answer the “missing baryon” problem.

On galactic scales, how the galactic winds from SN and AGN feedback including the AGN jets [99, 100] interact with cosmological inflows is the basis for the formation of galaxies. A key question in galaxy formation is how galaxies obtain mass from their CGM and when to stop growing [101]. Competition between inflows and feedback directly determines the growth rate of galaxies. Inflow will increase the mass of galaxies, and the galaxy wind can not only take away mass and metals from galaxies, but also reduce the accretion of new gas from the periphery. If this effect is significant, the inflow will be blocked and the star formation will be suppressed [73]. The converging location of inflow and outflow is the CGM. Therefore, the observation and study of the galactic media will provide important clues to the formation and evolution of galaxies.

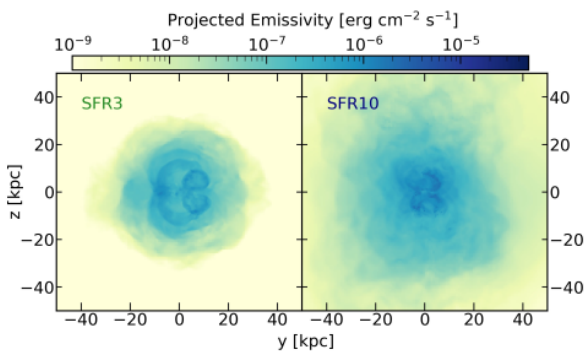


Figure 9 The cross-section of the MW-like thermal halo and the X-ray surface brightness. The left panel shows the case with the star formation rate of $3M_{\odot}/\text{yr}$ (current level), and right panel the star formation rate of $10M_{\odot}/\text{yr}$. (Vijayan & Li 2022)

To quantitatively constrain the strength of feedback and inflow, a number of attempts have been made. The Numerical Investigation of a Hundred Astrophysical Objects (NIHAO) project [102] simulated a total of 100 galaxies with masses ranging from dwarfs to the Milky Way (MW)-like galaxies. Compared with other simulations (e.g., Eagle, Illustris), the NIHAO simulation has some advantages in the number of samples and resolutions. The NIHAO simulation includes pre-stellar feedback, so it can reproduce the stellar-halo mass relationship and is suitable for studying the baryon cycle. The impact of SN feedback on the baryon cycle is further studied [103], where the percentage of baryons ejected out of the dark matter halo and returned to the galaxy are predicted respectively. Because the brightness of the thermal halo decreases with the increase of the radius, existing observations generally only see radiation within a few kpc from the galaxy.

It is expected that *HUBS* can increase the detectable physical scale by more than one order of magnitude, so that the current research on the inner region of the thermal halo can be extended to the entire CGM (even the IGM), thereby constraining radial profiles of various properties (e.g., density and temperature). Theoretically, inflow and outflow have very different effects on the properties of the thermal CGM (metal abundance, temperature, etc.). A remarkable feature is that the metal abundance in the outflow-dominated area will be much higher than that in the inflow. The outflow of different intensities will also produce very different effects. More energetic outflows launched by intensive star formation could enrich metals and heat up the gaseous halo at larger radii, which leads to a higher X-ray luminosity (see Fig. 9, numerical simulation results [104]). *HUBS*'s good spectral resolution can provide important clues to the properties of the thermal gas around the galaxy, such as temperature and metal abundance. Combined with its better spatial resolution, it can limit the inflow, outflow and the area where they interact, from which the feedback strength and the intensity of the inflow can be inferred. In addition, due to the invisibility of large-scale environments, there is no constraint on how many thermal gases there are in the media around the galaxy, while *HUBS*'s observation of large-scale thermal gas will provide an important constraint on this.

It was a long mystery that the expected amount of baryons around galaxies are not detected in existing multi-wavelength observations (e.g., [105-111]). For example, with the NIHAO galaxy formation simulations, [112] made predictions for the baryonic budget in present-day Milky-Way ($M_{200} \sim 10^{12} M_{\odot}$) type galaxies. They found that, compared to a universal cosmic baryon fraction of $f_b = \Omega_b/\Omega_m = 0.15$, haloes of this mass scale are typically “missing” 30% of the expected baryons, which are relocated to beyond two times the virial radii and are dominated by a diffuse warm-hot gas.

The game is to find this gas and map its distribution. As can be seen in Fig. 10, the temperature at the peak of the radiative cooling curve ($T \sim 10^{5.5}$ K) is close to the virial temperature of L^* galaxies. For L^* or super- L^* galaxies with more massive halos ($M_{\text{halo}} \gtrsim 10^{12-13} M_{\odot}$), the virial temperature could fall in the X-ray emitting range where the radiative cooling efficiency is relatively low compared to lower mass halos, as the latter has higher metal cooling efficiency. In this case, there could exist an extended and stable X-ray-emitting hot gaseous halo that potentially contains a significant fraction of the “missing baryons” (e.g., [109, 111, 113]).

The first science case in this regard is to observe nearby objects. In this case, the hot CGM could be studied in unprecedented detail even with moderate exposures (e.g., [84, 114]). The Andromeda galaxy (M31), with a stellar mass of $M_* = (1 - 1.5) \times 10^{11} M_{\odot}$, a dark matter halo mass of $M_{200} = (8 - 11) \times 10^{11} M_{\odot}$ [115], $\text{SFR} \approx 0.4 M_{\odot} \text{ yr}^{-1}$ [116], and $d \approx 0.78$ Mpc ($1' \approx 230$ pc), is thus the best case to search for the large-scale accreted hot CGM. It is the external galaxy with the largest angular size of the virial radius ($r_{\text{vir}} \approx 300$ kpc $\approx 23^\circ$), while the companion galaxy M33 locates at a projected distance of ~ 200 kpc from M31, within its dark matter halo (see Fig. 11 for the configuration). Such a large angular size of the dark matter halo makes M31 unique for the most detailed study of the multi-phase CGM. In particular, there are a lot of UV-bright background AGN projected within r_{vir} of M31 (Fig. 11), allowing for UV absorption line studies of the cool and warm gases from the CGM [117]. Furthermore, as our closest massive neighbor in the local group, M31 also received a lot of observations in many other bands, which help us to study both its dark matter halo and the multi-phase CGM (e.g., [118, 119]). These multi-wavelength observations, together with the proposed large sky area survey with *HUBS* will need $\sim (200 - 300) \times 15$ ks = (3.0 – 4.5) Ms observations to cover the entire area of interest, such as the M31-M33 stellar and gas stream ([120]). This will provide us with a unique panchromatic view of the baryon budget among the stars and the multi-phase CGM.

Fig. 12 shows the simulated *HUBS* spectrum extracted from the entire FOV toward the direction of M31, with an exposure of only ~ 15 ks. The real selection of the spectral extraction aperture depends on both the brightness of the feature of interest and the scientific goal. Here the $1^\circ \times 1^\circ$ aperture is still enough to separate the M31-M33 stream from the surrounding medium [120], which is a large-scale structure with gaseous counterparts [118]. In many cases when we do not need such a high signal-to-noise ratio, a higher angular resolution down to the instrument limit ($1' \approx 230$ pc) could be adopted, which is impossible for more distant galaxies. Due to the large angular size of the object, such *HUBS* observations of local galaxies are still very time-consuming and

typically require a few mega-seconds.

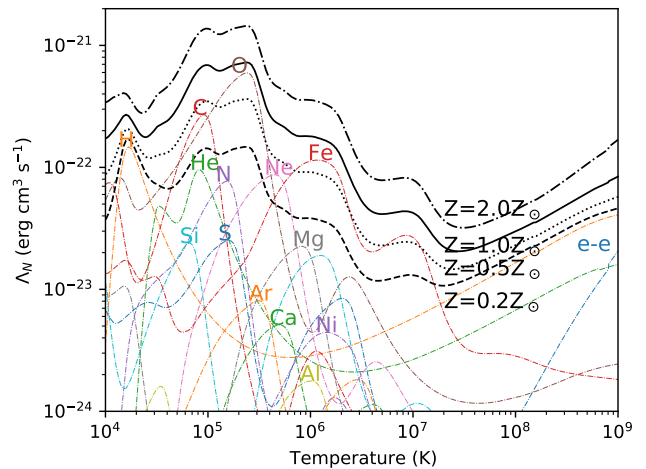


Figure 10 Radiative cooling curve of the thermal plasma under collisional ionization equilibrium (CIE) based on the AtomDB database (<http://www.atomdb.org>). The vertical axis is the normalized radiative cooling rate of the plasma defined as $\Lambda_N \equiv \frac{U}{\tau_{\text{cool}} n_e n_t}$ (in a unit of $\text{erg cm}^3 \text{ s}^{-1}$), where U is the internal energy of the gas [$U = \frac{3}{2}(n_e + n_t)kT$], τ_{cool} is the radiative cooling timescale, while n_t and n_e are the total ion and electron number densities, respectively. The horizontal axis is the temperature of the plasma. Different colored dash-dotted curves are the contribution by different elements (we only consider 14 elements with the strongest emissions) assuming an abundance of $Z = 1.0 Z_{\odot}$, with “e-e” denoting the electron-electron bremsstrahlung emission. The thick black curves are the sum of all these components under different abundances (the dashed, dotted, solid, and dash-dotted curves correspond to $Z = 0.2, 0.5, 1.0, 2.0 Z_{\odot}$, respectively).

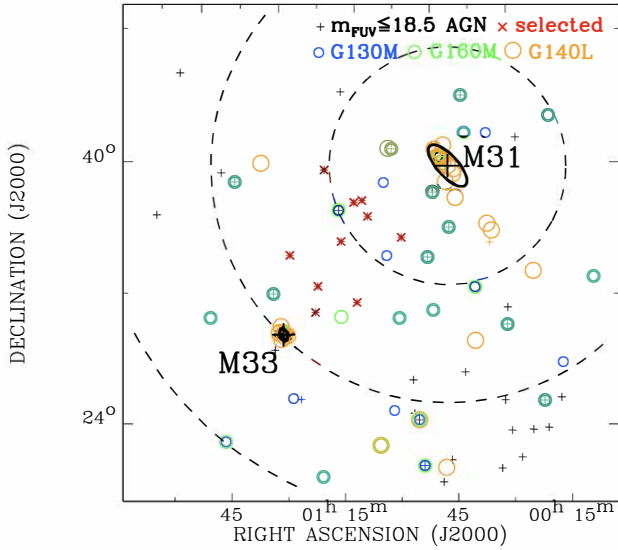


Figure 11 Location of UV bright (with GALEX FUV magnitude $m_{\text{FUV}} \leq 18.5$) AGNs (black plus) around M31 and M33. The large plus sign and the solid ellipse mark the location and extension of the optical disk of the two galaxies. The three large dashed circles have a radius of $r = 100, 200, 300$ kpc from the center of M31. Small colored circles as denoted on the top right are HST/COS observations of objects in the surrounding area [121], or are MW halo stars which allow for a determination of the absorption from the foreground MW halo [122].

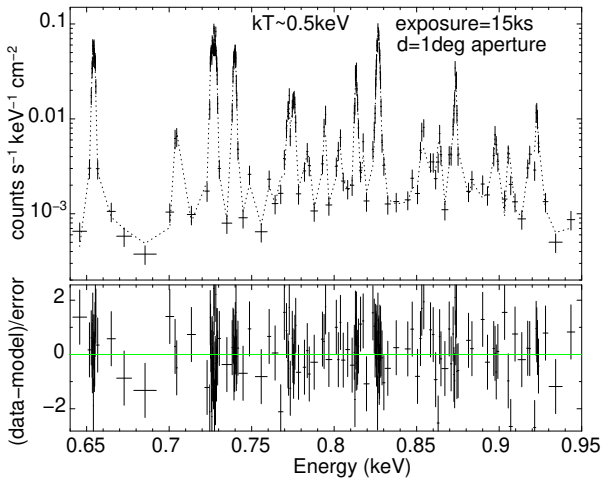


Figure 12 Simulated 15 ks *HUBS* spectrum extracted from the $1^\circ \times 1^\circ$ FOV coverage of the M31 halo. The dotted curve shows the $kT \sim 0.5$ keV model subjected to Galactic foreground absorption.

We also expect to collect a sample of $\lesssim 10$ massive galaxies at moderate distances for *HUBS*. The X-ray emission of the CGM could arise not only from the feedback of AGN and stellar sources (e.g., [123–125]), but also from the accretion shock heating and gravitational compression of the IGM (e.g., [126]). The relative importance of these two potentially interrelated mechanisms likely depends on a galaxy’s mass, as well as other properties such as the SFR and the environ-

ment. The extended hot CGM could potentially contain a large fraction of a galaxy’s “missing baryons”. However, due to its low density and metallicity, the X-ray emissivity of this extended hot CGM is extremely low [127]. In order to detect it and characterize its spatial distribution, we need a galaxy sample that is massive enough so the virialized gas has a temperature falling in the X-ray emitting band. These galaxies also need to be quiescent in star formation to avoid disproportionately strong X-ray emission from metal-enriched feedback material, as well as in a non-cluster environment such that the ICM would not contaminate the measurement of the CGM in the galaxy vicinity [113, 128]. Furthermore, it will also be better if the galaxies are located at a moderate distance of $d \sim (50 - 100)$ Mpc, so the *HUBS* FOV will cover at least a significant fraction of the virial radius, and the redshifted soft X-ray emission lines could be separated from the MW foreground emission ([129, 130]). The best cases are thus super- L^* quiescent galaxies (e.g., [131–134]). With the high energy resolution and low background of *HUBS*, we can extract narrow-band images covering individual emission lines with significantly suppressed MW foreground emission, and probe its radial distribution out to almost the virial radius.

When probing X-ray emission from low surface brightness features such as the extended CGM, the most important thing is not only the photon statistic, but also the level and fluctuation of the sky background. With broadband X-ray imaging observations, we can typically detect the hot CGM only within $r \lesssim (20 - 30)$ kpc or $r \lesssim 0.1r_{200}$ (e.g., [109, 113, 128, 129]). We present a simulated ~ 1 Ms *HUBS* spectrum of a $z = 0.01$ ($d \approx 50$ Mpc) massive quiescent galaxy in Fig. 13, using the spectral model from [128]. It is clear that some key diagnostic emission lines of the hot gas, such as the redshifted O VIII line at the rest-frame energy of 0.654 keV, could be separated from the same emission line arising from the MW halo. This will significantly increase the signal-to-noise ratio of the redshifted hot gas emission lines in narrow-band imaging observations.

We must note that the objects to be included in such observations need to be carefully selected according to their redshifts. A shorter distance will be helpful to collect more photons to study the physical and chemical properties of the brightest part of the hot CGM, but the contamination from the MW foreground makes it difficult to detect the faint extended hot CGM which potentially contains a larger fraction of the baryons [109, 110]. On the other hand, a too-large distance will significantly reduce the flux of the object and makes the project unfeasible. The best choice will be objects at $d \sim (50 - 100)$ Mpc, such as the CGM-MASS sample studied in [109, 113, 128]. We also would like to emphasize that the galaxies in the mass range of the CGM-MASS galaxies often have a large discrepancy in the measured hot CGM

mass based on X-ray or Sunyaev-Zel'dovich (SZ) observations [105, 111, 113, 135], which could be partially caused by the poorly constrained hot gas density profile [109, 133]. This is another reason to have deep X-ray observations probing the hot CGM from a large fraction of the dark matter halo. The total *HUBS* observation time needed to complete such a survey will be a few mega-seconds, depending on the real sample size and the adjustment of the exposure time for individual galaxies based on existing *Chandra* and *XMM-Newton* observations [113, 133].

recognized [3]. A number of theoretical models have been developed, predicting distinctively different CGM properties with a wide range of physical parameter spaces poorly constrained by existing observations. *HUBS* will be uniquely qualified to test these models and constrain the feedback physics in the CGM, which is discussed in detail as follows.

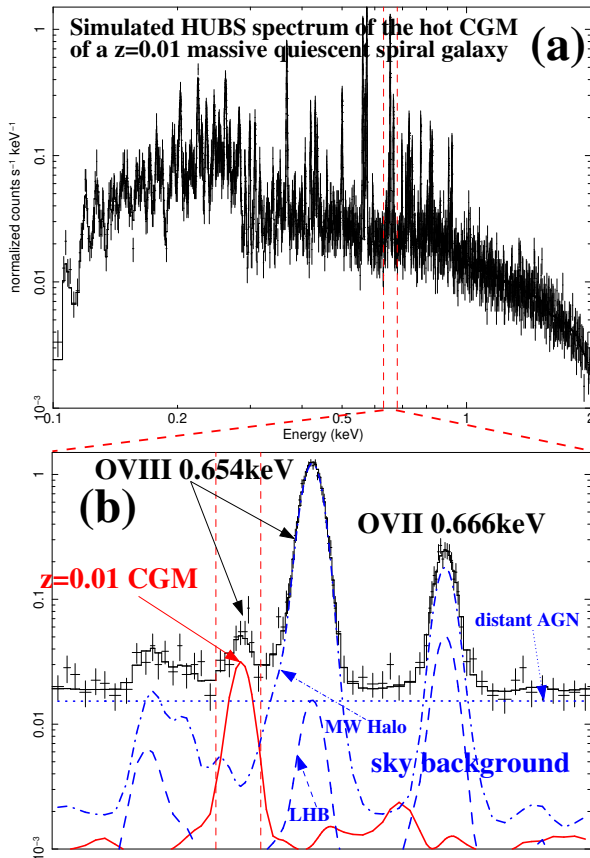


Figure 13 Simulated 1 Ms *HUBS* spectrum of the hot CGM at $r \leq 0.2r_{200}$ around a $z = 0.01$ ($d \sim 50$ Mpc) galaxy [128, 129]. Panel (b) is the zoom-in in the energy range of 0.63–0.68 keV of panel (a). The red curve is the hot CGM ($kT = 0.6$ keV plasma), while the blue curves are various sky background components (local hot bubble LHB; MW halo; distant AGN). The redshifted O VIII line from the CGM can be separated from the MW halo component.

2.4 Additional feedback physics

Due to the high level of complexity of galactic environments, the feedback processes might involve more physics than hydrodynamics and gravity. The impact of non-thermal physics on galaxy formation, such as magnetic fields and cosmic rays, has been long overlooked until recently the importance of these additional feedback physics starts to be investigated and

Magnetic fields: The magnetic field strength in the CGM is expected to be much weaker than that in the ISM, as the CGM is expected to be more diffuse and less dense. In the MW halo, the best-fitting B -field values are $\sim 1\text{--}10 \mu\text{G}$ [136, 137]. In recent years, the strength and topology of galactic scale magnetic field in the CGM started to be well constrained in radio observations, via either polarization or Faraday rotation measure (RM) synthesis ([138, 139]). The observed magnetic energy density in the CGM could be either higher or lower than the hot gas pressure [140–144], indicating a variety of roles the magnetic field plays in the global gas flows. On the simulation side, a variety of magnetic field strengths and topologies in the CGM are predicted by different sets of simulations, such as SURGE [145] and FIRE [146], which is still under active investigation. For instance, [145] found that the magnetic fields in the simulations even become dominant in the bi-conical regions. Therefore, the impact of magnetic fields in the CGM might not be negligible.

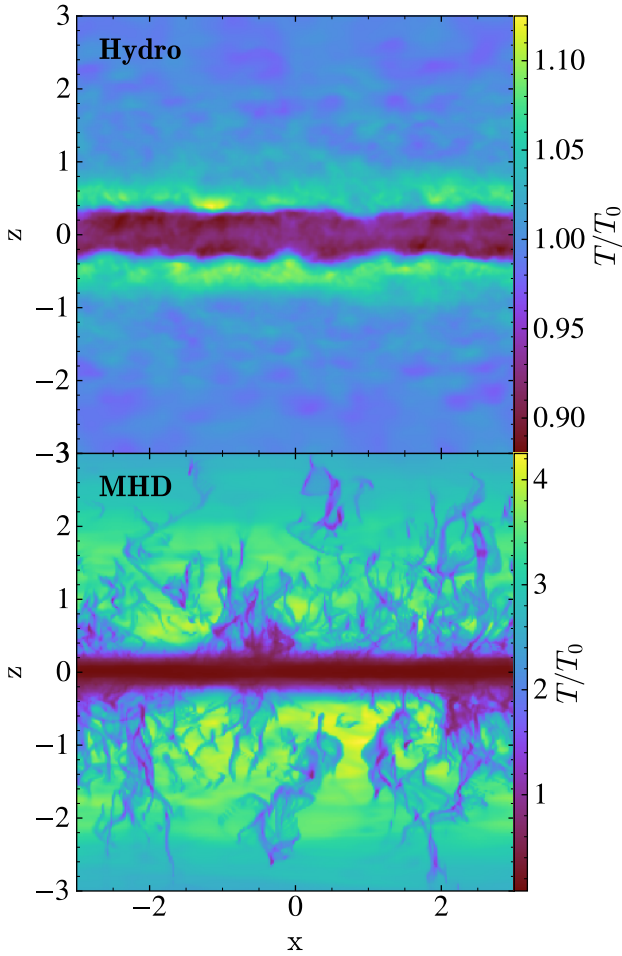


Figure 14 Projections of the gas temperature T (normalized to the initial temperature T_0) of simulated patches of the CGM in simulations without (top) and with (bottom) magnetic fields. Magnetic fields dramatically change the thermal states of the CGM by enhancing the thermal instability as well as the production of the cool gas, while the CGM remains single-phase in the case without magnetic fields. Datasets used in this figure are from [147].

Magnetic fields affect CGM in a few ways. First, magnetic fields can provide non-thermal magnetic pressure to the CGM, which could even be comparable to the local thermal pressure of the field strengths reaches a few μG . In this case, the halo gas is partially supported by the magnetic pressure $P_{\text{mag}} = |\mathbf{B}|^2/4\pi$, and can stay at a lower thermal pressure/temperature [145]. Second, magnetic fields can facilitate the production of cool gas in the CGM by enhancing thermal instability [147]. As shown in Fig. 14, at the presence of magnetic fields (where the magnetic energy and gas thermal energy are comparable), a significant amount of cool filaments arise in the CGM via enhanced thermal instabilities (bottom), in contrast to the case without magnetic fields where the CGM remains a single phase (top). Finally, magnetic fields help the survival of the cool gas by suppressing turbulent mixing with the hot phase via magnetic tension

[148-151], or reduce thermal conduction between the cool and hot phases via anisotropic conduction [152]. Therefore, the overall impact of magnetic fields is to increase the fraction of the cool gas in the CGM, and thus potentially alter the CGM thermal status which can be tested by *HUBS*.

Cosmic rays: Cosmic rays (CRs) are ultra-relativistic protons/electrons coupled with local plasma magnetic fields via Lorentz forces [153]. At the galactic/ISM scale, CRs at GeV energies (which dominates the CR energy spectrum) are produced by supernovae and AGN shock acceleration, and are transported by turbulence and magnetic fields in ISM and CGM. CRs are believed to be in roughly energy equipartition with the magnetic fields and thermal pressure in the ISM [154]. In recent years, the CR energy density and transport mechanisms have been better constrained via spatial analysis of the synchrotron radio continuum emissions detected above the galactic disks (e.g., [138, 155-157]).

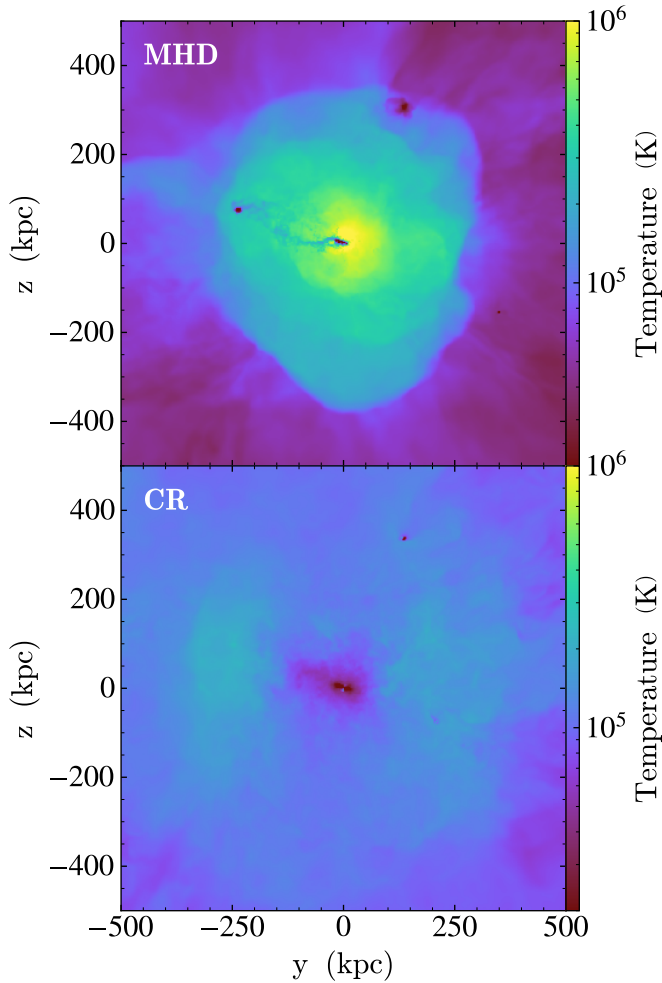


Figure 15 Projections of the gas temperature in MW-mass galaxy halos without (left) and with (right) cosmic rays. CGM is at the virial temperature of $T \sim 10^{5-6}$ K in the case without cosmic rays, with clear boundaries between the hot and cool phases around the virial radius ~ 250 kpc which traces the location of the virial shock fronts. In contrast, with cosmic rays, the galaxy halo is filled with much cooler ($T \sim$ a few 10^4 K) CGM without the signature of the virial shock. Figures are adapted from Fig. 1 in [158].

Recent theoretical studies suggest that with reasonable CR injection rates and transport coefficients, the CR energy density in the CGM can be comparable, or even significantly exceed, the thermal pressure in the CGM (e.g., [158-163]). Ji et al. 2020 ([162]) found that the CR pressure in the CGM can be one order of magnitude larger than the thermal pressure in the CGM, leading to a CR pressure-dominated galaxy halo where the halo gas is primarily supported by CR pressure rather than gas thermal pressure, and the temperature of the halo gas is much lower than the virial temperature of $\sim 10^{5-6}$ K, as shown in Fig. 15 from the FIRE-2 simulations¹⁾. In the meanwhile, virial shocks expected in massive ($M_{\text{halo}} \gtrsim 10^{11.5} M_{\odot}$) galaxy halos are also absent from the CR pressure-dominated CGM. Although this scenario is

roughly consistent with the observed CGM properties via quasar absorption lines such as H I and O VI column densities [106, 107], two-dimensional CGM emission maps which are expected from future *HUBS* observations can provide a more direct test of the CR pressure-dominated CGM. In particular, the morphologies and intensities of the soft X-ray emission from the CGM can be used to distinguish between the CR pressure-dominated and the thermal pressure-dominated CGM. In addition, the *HUBS* kinematics resolution can reach up to 1000 km/s in absorption and 300 km/s in emission, both of which are sufficient to probe the structures of virial shocks in the CGM.

2.5 Potential case studies on feedback physics tailored

1) The Feedback in Realistic Environments (FIRE) Collaboration: <http://fire.northwestern.edu>

for *HUBS*

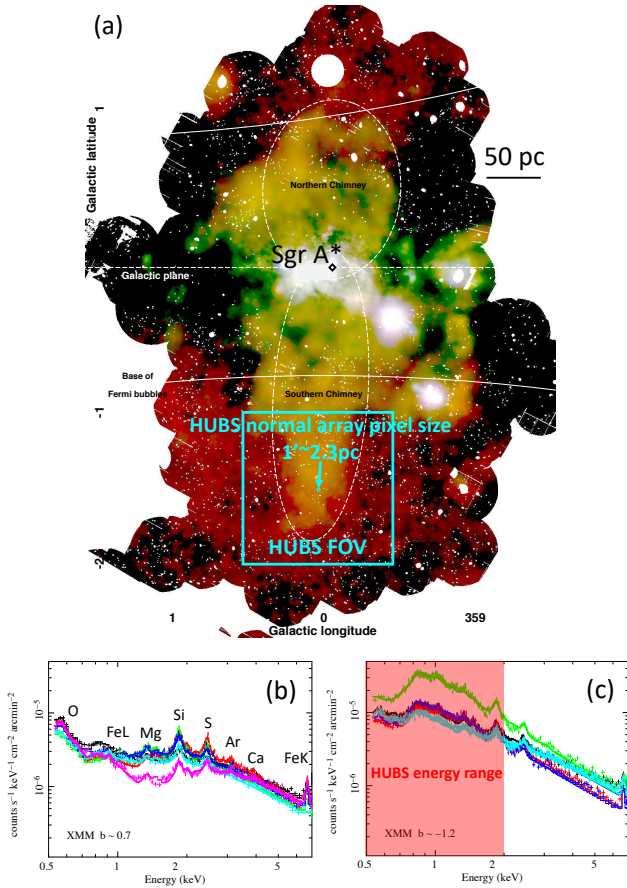


Figure 16 *XMM-Newton* observations of the “chimney” in the Galactic Center area [164]. (a) Tri-color X-ray images of the central 300×500 pc of the Milky Way: red: 1.5–2.6 keV; green: 2.35–2.56 keV covering the S XV lines; blue: continuum emission in the 2.7–2.97 keV band. The diamond at the center marks Sgr A*. The two dashed eclipses are the two chimneys indicating collimated bipolar outflows. The large cyan box shows the FOV of *HUBS* ($1^\circ \times 1^\circ$), while the tiny box marked with the arrow is the pixel size of the *HUBS* normal array ($1' \times 1'$). At the distance to the Galactic center (~ 8 kpc), a $1'$ *HUBS* pixel corresponds to ~ 2.3 pc. (b) and (c) are the *XMM-Newton* spectra extracted from a few regions at a Galactic latitude of $b \sim +0.7^\circ$ (b) and $b \sim -1.2^\circ$ (c), respectively. At $|b| \geq 1^\circ$, the foreground extinction is moderate, and many soft X-ray emission lines can be detected [emission line bumps of different elements are marked in (b)]. *HUBS* is sensitive to the soft X-ray line features at ≤ 2 keV [shaded area in (c)].

In order to probe the feedback physics mentioned above, we herein propose a few well-studied objects for some possible *HUBS* follow-up observations, which may lead to breakthrough scientific output in our understanding of stellar and AGN feedback.

Sagittarius A* (Sgr A*) located at the center of the Milky Way (MW) is the nearest supermassive black hole (SMBH), so provides us with a unique opportunity to witness the details of AGN or stellar (if more active star formation exists in

the past) feedback close to its launching site. There are increasing lines of evidence that outflows of energy and metal-enriched materials from the central tens of parsecs of galaxies have shaped the observed structures on a variety of larger scales [164–166]. Fig. 16 shows the *XMM-Newton* observations of the Galactic center area [164]. The two “chimneys” suggest collimated bi-conical outflows, which further connect to the larger-scale coherent structures such as the “Fermi bubbles” in γ -ray [167], the “*eROSITA* bubbles” in X-ray [168], or the “WMAP Haze” in microwave [169, 170], with typical sizes roughly on the order of the galaxy itself (more than one order larger than the “chimneys”). Existing X-ray observations of the Galactic center area already show interesting fine structures highlighted in the emission from special ions (e.g., the bipolar “chimneys” revealed in the S XV emission in Fig. 16a), many of them also have multi-wavelength coherent structures or counterparts (also see [165]). However, the energy resolution of the X-ray CCD spectrum is insufficient to separate individual emission lines (Fig. 16b,c), which limits the constraint of the physical and chemical properties of the outflows. *HUBS* will for the first time resolve fine spectral structures of the hot gas in a large area above the Galactic plane close to Sgr A*. Since the foreground extinction is very strong toward the Galactic center direction and *HUBS* is only sensitive at $\lesssim 2$ keV (Fig. 16b,c), the future *HUBS* survey will most likely focus on the area with the Galactic latitude $|b| \geq 1^\circ$ (e.g., the cyan box shown in Fig. 16a). We can either map the “chimneys” area shown in Fig. 16a or a larger sky area covering a significant fraction of the “*eROSITA* bubbles”, depending on the desired depth and the available observing time, or the required “effective angular resolution”.

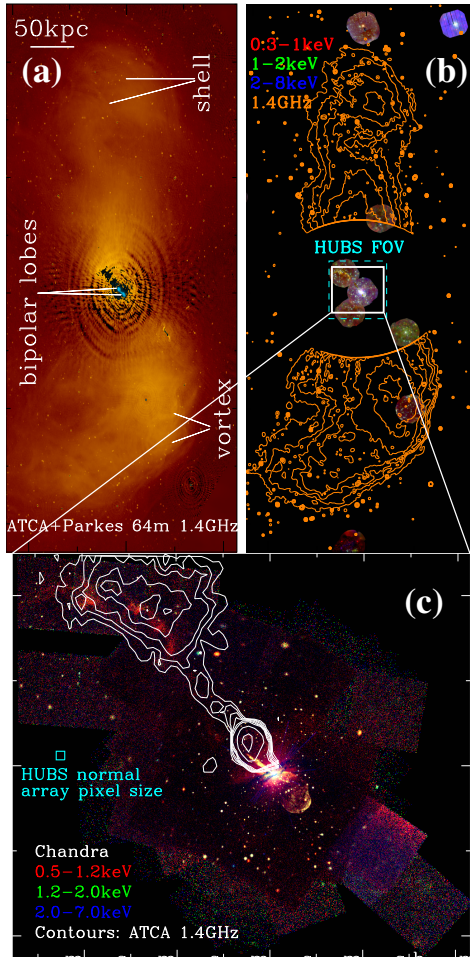


Figure 17 (a) ATCA+Parkes 64m 1.4GHz radio continuum image of the ≥ 500 kpc scale giant radio lobes in Cen A [171]. Some prominent radio continuum features identified by [171] are marked on the image (“shell” and “vortex”). The contrast of the image may not be high enough to clearly show these features as the dynamic range of the image is very large. The ~ 10 kpc scale bipolar radio lobes are plotted in blue in the very nuclear region. We also plot a scale bar of 50 kpc assuming a distance to Cen A of $d \approx 3.8$ Mpc. (b) *XMM-Newton* tricolor images of Cen A and the surrounding area with the same FOV as (a). The orange contours are the 1.4 GHz image in (a) with the central region masked. The cyan dashed box in the center is the *HUBS* FOV, while the white solid box is the FOV of the *Chandra* image in (c). (c) *Chandra* tricolor images of Cen A and the Northern Middle Radio Lobe. The contours are the high-resolution ATCA 1.4GHz radio continuum image from [172] (only covering the northern half). The small cyan box is the pixel size of the 60×60 *HUBS* normal array.

Centaurus A (Cen A; NGC 5128) is the nearest FR-I radio galaxy located at a distance of $d \approx 3.8$ Mpc ($1' \sim 1.1$ kpc; [173]). It is the central galaxy of one of the two subgroups comprising the Cen A/M83 group, and the 4th nearest galaxy group only after the local group, IC342, and the M81 group. Cen A is the 5th brightest external galaxy in optical, after LMC, SMC, M31, and M33; and 2nd brightest extragalactic radio source, only after Cygnus A. Fig. 17 shows the multi-scale radio and X-ray structures of Cen A, indicating complex interactions between the AGN jet and the galaxy envi-

ronment. The small distance and plenty of multi-scale structures related to the AGN-ISM/CGM/IGM interaction make Cen A unique for detailed analysis of AGN feedback. Combined with the study of the Galactic center region as described above, the proposed *HUBS* observations can be used to study the feedback processes over more than five orders of physical scales (from $\lesssim 10$ pc to ~ 1 Mpc). The large FOV of *HUBS* makes it ideal to observe a large object such as Cen A. We will need ~ 30 *HUBS* observations to cover the entire area of interest surrounding Cen A, which is much more efficient than the *Chandra* or *XMM-Newton* (Fig. 17b). The angular resolution of *HUBS* is still sufficient to resolve some fine structures such as the chain of knots in the northern jet (Fig. 17c). The energy resolution ($E/\Delta E \approx 500$ @1 keV for the 60×60 normal array; $E/\Delta E \approx 1000$ @0.6 keV for the 12×12 central sub-array) is sufficient to measure the physical and chemical properties of the hot gas, and is also typically marginally sufficient to measure the shift or broadening of the soft X-ray emission lines from a normal galactic outflow, especially for those from the gaseous medium strongly turbulated by the AGN (e.g., the Perseus cluster as observed by *Hitomi* [174]; the *HUBS* central sub-array has an energy resolution comparable to *Hitomi* at the Fe K lines).

As one of the nearest nuclear starburst galaxies with an edge-on orientation, M82 provides us with the best view of the multi-phase galactic superwind driven by starburst feedback [84, 123]. Existing high-resolution X-ray grating spectroscopy observations of the halo of M82 indicate complicated emission line spectra, with contributions from both the thermal plasma and some non-thermal components such as the charge exchange (CX; see the *XMM-Newton*/RGS spectra from [175]). However, such grating observations are limited to relatively compact objects. In most of the nearby galaxies like M82, we still rely on X-ray CCD imaging spectroscopy observations, with which the decomposition of different emission components, so the measurement of the physical and chemical properties of the hot gas, can be very uncertain (e.g., [84, 176]). Although located in the M81 group which has giant tidal tails detected in colder gas [177], most of the interesting features related to the galactic superwind (such as the northern “cap” ~ 11 kpc above the galactic plane; e.g., [178]) could be covered with a single *HUBS* observation. At a distance of $d \approx 3.53$ Mpc, the $1'$ *HUBS* normal pixel corresponds to ~ 1 kpc, which is still helpful to perform some spatially resolved analysis (e.g., [176]), although the fine structures of the superwind cannot be resolved. The $15''$ pixel size of the central sub-array could better sample the PSF, but cannot significantly increase the angular resolution. The velocity of the hot wind constrained in different ways should be $> 10^3$ km s^{-1} (e.g., [179, 180]), significantly exceeds the outflow velocity of the cold gas (typically

$\sim 500 \text{ km s}^{-1}$; e.g., [175]). Measuring the velocity difference of different gas phases is not only important in measuring the energy content of the outflow, but also in quantitatively estimating the CX contribution. Furthermore, we can also use the high-resolution spectra taken with the micro-calorimeter on board *HUBS* to better constrain the gradients of the intrinsic absorption column density, temperature, and metallicity, as well as some other derived parameters (electron number density, thermal pressure, cooling timescale, etc.), of the hot gas outflow [176]. These measurements can be compared to numerical simulations to determine the thermalization efficiency of supernovae (SNe) energy and the mass loading factor of the cool gas, which are key parameters of stellar feedback models (e.g., [176, 179]).

3 Galaxy cluster and large-scale structure

Quantifying the cosmic baryon budget, its multi-phase status, as well as its cooling and accretion activities, over a variety of physical scales from galaxies to groups/clusters or even the cosmic webs (e.g., [108, 181, 182]) can help us to understand various hidden drives of galaxy growth in their larger-scale environment [8, 183]. The baryonic matter abundance and distribution inside the cluster and group halos (e.g., [184-188]), as well as in the CGM of galaxies (e.g., [106, 107, 189-192]) have been extensively studied through multi-wavelength observations. On larger scales, a good fraction of the cosmological baryons at $z > 1$ have been detected inside the cosmic web with their abundance measured mainly through Lyman- α observations (e.g., [193, 194]). At lower redshifts, however, baryons inside the cosmic web are much more difficult to be probed due to the very low gas column density.

Many efforts have been made to search for cosmic baryons at such redshifts and it has been shown that approximately half of the total baryon budget at these epochs are locked up in the CGM of galaxies, the intragroup medium (IGrM), the ICM of clusters and the IGM in neutral and diffuse phases ([195]). The other half remain “missing” observationally and cosmological simulations have shown that they are locked up in a warm-hot ($10^5 \text{ K} < T < 10^7 \text{ K}$) phase in the IGM – referred to as the WHIM, as a result of significant heat-up and removal by star forming and feedback processes (e.g., [196-203]). Determining the “missing” baryon budget is expected to be most promising through the next generation X-ray spectroscopy (e.g., [204-207]). In this regard, *HUBS* will play a breakthrough role in probing the hot baryons in their multi-phase states on a variety of physical scales in the Universe. We herein present a few *HUBS* core science projects which could potentially greatly advance our understanding of

the hot baryon budget of the local Universe.

3.1 Multi-phase hot gas in galaxy groups and clusters

The hot gas inside the dark matter halo of galaxies, groups and clusters, referred to as the CGM, IGrM, and ICM, respectively, is an optically thin, collisionally ionized, multi-phase medium. The physical states and their spatial distribution are modulated by both external and internal factors (e.g., [183]). On larger scales, pristine gas is accreted from the connected cosmic web to the halo, together with relatively low metallicity gas stripped from the infalling satellite galaxy halos. On smaller scales, AGN and stellar feedback eject material, metal, energy/heat and momentum back to the halo environment, some of them can reach about several tens or even hundreds of kiloparsecs, where this hot polluted ejection meets the cold accretion from the outside and falls back when it sufficiently cools down. Overall the halo gas is experiencing gravitational accretion and heating, impact compression, collisional ionization and excitation, radiative cooling, etc.. Internally driven processes generally cause gas to move in the outward direction, although the angular distribution of inflows and outflows may be different and complex. Different spatial and time scales of the various processes involved therefore naturally lead to the multi-phased nature of this hot halo plasma. Observationally resolving the spatial structures in temperature, density, metallicity, and ionization state will be crucial to probe the contributions and strengths of individual processes that together modulate the hot halo gas across hundreds of kiloparsecs.

Regarding such a multi-phase IGrM or ICM gas, a cooler component is often detected in the central few tens of parsecs of relaxed (or nearly relaxed) groups and clusters, which accounts for up to several tens of percent of the total X-ray luminosity in 0.5 – 2 keV, after the projection effect is corrected (see [208] for a review). In the X-ray imaging spectroscopic analysis of the *Chandra* ([209]), *XMM-Newton* ([210]) and *Suzaku* ([211]) data, this cooler component is routinely modeled either as a single-phase, with a temperature decreasing inward monotonously, or as a cool spectral component coexisting with a hot component (i.e., the ICM defined in the ordinary sense). In this latter case, corresponding to a two-phase scenario, a relative “volume filling factor” that varies with radius is introduced to characterize the spatial distribution of the cooler gas. In these two scenarios, the formation and evolution of the cold gas are believed to be intrinsically different, which unfortunately cannot be distinguished by current data. In some cases (e.g., Abell 1795, [212]) a third weak gas component with an even lower temperature is necessary to improve the spectral fitting. The cooler components in the Virgo cluster and Abell 1795 are found to be

more metal-enriched than their hotter counterparts. However, in many other cases, the temperature range and metal abundances of the cooler component are poorly constrained, and are often fixed to certain values in the multi-component spectral fitting. Since the amount of gas cannot be well determined, a certain form of emission measure distribution as a function of temperature (e.g., a power-law form) has to be imposed. These uncertainties may have a considerable impact on the accuracy of measurements of metallicity (e.g., the so-called “Fe-bias”, see [213]) and other gas properties. For example, [212] reported that a systematic bias up to about $\sim 10\%$ can arise for the dynamical mass of the central region, which approximately equals the typical deviation between masses measured with the X-ray and the gravitational lensing techniques. Mounting evidence shows that the coexistence of cold and hot phases cannot be interpreted simply in terms of the hot bubble(s) inflated by the central AGN in the circumstance of a cooler environment. Although it has been proposed that the cold-phase gas may be the cD coronal gas confined by magnetic loops surrounded by the intruding hot ICM, or simply it may be a consequence of radiative energy loss in part of the ICM ([214]), direct observational evidence is still absent.

The large FOV and low instrumental background of *HUBS* make it best optimized to detect large-scale low surface brightness features, such as the extended multi-phase medium in cluster halos or even the cosmic web [5]. To detect the extragalactic hot gas emission with low-surface brightness, the foreground emission due to the MW hot CGM should be securely removed. With the high energy resolution of *HUBS*, a lower limit of redshift ensures the separation between the emission lines from the MW and targeted features (Fig. 13; also see [129, 130]). This will strongly help to remove the sky background, enabling the detection of extremely low surface brightness features. As demonstrated in the recent work of [130], which is implemented based on the IllustrisTNG simulation ([215-219]), *HUBS* is capable of detecting the soft X-ray emission of the IGrM in group halos out to $z = 0.3$, or that of the ICM in cluster halos located at slightly higher redshifts, when operating in either imaging or spectral mode for 1 Ms. Fig. 18 presents the X-ray emissivity maps (top) and the *HUBS*-observed O VII intensity maps (middle) of the hot gas in a cluster-sized halo (left column) and a group-sized halo (right column) simulated at $z = 0.11$. The metallicity-temperature ($Z - kT$) distributions of the gas particles in the two gas halos are plotted in the bottom panel, where two sets of black points are used to mark the bestfits of the adopted spectral model consisting of three APEC components. In particular, the mock images are made with the *HUBS* field of view and spatial resolution, i.e., 60×60 pixels in 1 square degree. The results also show that, although it

is possible to pick out the primary emission components by applying a simple spectral model (the three-APEC model in this case), more advanced tools designed for the analysis of high-resolution spectral data are needed to describe the gas properties more accurately.

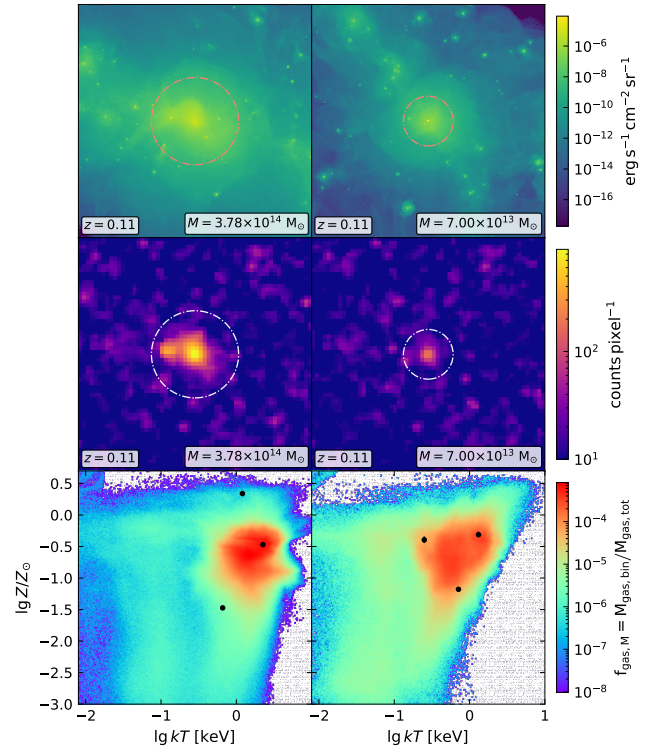


Figure 18 Top panel: X-ray emissivity maps of the hot gas in a cluster-sized halo (left) and a group-sized halo (right) selected at $z = 0.11$ from the IllustrisTNG simulation. The images are produced with 256×256 pixels for each, which covers a sky region of 1 square degree (the field of view of *HUBS*). The dash-dotted circles represent the virial radius (r_{200}). Middle panel: the mock *HUBS* O VII intensity maps for the two gas halos (i.e., the narrow-band images extracted at the position of (redshifted) O VII emission line) with 60×60 pixels in 1 square degree (1 arcmin/pixel, i.e., the resolution of *HUBS*). Bottom panel: the metallicity-temperature ($Z - kT$) phase diagrams of the two gas halos, where the black points represent the bestfits of the three-APEC spectral model. See [130] for more details.

3.2 Searching for hot baryons in the cosmic web

Recent studies have shown that it is possible to identify the baryonic filamentary structures of the cosmic web through stacking Lyman- α emissions ([220]), or the thermal Sunyaev-Zel’dovich signals ([221, 222]). An ongoing effort is, with the aid of cosmological hydrodynamic simulations, to find out the feasibility of detecting the X-ray emission of the hot baryons inside the filaments through the stacking technique [223, 224]. Due to the extremely low gas column density, direct observations are nearly impossible. However, this may be achieved with the help of optical tracers, because galaxies

that live inside filaments can be employed as a natural indicator of the cosmic web location. Many galaxy surveys, such as SDSS ([225]), GAMA ([226]), 2dFGRS ([227]), WiggleZ ([228]) as well as the Millennium Galaxy Catalogue Survey ([229]), have provided a variety of galaxy catalogs that together cover a good fraction of the full sky. Using the sky position and redshift information of these galaxies as inputs, edge-extracting software can readily reveal the large-scale structure of the cosmic web. With the optical tracers, we now have a great base for detecting the hot baryons hidden inside the filaments. However, the situation is still tricky, because a large spatial coverage and sufficient spatial resolutions in both transverse and sightline directions are necessary. *HUBS* is exactly suited for this purpose. The filaments have typically widths in the range of several hundred kiloparsecs to a few megaparsecs, our spectral resolution will be able to resolve them at a distance of up to a few hundred megaparsecs. This capability may be important to enhance the signal strength with or without stacking. The large field of view of *HUBS* can effectively cover a significant patch of the sky. With several tens of pointings, *HUBS* can collect X-ray emissions within a sufficiently large sky patch to allow mapping of the cosmic web structure (see Figure 3 of [230] for a demonstration of the cosmic web structure within a slice of a 10-degree cone out to $z \sim 0.1$). As shown in [130], out to redshift $z = 0.1$ *HUBS* will be able to detect hot gas in galaxies, groups, and clusters in both imaging and spectral modes given suitable exposure times. With an energy resolution of 2 eV, corresponding to a redshift resolution of $\delta_z \sim 0.003$ at such distances, the strong O VII and O VIII emission lines will essentially act as tomography tracers, indicating hot gas distributions at different redshifts. Selected patches in these line intensity maps *in both spatial and redshift dimensions* shall then be stacked according to the pre-identified cosmic web features as probed by optical tracers. The stacked signal will then be compared with signals derived from random stackings. Through such comparisons, not only will we perceive the existence of the hidden baryons inside the filaments, but also may we learn about the temperature and metallicity distributions of the hot ionized plasma inside the cosmic web.

3.3 Cluster observations for cosmology

HUBS will provide unprecedented opportunities for cosmology study with galaxy clusters, based on its large FoV, low instrumental background and superior spectral resolution. Cosmological constraints will mainly come from the following two aspects in the context of *HUBS* observations.

A. Constraints from cluster mass function

Galaxy cluster and group (“cluster” hereafter) population can be used as an important probe to constrain cosmological models and to investigate the properties of dark matter and dark energy [209, 231], the latter of which dominates within $z \lesssim 0.5$ [232]. In order to achieve cluster samples as complete as possible, wide-field surveys have been performed through the observations of the Sunyaev-Zel’dovich (SZ) effect, the weak gravitational lensing, and the X-ray emission of the ICM (e.g., [233, 234]). By obtaining cluster mass function, we can infer important parameters of the dark matter model, e.g., the matter density as Ω_M and the amplitude of linear matter density fluctuations as σ_8 when a flat universe is assumed. Furthermore, by combining X-ray and Sunyaev-Zel’dovich effect observations the absolute distances of galaxy clusters can be calculated, which allows the measurement of the Hubble constant [232].

The completeness of the detected cluster population, which is crucial to the constraints on cosmological parameters, is directly determined by the survey area and depth. Deep large surveys are time-consuming and expensive, thus the cluster population is comprehensively investigated only until $z \sim 0.1 - 0.2$ as of today. In the meantime, deficiency still exists in the faint end with a lower mass cut of about $10^{14} M_\odot$, making it very difficult to obtain a complete cluster mass function. Moreover, limited by the current FoV and instrumental background of detectors, very few clusters have been observed out to their virial radii, especially the low- z ones which are crucial to constrain dark energy models [235].

Several leading X-ray surveys were conducted in the last decade, among which the *ROSAT* All-Sky Survey (RASS) [236] is the first full-sky survey in soft X-rays. The studies of the few thousand RASS clusters, which are detected above the flux limit of $\sim 10^{-12}$ erg s $^{-1}$ cm $^{-2}$ and are mostly high mass systems located at the low redshift space, have offered a fundamental basis to cluster cosmology (e.g., [237, 238]). Recently, *eROSITA* All-Sky Survey (eRASS), the successor of RASS, is the most promising project for cosmological constraints in X-rays [239]. Upon completion²⁾, eRASS is expected to detect $\sim 10^5$ clusters, most of which are bright sources, in eight all-sky survey scans [241]. The depth of eRASS (an average exposure time of 2.5 ks per field), however, is relatively shallow and will limit its application in cluster cosmology (e.g., measurement of the gas fraction within the virial radius). In fact, although it is estimated that the eRASS survey will provide constraints of $\Delta\Omega_M = 0.012$ and $\Delta\sigma_8 = 0.036$ with combined probes from cluster number counts and angular clustering [241], $\Delta\Omega_M \sim 0.05$ and

2) However, the eRASS completion is currently uncertain, as *eROSITA* on board the German-Russian Spectrum-Roentgen-Gamma mission has been switched off since 26th February 2022, with only four of the eight planned all-sky survey passes finished [240]. The resumption of the telescope’s operation has not yet been determined.

$\Delta\sigma_8 \sim 0.07$ has just been achieved based on the first results from the proof-of-concept mini-survey with cluster number counts only, i.e., *eROSITA* Final Equatorial Depth Survey [242]; these are at similar levels of the constraints provided by the *Chandra* and *ROSAT* cluster archives [238] or by the XXL survey of *XMM-Newton* [210, 243]. Deeper investigations with a considerably wide field are desired in order to achieve a complete cluster sample out to $z \lesssim 0.5$, including those low-mass systems.

HUBS, due to its large FoV and low instrumental background, has great potential to collect a complete sample of clusters extending to larger redshifts, by carrying out a deep survey covering an area of $\sim 15 \text{ deg}^2$ with an average exposure of 300 ks. This surveying field, hence being named *HUBS-DF* (*HUBS* deep field), will be sited in the Galaxy And Mass Assembly (GAMA) survey footprint, particularly the GAMA02 field [244], therein abundant multi-band survey data have been archived, which is very important to assist cluster identification and study.

With a low instrumental background and superior 2 eV energy resolution [5], *HUBS* has the superb capability to resolve galaxy groups (or the faintest clusters) among crowded foreground/background AGNs and normal galaxies in narrow-band (vicinity of O VII and O VIII lines) images based on a recently published work of the *HUBS* team [130]. By extrapolating this result, it can be easily seen that a cluster with $M_{500} = 5 \times 10^{13} M_{\odot}$ at $z \sim 0.5$ can be resolved in the O VIII line with an exposure of 300 ks (Figure 19). We consider this quasi-monochromatic imaging of *HUBS* a novel method to identify faint and/or distant clusters, and believe that *HUBS* has excellent feasibility to measure ICM in extended redshift range (see also [130]). However, to achieve a complete cluster sample within $z \sim 0.5$, strong background source confusion of *HUBS* with flux limit of $\sim 5 \times 10^{-15} \text{ erg s}^{-1} \text{ cm}^{-2}$ must be removed. A drift scan or an assembly of 4500 stacked shallow observations (1 ks for each) with each pointing shifted by $3'$ is proposed, to improve the angular resolution of the central 11.3 deg^2 of *HUBS-DF* to $15''$ with the core 12×12 detector array [5], so as to lower down source confusion limit by one magnitude in this area.

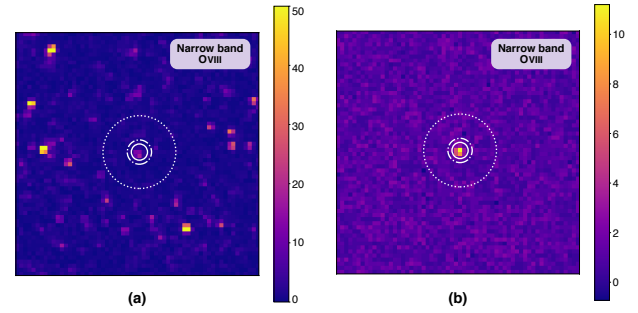


Figure 19 Mock X-ray images of a cluster with $M_{500} = 5 \times 10^{13} M_{\odot}$ at $z \sim 0.5$. (a) is the 18 eV narrow band image around the redshifted O VIII emission line; (b) same as (a) with the point sources above 5σ of the background removed. See [130] for details of the simulation. The dashed, dot-dashed, and dotted circles denote the radii r_{500} , r_{200} , and $3r_{200}$, respectively.

Since one of the most important issues is the synergies between *HUBS* and multi-wavelength facilities for source identifications, the survey will be performed within the 25 deg^2 north portion of the XMM-XXL survey in GAMA02, which also overlaps with the VIPERS redshift survey [245]. In the narrow-band image of *HUBS*, background AGNs above $10^{-15} \text{ erg s}^{-1} \text{ cm}^{-2}$ (in 0.5-2.0 keV) can be efficiently removed according to the existing XMM-XXL source catalog, and meanwhile, the candidate clusters can be confirmed by utilizing existing cluster catalogs (especially XXL cluster catalog [233], the Atacama Cosmology Telescope (ACT) SZ cluster catalog [246], and Wen-Han (WH2022) cluster catalog [247]) and ancillary multi-frequency observations, such as the Sloan Digital Sky Survey (SDSS) [248], the Wide-field Infrared Survey Explorer (WISE) [249], the Galaxy Evolution Explorer (GALEX) [250], and the Canada-France-Hawaii Telescope Lensing Survey (CFHTLenS) [251].

We have quantitatively estimated the completeness of the expected cluster sample from the proposed *HUBS-DF* survey, and its constraints on the cosmological parameters. Assuming an average CXB background derived from the *Chandra* or *XMM-Newton* observations, the *HUBS* 300 ks deep exposure will allow us to achieve the most complete X-ray sample of clusters within $z \lesssim 0.5$ with $M_{500} > 5 \times 10^{13} M_{\odot}$. Under such mass limit, *HUBS* detection will be 100% complete within $z \lesssim 0.48$, 93.2% complete at $z = 0.5$, 30.5% complete at $z = 0.75$, and 10.6% complete at $z = 1$. Although *HUBS* will detect a much smaller total number of clusters than all-sky surveys, the expected detected number density will be one order of magnitude better than the *eROSITA* shallow survey. The depth of our survey guarantees that there will be > 2600 photon counts for each target, which is crucial in measuring gas properties. Compared to the extremely low counts (50 counts per target used as detection limit in forecast [241]) of the *eROSITA* detected clusters, the remarkably improved

spectral quality will allow us to directly constrain the gas temperature in the spectral fittings, and estimate the cluster mass more accurately via the mass-temperature (M - T) scaling relation. By applying the weak-lensing measurements and the excellent spectroscopic redshift measurements of the GAMA survey to, e.g., perform the mass calibration, we expect that our error budget can be notably reduced compared with that of the wide but shallow survey of eRASS. Finally, an early prediction of the cosmological constraints for Λ CDM models has been estimated using the cluster detection limit mentioned above and the Markov chain Monte Carlo (MCMC) exploration of the parameter space (20), which shows that *HUBS* can greatly improve the constraints on cosmological model parameters as compared to the existing results of *ROSAT*, *Chandra* and the *eROSITA*.

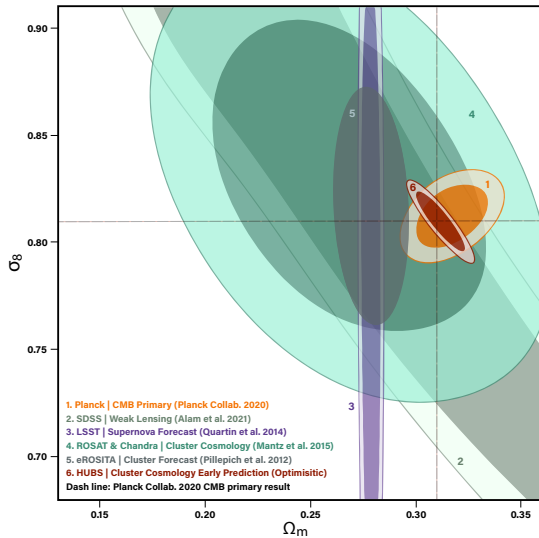


Figure 20 Predicted *HUBS* constraints on Ω_M and σ_8 , which is compared to the results derived from *Planck* CMB study, SDSS weak lensing study, LSST supernova forecast, *ROSAT* and *Chandra* cluster survey, and *eROSITA* cluster forecast (references in the picture). Note the last three constraints all used the cluster number counts method.

The *eROSITA* cluster forecast marks the 1σ distribution of the parameter space. For the rest, the darker and the lighter shades denote 1σ and 2σ level of the constrained parameter space, respectively. All the contours are smoothed for illustrative purposes. Our simulation input is based on the new Planck 2018 CMB primary results, hence the contours are centering at a different location.

B. Constraints from cluster gas fraction

In contrast to the methods that use the abundance of galaxy clusters as a function of mass and redshift to constrain cosmological models, the method via calculating gas mass fraction (f_{gas}) does not rely on the completeness of the cluster sample. This method focuses on the study of gas ratios and their dis-

persion, and the dependence of these quantities on the cluster mass, aperture and redshift. With the deduced gas mass fraction we can constrain Ω_m , using a combination of the Hubble parameter and cosmic baryon fraction as $h^{3/2}(\Omega_b/\Omega_m)$. The results obtained with this method, although to be improved, are competitive as well as consistent with those from recent CMB, Type Ia supernova and baryon acoustic oscillation data, and in the meantime to explain why f_{gas} is lower than expected in some low-temperature ($kT_{2500} < 5$ keV) systems.

The current relevant work from *Chandra* [252, 253] is based on a morphological selection of relaxed clusters above 5 keV, with the study only confined within r_{2500} . However, at r_{2500} the influence of various astrophysical processes, e.g. stellar winds from massive stars, AGN jets and supernova explosions, cannot be neglected. The study of [235] indicated that even at $\sim r_{500}$ hot gas is still relatively significantly affected by various astrophysical processes, giving the dependence of the baryon fraction upon radiative cooling, star formation, feedback through galactic winds, conduction, and redshifts. As a result, extended investigation of f_{gas} until the virial radius (roughly r_{200} where gravity dominates) is more cosmologically crucial.

The large FoV of *HUBS* brings a huge advantage to addressing this issue by allowing us to cover the entire virial region of a cluster with one pointing close as $z \sim 0.02$. Moreover, its superior spectral resolution provides unique means to identify ICM bulk motions with radial velocities possibly from 90 to 6000 km s $^{-1}$, to crosscheck whether the cluster is truly relaxed. We expect to observe $\sim 30 - 50$ relaxed brightest galaxy clusters to r_{200} with ~ 50 ks single pointing for each. The selection should satisfy two criteria. Firstly, high-quality multi-band data are available for the target, for synergistic investigations to remove possible background pollution. Secondly, once weak lensing data is available, the total gravitating mass obtained in the X-ray will be calibrated, in order to guarantee high accuracy in the gas fraction calculation.

When the gas mass fractions of low- z clusters are incorporated with baryon fraction measurements via the CMB, or with priors on the cosmic baryon density and the Hubble constant, the Hubble constant or the dark energy density as well as the equation of state can be deduced. Thus galaxy clusters in the low- z region can not only help provide a more accurate sample for our measurements, but also have more important cosmological significance for they are in the dark-energy-dominated window of cosmic history. Finally, if the gas mass fraction of clusters is indeed constant, it can be used as a ‘standard ruler’ to measure the space-time geometry of the Universe with the Hubble parameters determined by other measurements.

4 Galactic Science

Close to home, the Milky Way provides the nearest targets for detailed study of the ISM, energetic explosions, stars, compact objects, and so on. Hot gas is thought to permeate the ISM. It is most certainly related to supernovae, stellar wind, and the central supermassive black hole, and thus offers an excellent laboratory for studying the physics of feedback processes. There are a number of unresolved issues, including the origin of the soft X-ray background radiation, the origin of the *eROSITA* Bubble (which might be related to the Fermi Bubble), and the properties of the hot halo, which likely bear relevance to the physics of CGM and feedback processes.

4.1 The Cosmic X-ray background

The cosmic X-ray background (CXB) is one of the first discoveries of X-ray astronomy, along with the first extrasolar X-ray source Scorpius X-1 [254]. Later the flux level of the soft X-ray band (44 – 70 Å) was successfully measured by [255] and [256], and interpreted as truly diffuse emission of hot plasma [257, 258]. Our understanding of the soft X-ray background has progressed considerably in the ensuing more than 50 years, with generations of X-ray instruments. Aside from the in-service all-purpose telescopes such as *Chandra* X-ray observatory and *XMM-Newton*, as well as retired ones such as *ROSAT* and *Suzaku*, many kinds of space missions have been dedicated to probing the nature of the soft X-ray background. Recent missions include the space shuttle payload “*Diffuse X-ray Spectrometer*” (*DXS*, [259]), dedicated explorer “*Cosmic Hot Interstellar Plasma Spectrometer*” (*CHIPS*, [260]), sounding rocket mission “*Diffuse X-rays from the Local galaxy*” (*DXL*, [261, 262]), and the recent soft X-ray surveyor *HaloSat* [263].

In general, the CXB can be decomposed into two kinds of origins, galactic and extragalactic. The galactic soft X-ray emission comes from three distinct components, the solar wind charge exchange (SWCX), the Local Hot Bubble (LHB), and the Galactic halo, while the extragalactic origin is dominated by AGNs. Distinguishing these components from each other and quantifying their contribution to the soft CXB are limited by the spectral resolution of current space missions and model dependent. For example, it is still an open question whether the observed soft X-ray emission at 1/4 keV is due to LHB or purely from SWCX (e.g., [264-266]).

HUBS can provide unprecedented line diagnostics to help to understand the origin of the CXB. On the other hand, both in-service and past missions barely cover the 0.1 – 0.5 keV band, which seems to be a turnover in the spectral energy distribution of cosmic UV/X-ray background ([267-269]). With *HUBS*, we can obtain finer constraints on the UV/X-ray back-

ground modeling.

4.1.1 Local hot bubble

It has been identified that the solar system resides in a cavity of low-density and ionized gas, surrounded by a shell of cold neutral gas and dust. The existence of such a cavity was implied by the soft X-ray emission seen in the *ROSAT* map at 1/4 keV [270], and was dubbed as the “local hot bubble” [271, 272]. Though debates on the model exist, the LHB still led its popularity and was strongly supported by recent studies [273, 274]. Followup studies revealed its irregular shape and extent, suggesting a pathlength of order 100 pc [274-276], possibly created and maintained by stellar winds or supernova explosions due to nearby star formation activities.

Despite the change in intensities, soft X-ray emission from the LHB can be characterized by a hot phase plasma with $k_B T \sim 0.1$ keV [259, 277]. However, possible contamination arises from foreground SWCX, and Galactic halo at intermediate and high latitudes.

X-ray shadowing method is invoked to divide the observed emission into the foreground and background components [273, 278]. Based on the *DXL* data, Liu et al. [275] removed the contribution by SWCX and reported a uniform temperature $k_B T = 0.097 \pm 0.013$ keV, consistent with previous results. In addition, combining the *DXL* result and other measurements, Snowden et al. [274] showed the total pressure in the LHB is in pressure equilibrium with the local interstellar clouds, eliminating the long-standing pressure problem of the LHB [279].

4.1.2 Galactic halo

The hot gaseous halo was first predicted by [280], while the first hint of the hot gaseous halo was observed by RASS [281]. It was implied by the anti-correlation between the soft X-ray emission at 1/4 keV and the column densities of the neutral hydrogen (e.g. [282]). After *ROSAT*, high spectral resolution spectra obtained by *DXS* revealed that the soft X-ray emission was dominated by thermal emission of hot gas ($k_B T \approx 0.1 - 0.2$ keV), which favored a galactic halo origin [283]. Furthermore, the launch of flagship telescopes *XMM-Newton* and *Chandra* enabled high spatial resolution observations to decompose the diffuse contribution seen by *ROSAT* into the extragalactic point sources (e.g., AGN; [284]) and truly diffuse emission (e.g., [84]).

In the past two decades, the understanding of the Galactic hot halo has been improved a lot by deep *XMM-Newton* and *Chandra* observations in both emission and absorption. Particularly, the spatial distribution of the Milky Way hot halo

has been established as the first-order approximation assuming the spherical symmetry (e.g. [285-287]). Furthermore, the temperature distribution of the hot halo has been investigated, showing another extremely hot phase at $k_B T \approx 0.7$ keV (e.g., [288]). In the current decade, newly launched surveyors *eROSITA* and *HaloSat* also continuously provide new insights, such as the discovery of the soft X-ray bubbles on both sides of the Milky Way (i.e., *eROSITA* bubbles; [289]).

Although it has been astounding progress to understand the Galactic hot halo from decades ago, there are still fundamental open questions in the field. For instance, the metallicity of the hot halo is still controversial. On one hand, the continuum of the thermal emission due to the Galactic hot halo is hard to be decomposed from other contributors to the continuum (e.g., the CXB or the soft proton), limited by the relatively poor spectral resolution of the existing instruments. On the other hand, the SWCX contributes to the soft X-ray line emission, which is also blended with the emission of the Galactic hot halo. These difficulties make it a hard problem to determine the hot halo metallicity. The high resolution and spectral coverage down to 0.1 keV of *HUBS* could bring new possibilities to determine the metallicity by clearly decomposing line emission and the continuum or determining the line ratios between forbidden and resonant lines.

Another intriguing question is about the potential extremely hot phase in the Galactic halo. Currently, detection of an extremely hot phase at $k_B T \approx 0.7$ keV has been claimed in both emission and absorption. However, these pieces of evidence have limitations in different ways. The absorption line analyses rely on weak detection ($\approx 2 - 3\sigma$) of Ne IX and Ne X in two sight lines [288, 290]. The modeling of this absorption system requires both super high temperature and super solar neon abundance of $[\text{Ne}/\text{O}] \approx 0.7$, which raises questions about its origin (e.g., in the Galactic disk or the Galactic halo). The emission evidence of the super hot component is mainly the unexpected enhanced feature at 0.8 – 0.9 keV in the single-temperature hot halo model. However, as suggested in [277], the similar feature observed at low Galactic latitudes can be explained by the hot corona of M dwarf stars in the disk. Adopting the model in [277], M dwarf stars can contribute $\approx 2 - 4 \times 10^{-7}$ kpc cm⁻³ at high latitudes, which can be 50 - 100% of the claimed detection of extremely hot phase (e.g., [291, 292]). The high spectral resolution and relatively high spatial resolution of *HUBS* could provide unique insights into the extreme hot phase by constraining line ratios (determining radiation mechanisms) and resolving possible M dwarfs in the field. Therefore, although *HUBS* is not a dedicated surveyor focusing on the diffuse emission of the Galactic hot halo, its unique combination of large FOV and high spectral resolution opens a special window to study the Galactic hot halo.

4.1.3 Extragalactic sources

While the diffuse Galactic and the local emission dominate the CXB in the 0.5 – 1 keV band, the majority of the X-ray background has been recognized as discrete extragalactic sources, mostly AGN and star-forming galaxies. According to the deepest observations by *Chandra* and *XMM-Newton*, in the 0.5–2 keV band, the resolved fraction of the extragalactic background reaches about 80 – 90% (e.g., [293-297]). As a consequence, insights into the extragalactic background may serve as a constraint on the integrated SMBH growth and the accretion physics of galaxies.

However, there still remains unresolved CXB of unknown origin, for instance, about 10% diffuse emission in the 1 – 2 keV band [295]. It may be from CGM of galaxies within their Virial radii [298] or “warm-hot” intergalactic medium with the temperature of 10^{5-7} K (WHIM; [299]). On the other hand, with the current CCD energy resolution, some models for the components of CXB are oversimplified, for e.g., a single-T APEC model for describing the local thermal-like emission cannot interpret the emission excess of CXB below 0.5 keV [295]. Consequently, the uncertainties of the AGN contribution are larger in the 1 – 2 keV band, which is essential for disentangling the obscured and the unobscured AGNs (e.g., [300]).

HUBS has a large FOV (~ 1 deg²), and therefore most observations will partly cover the region of CXB, with a remarkable effective area (~ 500 cm²). The X-ray integral field units in *HUBS* cover the 0.1 – 2 keV band which is complementary to the bands of *Chandra* or the future *Athena*, and together can give better constraints on the composition of CXB. With the 2 eV high energy resolution, the local diffuse emission can be exclusively determined, and the obscured fraction of AGNs would be more precise. Taking that *HUBS* is designed for observing CGM and WHIM (e.g., [130]), it will quantitatively predict their contributions in the CXB and fill the final gap of the unresolved CXB.

4.1.4 Solar wind charge exchange

SWCX is generated when the highly ionized solar wind ions interact with the neutral materials within the solar system, gaining an electron in a highly excited state which then decays emitting an X-ray or UV photon with the characteristic energy of the ion. It was first proposed to explain the cometary soft X-ray emission [301], and then identified as the source of the long-term enhancements observed in the *ROSAT* All-Sky Survey (RASS; [282, 302]).

Based on the target neutrals, there are in general two kinds of SWCX, i.e., the geocoronal SWCX and the heliospheric SWCX. The former is due to the interaction between the compressed solar wind ions in the magnetosheath and the neu-

trals (mostly hydrogen) in the exosphere of the Earth. Its strength and location depend strongly on the strength of the solar wind. The latter, on the other hand, is due to the interaction between the free-flowing solar wind and the neutral ISM within the entire heliosphere (up to ~ 100 AU). Heliospheric SWCX shows direction dependence as a consequence of the structured solar wind and the neutral distribution in the heliosphere.

Due to its ubiquity, SWCX emission contaminates every X-ray observation of astrophysical objects. In particular, the spectrum of SWCX contains rich lines, some of which are the same lines used for the diagnostics of astrophysical plasma. The inclusion of SWCX emission could significantly change the derived plasma temperature of the astrophysical object, and/or mimic a separate diffuse soft X-ray component.

Despite the difficulties in separating SWCX emission from that of astrophysical plasma, different groups have developed models to calculate SWCX emission based on solar wind conditions, neutral distributions, and theoretical interaction cross-sections (e.g., [303-306]). However, there are, sometimes, large discrepancies between the model predictions and the observational results (e.g., [307-309]). The largest uncertainties of these models are mainly due to the lack of detailed information about the solar wind abundance and ionization state, and the theoretical and experimental interaction cross-section.

Owing to its high spectral resolution, *HUBS* will allow us to resolve most of the fine-structure lines, which suits well for learning SWCX. In principle, line intensity ratios in triplets of the He-line ions (e.g., O VII) from SWCX emission are different from those in astrophysical thermal emission (e.g., [310]), and the *HUBS* spectroscopy will help to distinguish and separate SWCX emission from the thermal components, e.g., from the LHB, the Galactic halo, and other distant components.

Due to the low-Earth orbit, *HUBS* observation will be inevitably affected by the geocoronal SWCX. One strategy to study the SWCX in the near-Earth environment is through *HUBS* observations of the Moon. *HUBS* observation will cover the full Moon with its field of view and clearly resolve the SWCX lines with its superior energy resolution (see Fig. 21). On the bright side, strong fluorescence lines from O, Mg, Al, and Si can serve as a remote sensor of the element composition on the lunar surface. While the observation of the dark side of the Moon will maximize the SWCX signal by blocking the thermal emission from our galaxy and distant objects. The X-ray emission from the dark Moon mainly consists of two parts: the emission from the magnetosheath (the near-Earth environment $< 10 R_E$) and from the region be-

tween the bow-shock ($\sim 10 R_E$) and the Moon ($60 R_E$). For the near-Earth environment, the high variability of SWCX is complicated by the solar wind temporal variation. Real-time monitoring of the solar wind is necessary for accurate data analysis. In-situ measurements from ACE³⁾ and/or the future Chinese space mission SMILE⁴⁾ will provide valuable data. Another important factor in the SWCX luminosity is the neutral distribution in the magnetosheath, which requires sophisticated magneto-hydrodynamic modeling for the solar wind interaction with Earth's atmosphere [311]. The high-resolution spectra obtained by *HUBS* will precisely measure the SWCX contribution in the near-Earth environment and help to test the results of MHD models. In addition, *HUBS* data can be used to constrain the charge exchange cross-sections measured in the laboratory.

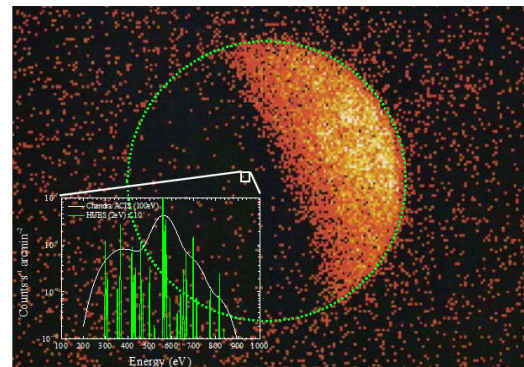


Figure 21 The *ROSAT* PSPC observation for the Moon [312, green dotted circle], inside panel shows the *HUBS* simulation (2 eV, green curve) for an average slow solar wind ($v = 400$ km/s) at one chip marked by open white box along with the comparison to *Chandra*/ACIS simulation (100 eV, white curve). Here, the CX model uses the same exospheric hydrogen as in previous work [313].

4.2 Supernova remnants

Supernovae (SNe) are among the most violent explosions in the universe, which release a typical energy of $\sim 10^{51}$ erg in a rather short timescale. As an essential part of the galactic ecosystem, SNe play an important role in the baryon cycle and the energy feedback. Supernova remnants (SNRs) are SNe interacting with the surrounding circumstellar material (CSM) and interstellar medium (ISM), which provide an important means to study the physics of both sides of the interaction.

SNRs are bright sources in the X-ray sky and the nearest targets to observationally constrain how SNe influences galactic ecosystems. Over a hundred X-ray-bright SNRs have been found thus far in our Galaxy, LMC, and SMC. These extended sources are actively heating the interstellar medium

3) <https://solarsystem.nasa.gov/missions/ace/in-depth/>

4) <http://english.cssar.cas.cn/smile/>

with fast shocks and enriching it with heavy elements. The X-ray observations in past decades have greatly advanced our knowledge on SNRs [314], but also post some challenges that require X-ray observations with high spectral resolution.

Some crucial questions in SNRs are yet to be answered with future X-ray instruments with high spectroscopic capabilities: 1) What are the metal compositions in diverse SNRs and how do different supernovae contribute to producing heavy metals in our Universe? 2) How are the hot plasmas in non-equilibrium ionization produced? 3) How to constrain charge exchange and resonant scattering processes using emission lines? Below we summarize why *HUBS* will help us address these key questions.

4.2.1 Associate SNRs with their progenitors

One of the major challenges in the SNR study concerns the identification of the progenitor type. The two major types of SNe — the core-collapse SNe and the Type Ia (thermonuclear) SNe — can be well-defined and easily distinguished based on their optical spectrum around maximum light. However, it is not that straightforward to associate an evolved SNR with its original progenitor system, which needs a detailed investigation into the properties of the SN ejecta and the CSM.

Type Ia SNe represents the thermonuclear explosions of C/O white dwarfs. The nuclear burning in Type Ia SNe typically results in a large amount of iron-group elements (IGEs) such as Fe and Ni as well as intermediate-mass elements (IMEs) such as Si, S, Ar, and Ca [315, 316]. However, in the case of core-collapse SNe, one may expect oxygen as the major product of the nucleosynthesis [317, 318]. Therefore, the SN ejecta metal abundances (or abundance ratios) can be used as diagnostics for typing their remnants [319]. SNRs showing evidence of enhanced oxygen abundances (so-called oxygen-rich SNRs) are commonly considered from the core-collapse explosions of the most massive stars, while SNRs dominated by IGEs and IMEs are more likely from Type Ia events. The X-ray spectra of SNRs contain most of the prominent emission lines from these metal species, which are essential for constraining the ejecta properties. However, the X-ray spectra of SNRs can always be a combination of the non-thermal emission from the accelerated particles and the thermal emission from both the shocked ejecta and CSM/ISM. Therefore, a precise measurement of the metal abundances relies on high-resolution X-ray spectroscopy that allows us to separate, identify, and measure the individual emission lines, and to distinguish the ejecta from other components. This can be challenging for the CCD instruments. For example, with a typical energy resolution $\Delta E \sim 100$ eV, CCD instruments can hardly resolve the Fe-L complex and

the Ne He α lines around ~ 0.7 – 1.0 keV, which will be seen as a bump-like structure or a pseudo-continuum and lead to large uncertainties in the measured abundances. The current grating instruments such as *XMM-Newton* RGS and *Chandra* LETG/HETG may partially solve this problem, but they are limited to those bright remnants with small angular sizes and the remnants with bright knot/filament structures.

The constraint on the X-ray properties of the shocked plasmas in SNRs, and our understanding of the SN-SNR connection, will be greatly improved with the help of *HUBS*. The *HUBS* energy band (0.1–2 keV) covers most of the He-like and H-like emission lines from C, N, O, Ne, Mg, Si, and L-shell emission from Fe and Ni. With an ultra-high energy resolution of ~ 2 eV of the main array and $\lesssim 1$ eV of the central sub-array, *HUBS* is capable of resolving individual emission lines, especially the He-like triplets (i.e., the resonant lines, the forbidden lines, and the intercombination lines) and the Fe-L complex. Figure 22 shows the simulated 100 ks *HUBS* spectrum of a mix-morphology SNR 3C 400.2, which provides an illustration of its extraordinary capability on detecting and resolving diverse metal species under different ionization states in SNRs. On the other hand, the spatial resolving ability and the large field of view may help to map the spatial distributions of the plasma parameters over the whole remnant.

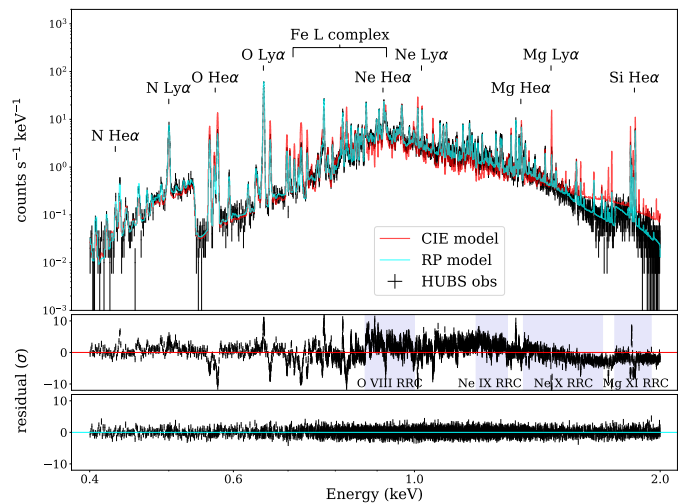


Figure 22 Simulated 100 ks *HUBS* spectrum of SNR 3C 400.2 (black data points), fitted with a collisional ionization equilibrium plasma model (CIE model, the red curve) and a recombining plasma model (RP model, the cyan curve), respectively. The lower panels show the residuals.

4.2.2 Constrain the origins of non-equilibrium ionization plasmas

At the early phase of the SNR evolution, due to the low density of the shocked plasma, the ionization process may take a rather long timescale before reaching equilibrium

($n_e t \sim 10^{12} \text{ cm}^{-3} \text{ s}$). Therefore, the shocked plasma in young SNRs is expected to be in the non-equilibrium ionization (NEI) state, where the plasma is still under-ionized (ionizing plasma, IP), characterized by an ionization temperature kT_i which is lower than the electron temperature kT_e . The observational evidence for this under-ionized NEI plasmas has been extensively established for a number of young SNRs such as Cas A, Kepler's SNR, SN 1006, SN 1987A, etc (e.g., [320-324]). However, recent X-ray spectroscopic studies have revealed the existence of over-ionized plasma (recombining plasma, RP) in several SNRs, where kT_i goes even higher than kT_e (e.g., IC 443, G359.1-0.5, W28, W44, etc., [325-329]). So far, RPs have been found in over a dozen of SNRs, which may represent a new subclass of SNRs [330].

The physical origin of the RPs in SNRs has not yet been fully understood. Theoretically, there are two approaches to an over-ionization state of the plasma: increase of kT_i (extra ionization) or decrease of kT_e (electron cooling). The extra ionization can be caused by suprathermal electrons [327], high-energy photons [325], and low-energy cosmic ray protons [331]. On the other hand, the electron cooling scenario, which is considered to be better applied to the SNR evolution, may arise from adiabatic expansion [332] and thermal conduction [325, 333]. In addition, simulations indicate that various scenarios, such as the adiabatic expansion and the thermal conduction, may simultaneously contribute to the formation of RP [333, 334].

The X-ray emission of RPs is characterized by several distinct spectral features, including the radiative recombination continua (RRCs), enhanced $\text{Ly}\alpha$ to $\text{He}\alpha$ line ratios, and enhanced He-like ion G ratios (defined as $G = (f + i)/r$, where r , f , and i stand for the resonant, forbidden, and intercombination line flux, respectively). Limited by the energy resolution of the current CCD instruments, the studies on RPs by far are mostly based on the RRCs and $\text{Ly}\alpha$ lines lying in the $\geq 2 \text{ keV}$ band (covers mainly the heavier elements such as Si, S, and Fe), and thus may leave some bias. *HUBS* will extend our study into lower energy band (0.1–2 keV). SNR 3C400.2 is one of the few remnants in which people have detected recombining features in the $< 2 \text{ keV}$ band so far [335] (another possible example could be SNR CTB 1 [336]). In Figure 22, we present a simulation of the 100 ks *HUBS* spectrum of 3C 400.2. A collisional ionization equilibrium (CIE) plasma model leaves significant residuals at the RRCs of O VIII, Ne IX, Ne X, and Mg XI, as well as the $\text{He}\alpha$ and $\text{Ly}\alpha$ lines, which can be clearly identified with the help of *HUBS*. In addition, the spatial resolving ability of *HUBS* can help to map the distribution of RPs in SNRs, which is crucial in determining their physical origins.

4.2.3 Diagnose charge exchange and resonant scattering processes

The excellent energy resolution of *HUBS* is especially suitable for line-oriented studies. Here, we bring up two examples in SNR physics, concerning the charge exchange process and the resonant scattering effect.

Charge exchange (CX) takes place in various astrophysical environments where the hot ionized plasma interacts with the neutral gas, such as solar wind interacting with planet atmospheres, comets, and the heliosphere. The collisionless shocks in SNRs provide a promising site for the CX study. Right behind the SNR shock front, unshocked cold neutrals may collide with the shocked hot ions and go through the CX processes, resulting in a population of highly excited recombined ions (or neutrals) which then produce cascade emission lines. Observational evidence of CX emission has been obtained from the optical band in many SNRs for over 30 years [337, 338]. However, the study of CX-induced X-ray emission in SNRs is still limited. Possible evidence has been found for a number of SNRs, including Galactic remnants Cygnus Loop [339-341], Puppis A [342], and G296.1-0.5 [343], SMC remnant 1E0102.2-7219 [344], as well as LMC remnants N132D [345] and J0453.6-6829 (SNR B0453-68.5) [346]. These studies are mostly based on investigations into the O VII triplets: the CX emission could be indicated by an unusually high G ratio. However, the precise measurement of G ratios could still be challenging with current X-ray instruments. CCD cameras are not able to resolve the He-like triplets, which are shown as one single line in the spectrum. Thereby one can only roughly estimate the G ratio based on the line centroid energy, which may lead to large uncertainties. In addition, CCD observations may be contaminated by the emission from solar wind charge exchange (SWCX). Grating instruments can help to resolve the triplets and to improve the constraint on G ratios, but the energy resolution may still be affected by the angular size of the source (morphological broadening). On the other hand, an enhanced G ratio is not necessarily originated from CX, it can also be induced by other mechanisms such as resonant scattering and inner-shell ionization. One possible way to distinguish CX from other mechanisms is to look for enhanced high-level excitation lines (e.g., enhanced $\text{Ly}\gamma/\text{Ly}\beta$ line ratios), which is another prominent and unique feature of CX emission. However, these lines are usually too weak to be detected or blended with other emission lines. Taking together the spatial resolving ability, the high energy resolution, and the large effective area, *HUBS* provides us with an unprecedented opportunity to study the CX phenomenon in SNRs.

Due to the rather low density, the hot X-ray plasma in SNRs can be safely assumed as optically thin in most cases.

However, for some emission lines with large transition oscillator strengths, the resonant scattering (RS) effect may not be ignored when the remnant contains a large column density. The optical depth at the line centroid can be estimated following [347]:

$$\tau = \frac{4.24 \times 10^{26} f N_{\text{H}} (n_i/n_z) (n_z/n_{\text{H}}) (M/T_{\text{keV}})^{1/2}}{E_{\text{eV}} \left(1 + 0.0522 M v_{100}^2 / T_{\text{keV}}\right)^{1/2}} \quad (1)$$

where f is the oscillator strength of the line, E_{eV} the line centroid energy in eV, N_{H} the hydrogen column density in cm^{-2} , n_i the ion density, n_z the element density, M the atomic weight, T_{keV} the plasma temperature in keV, and v_{100} the turbulence velocity in 100 km s^{-1} . Taking the O VII resonant line ($f \sim 0.72$) as an example, in a dense remnant like SN 1987A ($n_e \sim 2400 \text{ cm}^{-3}$ [324]) or a large remnant like Cygnus Loop (diameter of $\sim 2.8^\circ$ at a distance of $\sim 540 \text{ pc}$ [348, 349]), the column density may go to $N_{\text{H}} \gtrsim 10^{20} \text{ cm}^{-2}$, resulting in an optical depth $\tau \sim 1$. The RS process will scatter the incident photon into another random direction. For a non-uniform distribution of the plasma or an asymmetric remnant, it will then change the line flux and modify the surface brightness distribution. Therefore, similar to CX, RS may also be indicated by an enhanced G ratio — in this case, it is due to the reduced resonant line flux rather than the enhanced forbidden line flux. The RS effect in X-rays has been extensively studied in diffuse hot plasma of massive elliptical galaxies, galactic bulges, and clusters of galaxies [350-352]. The current study on the X-ray RS effect in SNRs is still quite limited. One possible observational evidence comes from the LMC remnant N49, for which people find enhanced O VII G ratio as well as O VIII $\text{Ly}\beta/\alpha$ and Fe XVII $(3s-2p)/(3d-2p)$ ratios, indicating RS effect on several resonant lines [353]. *HUBS* will be capable of resolving all of the bright resonant emission lines lying in the 0.1–2 keV band. Taking advantage of its spatially-resolved high energy resolution and the large field of view, we will be able to map out the surface brightness distributions of individual emission lines for the whole remnant, which has never been done before and will certainly improve our insight into the RS effect in SNRs.

4.3 Stars and compact objects

As the fundamental units of galaxies, stars play a key role in the recycling of matter. X-ray observations associated with stars not only deepen understanding of a wealth of astronomical phenomena, but also contribute to the understanding of extreme physical processes.

Several crucial questions have to be answered with *HUBS*:

1) Can we detect spectral features on the neutron star surface or the surrounding accretion disk to constrain the equation of

the state of compact objects? 2) How does the hot plasma near the WD surface in the accretion column/boundary layer cool and how are the emitted X-ray photons absorbed by the accreted matter? 3) How to understand the X-ray flare mechanism and coronal heating process?

HUBS, with its large area and high spectral resolution, will clarify these unanswered questions about neutron stars, white dwarfs and active stars.

4.3.1 Neutron Stars

Neutron stars formed by supernova explosions are the most compact objects in the universe. The equation of state for cold and dense matter is still inconclusive with respect to the understanding of the non-perturbative nature of the fundamental interactions between quarks [354]. The equation of state of a neutron star and a strangeon star predicts different mass-radius relations [355, 356]. The accurate measurements of neutron star mass and radius could put stringent constraints on the equation of state [357]. Mass measurements of massive neutron stars, $M > 2M_{\odot}$, have already excluded a number of equations of state that predict the maximum mass smaller than $2M_{\odot}$ [358]. Although a number of masses of neutron stars in compact binaries have been measured from radio observations with high precision, radius measurements are much more difficult to achieve with comparable precision.

Usually, neutron star mass and radius can be measured from type I X-ray bursts occurring in NS LMXBs, pulse profile modeling of X-ray pulsars and so on. NS low-mass X-ray binaries (NS LMXBs) are composed of NS and a main sequence donor orbiting each other. The masses of the NS and its companion can be determined by kinetic methods, with the orbital motion of the star in the NS LMXBs causing its spectral lines to undergo periodic redshifts and blue shifts due to the Doppler effect. The optical and/or near-infrared (NIR) spectroscopic observations can determine the mass function (stellar apparent velocity profile) of the star. Over the past decades, optical/NIR observations have shown that this method has the potential to constrain the compact object mass of LMXBs. However, there are also some shortcomings, mainly in that (1) this method requires a relatively bright optical/infrared flux of stars in LMXBs with strong absorption or emission lines, which is difficult with current optical/NIR telescopes for optically faint LMXBs; (2) This method can only measure the stellar mass function, but not the dense stars. If we can use an X-ray telescope with high energy resolution and a large effective area, we will be able to measure the velocity profile of dense stars and obtain the mass function of dense stars, which can be combined with optical/NIR observations to measure the binary mass ratio. The masses of dense stars can be constrained more precisely

if the stellar masses can be determined from optical observations. This has important implications for the mass spectrum of black holes and neutron stars, and for the solution of the “mass gap” problem. Even if the stellar masses cannot be determined, the mass ratio of the two objects, combined with other measurements, can be used to constrain the binary masses very well.

Zhang et al. [359] suggested that absorption lines from accretion disk winds are redshifted or blueshifted due to the Doppler effect of orbital motion. These spectral features are produced in the vicinity of compact objects and trace their motion, which can constrain the mass of compact objects in LMXBs. This approach was subsequently applied to the eclipsing NS LMXB MXB 1659–298, but the uncertainties of the measured apparent velocities are large because the energy resolution of *Chandra* and NuSTAR is not high enough [360]. In general, the maximum apparent velocity of compact objects in X-ray binaries is in the order of 100 km/s, which causes a spectral shift of order 10^{-4} . Therefore a high energy resolution of the detector is required. The energy resolution of *HUBS* has the possibility to measure the Doppler effect of the spectral lines with high precision.

The LMXB 4U 1700+24 has a red giant companion, and the X-ray emission is dominated by wind accretion. In the X-ray spectrum of 4U 1700+24, the O VIII (hydrogen-like Ly- α) emission line is found with a central energy of about 0.65 keV [361]. The spectral line structure is corresponding to a gravitational redshift of 0.009, suggesting that 4U 1700+24 is a candidate for a low-mass neutron star, which has to be verified by *HUBS* observations [362].

Type-I X-ray bursts are the unstable thermonuclear burning of accreting matter on the NS surface. The unstable thermonuclear burning of the hydrogen and helium, also known as type I X-ray burst, usually has a duration of $\sim 10 - 100$ s with a typical energy release of 10^{39} erg, recurs from few hours to days, and ignites at a column depth of $\sim 10^8$ g cm^{-2} [363]. In a rare case, superbursts, which are believed due to burning carbon, have been identified from the total energy release of $\sim 10^{42}$ erg and the duration of $> 10^3$ s [364]. Cottam et al. [365] reported the identification of absorption lines by stacking of *XMM-Newton* spectra over dozens of type-I X-ray bursts from NS LMXB EXO 0748–676, which they claimed were gravitational redshifted Fe and O lines from the stellar surface. However, the spectral lines have not been confirmed by the following observations. This particular source is now believed to be rotating rapidly with the frequency of 552 Hz from its burst oscillation [366], which makes it challenging to explain the relatively narrow spectral features. In’t Zand et al. [367] also reported the none detection of spectral lines in Rapid Burster from *Chandra*/HETG observations. Rauch et al. [368] calculated the possible spectral lines in the soft X-

ray band, i.e., Fe and O, that can be generated during X-ray bursts. *HUBS* provides a larger effective area accompanied with a high energy resolution than *XMM-Newton* and *Chandra*, which could resolve spectra features with a high S/N ratio from NS in LMXBs also by adding many X-ray bursts, or from a single superburst.

The X-ray dimmed isolated neutron stars (XDINS) mainly emit blackbody spectra in X-ray bands, and show optical/ultraviolet (UV) excesses [369]. All seven known XDINSs were found by soft X-ray detectors. RX J1856–3754 is the brightest and closest neutron star. *Chandra* observations showed that RX J1856–3754 had an almost blackbody spectrum in the soft X-ray band, with no emission or absorption lines [370], but absorption lines may be present in other XDINS. It is generally believed that the soft X-ray thermal spectrum of XDINS comes from the surface of the star. The absorption lines in the XDINS spectrum are produced in the magnetic environment of the neutron star. Moreover, the structure of the absorption lines is related to the stellar surface properties. The temperature and stellar radius determined by the continuum spectrum depend on the equation of state of the compact object (see [371] for neutron stars; [372] for strangeon stars). Therefore, XDINS is also an excellent target to study the surface properties and the equation of the state of NSs.

Besides measuring the NS mass and radius, *HUBS* can also study the magnetic field of anomalous X-ray pulsars (AXPs) and soft- γ -ray repeaters (SGRs). AXPs and SGRs are slowly rotating, isolated and ultra-magnetized neutron stars [373, 374]. Their X-ray activities, short bursts and outbursts, are powered by magnetic energy. During outbursts, the X-ray spectra of AXPs and SGRs may show absorption lines, which is interpreted as a proton cyclotron feature. *HUBS* could resolve the absorption features in 0.1–2 keV from AXPs and SGRS, and measure the magnetic field (see e.g., [375]).

4.3.2 Cataclysmic Variables

Cataclysmic variables (CVs) are binaries consisting of a white dwarf (WD) and a late-type main sequence or sub-giant star. CVs are the most populated binaries consisting of a compact star and their spatial density can reach up to 10^{-6} to 10^{-5} pc^{-3} in the solar neighborhood [376]. The WD in a CV accretes matter from its companion and emits mostly in UV and X-ray energy range. CVs are not only laboratories of stellar evolution theory, but also related to other important astrophysical questions. For example, CVs collectively contribute up to 80% of the Galactic Diffuse X-ray Background (GDXE). What’s more, CVs are closely related to the progenitor of type Ia supernovae since the latter are supposed to

be binaries harboring one or two WDs.

X-ray observations provide unique information to understand the accretion and emission process of CVs. The X-ray luminosity of CVs can reach 10^{33-34} erg s⁻¹, high enough to study the structure of the X-ray emitting region through X-ray spectroscopy. For example, the hard X-ray (around 2 to 50 keV) spectra of CVs have been well described by the multi-temperature thermal plasma model (mkcflow), and are used to constrain the maximum emission temperature and the mass of the WD. In contrast, the soft (0.1-2 keV) X-ray spectra of CVs are less well understood, and the usual characterization (the same mkcflow emission partially covered by the accreted matter) failed to explain the He-like and H-like lines from different elements (e.g., C, N, O) [377, 378]. Until now, there are only 15 CVs with high-resolution X-ray spectra at present, and about half of them are not well explained. Since the soft X-ray are supposed to be originated from the region fairly close to the surface of the WD, the failure of a widely-accepted model in this energy range leads to the lack of understanding of the accretion process near the WD itself.

HUBS provides a unique opportunity to explore the details of the emission region in CVs. The high-resolution spectra would certainly allow a detailed investigation of the distribution of the differential emission measure (dEM) and the metallicity on a large sample of CVs. Combined with hard X-ray data, a thorough understanding of the structure and evolution of the accreted matter in CVs could be reachable.

A rough estimation of the exposures could be done. For CVs within 50 pc, the typical 0.1–2 keV X-ray flux is $\sim 10^{-12}$ to $\sim 10^{-11}$ erg s⁻¹ cm⁻². Simulation shows an *HUBS* snapshot of 10 to 100 ks (depending on the flux of the target) could provide a spectrum with sufficient photons for a targeted CV to identify the important emission lines (e.g., of the O and Ne elements) of one targeted CV for further investigation. A total sample of 30 bright CVs in the solar neighborhood requires 30 snapshots with a total exposure of 1.4×10^6 s (16 days).

With the large effective area and high spectral resolution, *HUBS* can greatly improve our understanding of the accretion process in CVs.

4.3.3 Stars

Stars located across almost all regions of a Hertzsprung-Russell diagram have been identified as X-ray sources, although with different mechanisms. Stellar magnetic corona is the predominant origin of X-rays for late-type stars, while for massive and hot stars, the X-ray emission is from shocks forming in unstable winds. The X-ray radiation of pre-main sequence stars may originate both in hot coronal plasma or shocks [379].

The stellar magnetic activity provides substantial information on the magnetic dynamo and the coronal heating process. It is also of great value for exploring the interaction between stars and their planets and determining the habitable zone of different stars [379, 380]. Stellar magnetic activity is ubiquitous in late-type stars, which can be traced by various proxies, including spots and flares from the photosphere, emission lines from the chromosphere, and X-ray and radio emissions from the corona. The activity level strongly depends on stellar parameters (e.g., stellar mass, age).

X-ray astronomy has played a key role in stellar activity studies. The X-ray luminosity of active stars in the quiet state ranges from 10^{27} to 10^{31} erg s⁻¹, while it is 1–2 orders of magnitude brighter during flares [379, 381, 382]. It helps establish the famous activity-rotation relation (e.g., [383, 384]). In the relation, the X-ray activity is described as the ratio between X-ray luminosity and bolometric luminosity, while the Rossby number is used to trace stellar rotation, which is defined as the ratio of the rotation period to the convective turnover time. The relation is usually suggested to consist of two distinct sequences: the saturated region for rapidly rotating stars, in which the activity level keeps constant, and the power-law decay region for slowly rotating stars, where the activity level is rotation-dependent [384].

X-ray spectral observations have yielded a typical temperature of about 0.1–1 keV for the stellar corona, belonging to the soft X-ray band. Previous studies using the low-resolution spectra (e.g., *Chandra*/ACIS, *XMM-Newton*/MOS) have measured the coronal temperatures and discussed the distribution of differential emission measures (dEM) for some nearby active stars [385]. High-resolution X-ray spectroscopy, on the other hand, is mainly done with *Chandra*/HETG and *XMM-Newton*/RGS high-resolution spectrometers. By using the He-like and H-like lines from different elements (e.g., C, N, O), the distributions of some physical parameters (e.g., coronal temperature and density, dEM, metallicity) during quiet states and flares have been well constrained for dozens of stars [381]. High-resolution spectra of active stars revealed a new trend that runs opposite to the solar FIP effect, called the “inverse FIP (IFIP) effect” [386].

Although previous studies provide a number of surprising findings, there are many key issues unresolved. The standard picture of the activity-rotation relation has been challenged by recent studies, such as the variable activity level in the saturation region [387] and more sequences possibly divided in the relation [388]. It is also doubted that the distribution of coronal physical parameters is universal among stars due to the small and incomplete sample with high-resolution spectroscopic observations. For example, more than 900 F/G/K-type stars are located within 30 pc of the solar system [389],

but only about 40 ones were observed; most stars around the solar system are M-type dwarfs, but only a few were observed (e.g., Proxima Cen [390] and CN Leo [391]). More importantly, some basic physical questions including the mechanism of the saturation and the connection between the relation and magnetic dynamo are poorly understood. A large sample covering different types of stars, with well-measured activities and spectral parameters, can help investigate the physical properties of the stellar magnetic dynamo and provide potential diagnostics of heating mechanisms.

HUBS can help establish a large high-resolution X-ray spectral sample for stars with different spectral types, rotation periods, ages, and metallicities. For single stars, detailed diagnostics of the coronal temperature and density can be done with the emission lines from different elements. With further investigation of the dEM, the FIP and IFIP effects, and the area of the active region, a comparison with the Sun can help explore the flaring mechanism and heating process. On the other hand, by using the large sample, the distribution of these parameters and their relationships with different stellar parameters (e.g., mass, age, rotation) will help understand the structure and evolution of stars.

For typical active stars, an exposure of 100 ks by *HUBS* can obtain a spectrum with a sufficiently high signal-to-noise ratio for the following studies; for close stars, the exposure time can be reduced to around 10–30 ks. Therefore, the exposure time of 100 stars is about 10^3 to 10^4 ks. Taking Proxima Cen as an example, the simulation shows that *HUBS* can clearly distinguish emission lines in its spectrum (typical for M-type active stars) compared with *XMM-Newton*/RGS observations with an exposure time of ≈ 800 s.

With the large effective area and high spectral resolution, it can be predicted that *HUBS* will provide a valuable opportunity to advance stellar magnetic activity studies.

5 Exploiting the Capabilities of *HUBS*

As shown in previous sections, *HUBS* will observe various types of warm and hot plasmas across more than ten orders of magnitude in size, such as stellar coronae, supernova remnants, AGN winds, hot plasmas around individual galaxies and galaxy assemblies, and cosmic web filaments. Characteristic emission and absorption lines in the high-resolution X-ray spectra will enable us to measure various physical properties of these astrophysical plasmas, including but not limited to temperature, density, elemental abundances, and kinematics [18,392,393]. These fundamental parameters are essential to fill the gaps in our understanding of the role of warm and hot plasmas in the formation and evolution of the hot Universe. These astrophysical plasmas, play an important role in

the galactic ecosystem [3, 7, 14, 15, 394–396].

As we have experienced with the era of diffractive grating spectrometers aboard *XMM-Newton* and *Chandra* [397–399], the next-generation high-resolution X-ray spectroscopy will offer both an opportunity and a challenge. On one hand, they will greatly advance our knowledge of the Universe more than what we have learned from *XMM-Newton* and *Chandra*. On the other hand, they will also challenge us on how to quantify key observables precisely and efficiently. To better prepare us for the upcoming new era, we need to improve the status quo in the following three aspects: atomic data, plasma models, and spectral analysis techniques.

5.1 Atomic data

Various types of microscopic atomic processes give rise to continuum and line features in the observed spectra. Generally speaking, the interactions between electrons, ions, and photons can be divided into collision, ionization, and recombination [400]. Each category can be further divided into several sub-classes. For instance, radiative, di-electronic, and multi-electron recombination all contribute to the continuum and line emission in the observed spectrum. Even if we are limited to the simplest radiative recombination rates of H- to Na-like ions with $Z \leq 30$, there are 3×10^4 levels to consider [401]. Each level-resolved rate is provided either on a few temperature grids or described with a few parameters [401]. The entire atomic database can easily grow to a significant size.

The associated large amount of atomic data is the building block of astrophysical plasma codes widely used in the community: APEC [402, 403]/ACX [404]/NEI [405], CHIANTI [406, 407], Cloudy [408, 409], SPEX [410, 411], SASAL [412, 413] and XSTAR [414, 415]. Caution that the underlying atomic databases are not perfect (e.g., [416, 417]). Continuous developments including both theoretical calculations and lab measurements are required [418–420].

In 2016, we had a test of the next generation of high-resolution X-ray spectroscopy with *Hitomi* [421]. While the statistical uncertainty of the observed spectrum is less than 1%, the Fe abundance measured with APEC and SPEX differ by 16% [422]. This is mostly attributed to the different atomic data used by these two plasma models [422]. The Fe abundance is measured from H- and He-like lines, but their transition rates (i.e., A-values) and electron-impact excitation rates can differ up to 40% [422]. That is to say, the accuracy of the atomic data is not adequately converged to match the accuracy of the observed data.

When the mysterious 3.5 keV line was in the spotlight [423, 424], it was unclear whether natural atomic processes like di-electronic recombination and charge exchange pro-

cess can account for this instead of the dark matter decay process. This was largely due to the incompleteness of the atomic database. New theoretical calculations and lab measurements were then pursued to quantify the role of these two recombination processes [425-428]. Ar xvii di-electronic recombination line is at 3.62 keV, while the S xvi charge exchange recombination line is at 3.47 ± 0.06 keV. Due to insufficient energy resolution of CCD instruments, the line center of the 3.5 keV line is not tightly constrained: 3.57 ± 0.02 keV by [423] and 3.52 ± 0.02 keV by [424]. On the other hand, while the 3.5 keV line is found in some mega-second CCD observations, it is absent in the ~ 300 ks microcalorimeter (Hitomi/SXS) observation. Deeper microcalorimeter observations with fine energy resolution (e.g. HUBS) are certainly required.

5.2 Plasma diagnostics

Plasma diagnostics play a crucial role when interpreting characteristic continuum and line features in the observed high-resolution spectra. Fundamental physical properties of the observing target are measured by matching the data and model.

In the 0.1 – 2 keV soft X-ray bandpass covered by *HUBS*, H-like Lyman series and He-like triplets are the most prominent emission line features. In a low-density CIE plasma, such as the majority of hot gas in individual galaxies and galaxy assemblies, the Ly α lines should have the highest intensity among the Lyman series. Ly α might be optically thick in some astrophysical environments so that the intensity of Ly α will be reduced by resonance scattering (a fraction of Ly α photons are scattered out of our line-of-sight). Other Lyman series lines with smaller oscillator strength suffer less from this issue, leading to larger ratios of Ly β /Ly α , Ly γ /Ly α , and Ly δ /Ly α . Furthermore, at the interface between the hot plasma and cold media (e.g., comets), the charge-exchange process can selectively increase the intensity of e.g., Ly γ or Ly δ [426].

The He-like triplet consists of the resonance (w), intercombination (x and y), and forbidden (z) lines. The line ratio among the three is rather sensitive to a wide range of plasma temperature, density, and the astrophysical environment of the plasma [393]. In a CIE plasma, the $G = (x+y+z)/w$ ratio decreases with an increasing plasma temperature, while the $R = z/(x+y)$ ratio decreases with an increasing plasma density [393]. In photoionized plasmas (e.g., the X-ray narrow line region of AGN), the external radiation field can boost both the G - and R -ratios [393, 429]. The charge exchange process can also increase the G -ratio [426, 430, 431]. The optical depth effect also applies to He-like resonance lines as well [432-435].

Apart from H- and He-like lines, the Fe-L complex is also prominent [436-441]. These $n \geq 3$ to $n = 2$ (i.e. L-shell) transitions of Fe xvii to Fe xxiv are susceptible to a wide range of atomic processes: direct and resonance excitation, radiative and di-electronic recombination, inner-shell ionization. Consequently, they are notorious for spectral modeling. The line ratios among the Fe xvii 15.01 Å (3C), 15.26 Å (3D), 17.05 Å (3G), and 17.09 Å (M2) lines have been the hot topic for both theoretical calculations and lab measurements for decades [442-451].

Thanks to the fine energy resolution and large effective area of *HUBS* (Figure 1), some weak line diagnostics become possible and effective. The width of radiative recombination continua (RRC) is an effective measure of plasma temperature. These RRC can be found in the hot recombining plasma of supernova remnants [452, 453] or warm photoionized gas of X-ray binary [454] or AGN [455, 456]. Di-electronic recombination satellite lines of He-like ions can effectively verify the presence of non-Maxwellian electrons, such as those supra-thermal electrons behind the shock of merging galaxy clusters [457]. Meta-stable absorption lines of Be-like to F-like ions can probe a wide range of number density for AGN winds [18].

All these diagnostics have been implemented in the astrophysical plasma codes widely used for X-ray spectral analysis: APEC/ACX/NEI, CHIANTI, Cloudy, SPEX, and XSTAR. Continuous developments of these plasma codes are still required. For instance, pre-calculated charge-state distribution tables [458, 459] are not applicable to high-density plasma [460, 461]. Self-consistent charge-state distribution calculations involving excitation, recombination, and ionization from and to meta-stable levels are required. Radiation transfer for the high-density plasma is also required. On one hand, this calls for a large amount of atomic data that is not yet available. On the other hand, as the complexity grows, computational efficiency needs to be improved.

5.2.1 Laboratory benchmark required by *HUBS*

Plasma diagnostics for various objects are strongly dependent on the above-listed models, including SPEX/CX [426] and ACX [404] for charge-exchange emissions in SWCX foreground and SNRs. However, these two models are not perfect. To obtain high-resolution spectra, both models use some approximations to redistribute total or n - or nl -resolved cross-sections. For the n -resolved cross-section, limited experimental data are available in collisions with different neutrals at some energies [462]. For the nl -resolved cross-section, only theoretical calculations are available while experiments are lacking. In the high-resolution spectra obtained with *HUBS* ($\Delta E \leq 2$ eV), most of the lines are fine-structure

levels (nLJ) resolved. However, the present CX models including ACX and SPEX-CX, have rather large uncertainties [463]. This calls for the laboratory benchmark of the CX model.

By comparison of the resultant spectra from both the experimental and theoretical cross-sections, the accuracy of the CX model will be examined at given collision energies. In some cases, CX high-resolution spectrum can be measured directly in the laboratory, which can be used to fit the *HUBS* observation. Besides the charge-exchange data, laboratory measurements on other atomic data including ionization, dielectronic/radiative recombination, excitation as well as spectra, will improve our interpretation of the *HUBS* observations.

In turn, the *HUBS* spectroscopy will prompt the progress of the collision theories in atomic physics, including the nl -resolved charge-exchange cross-section. Generally, the n -resolved CX cross-sections can be obtained in a heavy ion source by the cold target recoil ion momentum spectroscopy (COLTRIM) apparatus with the electron energy resolution of ~ 10 eV [462]. The nl -resolved cross-section of He-like captured ions has never been obtained by experiments. For the collision of O^{7+} with H, the dominant capture channel by O^{7+} projectile of the bound electron from the H donor is $n = 4$ captured ion states by accurate close-coupling calculations. The radiative decay rates of the dipole transitions of O VII have an accuracy of $\leq 5\%$. The O VII resonance, intercombination, and forbidden lines at the rest-frame energy of 561 eV, 569 eV, and 574 eV are well resolved in the *HUBS* observation. The observed data can be used to determine the l -distribution in the $n = 4$ channel with an accuracy better than 10% by an iterative algorithm.

In summary, the *HUBS* spectroscopy with high resolution requires laboratory measurements to benchmark the CX model, it also gives some constraints for the nl -distribution of the cross-sections measured in the laboratory. Both of them complement each other.

5.3 Spectral analysis techniques

With diffractive grating spectrometers, we typically obtain one high-resolution X-ray spectrum for each observation. It might take weeks or months for experts to finish a thorough spectral analysis. With X-ray integral field units like those on *HUBS*, we might get up to thousands of high-resolution X-ray spectra in one single observation. We need to quantify key observables precisely and efficiently with limited manpower and computation resources.

For observations targeting point-like sources, an efficient and automated line detection algorithm without any prior knowledge of the targets is required as the first step [429]. If the spectrum is not featureless, we need to identify these lines

and extract preliminary information such as the line center, velocity shift, line broadening, equivalent width, and plasma types according to the intensities of characteristic lines. This might call for a machine-learning approach. For observations targeting extended sources, imaging spectroscopic approaches including but not limited to Weighted Voronoi Tessellations [464] and smoothed particle inference [465] are to be pursued to get a comprehensive and self-consistent view of the observing target.

6 Status of *HUBS*

The *HUBS* project is being funded by the *China National Space Administration* for key technology development (which corresponds roughly to Phase A, in terms of NASA project cycles). The critical technologies identified include superconducting microcalorimeter (detector), wide field-of-view X-ray focusing optics (telescope), multiplexing signal readout electronics, mechanical cooler and adiabatic demagnetization refrigerator. The goal is to advance the technical readiness levels (TRLs) of those technologies sufficiently by the end of 2023, before the project can enter the next phase. Looking ahead, the important milestones will include the completion of technology development and payload design, the construction of the *HUBS* satellite, and the launch and operation of the satellite (around 2030 and beyond).

Mock observations have been made to assess the scientific capabilities of *HUBS* and also to help formulate observing strategies [130]. The results suggest that CGM studies require deep exposures on carefully-selected targets, while group or cluster observations are likely quite efficient at low redshifts, thanks to the large field of view. For IGM studies, on the other hand, medium-exposure mosaic observations will be necessary to acquire sufficient spatial coverage, so the total exposure time is also expected to be long for each selected field. It is, therefore, clear that target selection is critical to the success of *HUBS*. Discussion is ongoing on the scientific values (vs resource investment) of an all-sky survey in the extended mission period.

7 Summary

The *Hot Universe Baryon Surveyor* mission aims at studying the hot gas in the universe with unprecedented sensitivity and spatial resolution in X-rays. Among the core sciences for which the *HUBS* is tailored, the feedback in the galactic ecosystem and the cosmic baryon budget are of particular importance. The *HUBS* will provide a unique opportunity to study the hot gas in the ISM, the CGM and the ICM by re-

solving the X-ray spectrum in both emission and absorption, from which the spatial distribution and the kinematics of the hot gas can be confidently obtained. Since the thermal and kinematic status of the hot gas is closely related to the star formation and the AGN activity, the *HUBS* mission will be a huge leap forward in our understanding of galaxy formation and evolution. Moreover, with its high sensitivity and large field of view, the *HUBS* is highly capable of searching for multi-phase hot gas in galaxy groups, clusters and the cosmic web, which will pave the way for the future study of the cosmic baryon budget.

The *HUBS* may also extend its application to other X-ray-related observatory sciences. For instance, *HUBS* will be able to directly constrain the gas number densities and opening angles of the AGN-driven outflows. The *HUBS* can also probe the nearest X-ray sources within our Galaxy, such as cosmic X-ray background, supernova remnants, activities of stars and compact objects, and the emission from the Solar system.

The capability of the *HUBS* can be exploited further by renovating the knowledge of atomic data, plasma models and the techniques of spectral analysis. The laboratory measurements on atomic data will be used to benchmark the CX model and to improve the interpretation of the *HUBS* observations. In addition, since the *HUBS* will be able to obtain thousands of high-resolution X-ray spectra in one single observation, the spectral analysis techniques will be developed to quantify key observables precisely and efficiently with limited manpower and computation resources.

A staged construction plan has been carefully designed for the *HUBS* mission. With the support from the *China National Space Administration* for key technology development, a number of critical technologies have been identified, and the current goal is to sufficiently enhance the technical readiness levels of those technologies by the end of 2023 before entering the next phase. Besides, mock observations have also been developed to test the feasibility of observing targets and strategies.

As we celebrate the 60th anniversary of X-ray astronomy, the field is about to enter a new era, in which spatially-resolved, high-resolution spectroscopy is expected to become increasingly exquisite and routine, thanks to the advancement of new detector technologies. The imminent launch of *XRISM* [466] is highly anticipated, as the first mission employing microcalorimeters for spectroscopy observations. The scientific potential of such a spectrometer has been well illustrated by sounding-rocket experiment [467] and the *Hitomi* satellite mission [421], so breakthroughs are expected of *XRISM*, especially in the studies of ICM and AGN, as it is optimized to detect emission lines at higher energies than *HUBS*. With the new generation of microcalorimeters,

HUBS, as well as *Athena* [468], will not only provide higher spectral resolution, but significantly improve the detection sensitivity at energies where the emission lines associated with hot CGM/IGM are expected to lie and thus provide new avenues to exploring baryonic processes in the cosmos. These improvements are expected to significantly advance our understanding of many important astrophysical fields, as we have stated in detail in the present paper.

This work is supported by the National Natural Science Foundation of China (Grant Nos. 11721303, 11821303, 11825303, 11873029, 11890693, 11973033, 11991052, 12025303, 12033004, 12041301, 12121003, 12133008, 12173018, 12192220, 12192223, 12221003, 12233001, 12233005, 12273010, 12273030, 12273057, 122011540375, U1931140), the China Manned Space Project (Grant Nos. CMS-CSST-2021-A04, CMS-CSST-2021-A06, CMS-CSST-2021-A10, CMS-CSST-2021-B02), the Ministry of Science and Technology of China through its National Key R&D Program (Grant No. 2018YFA0404502), the National SKA Program of China (Grant No. 2020SKA0120300), the National Key Research and Development Program of China (Grant No. 2022YFA1602903), the Outstanding Young and Middle-aged Science and Technology Innovation Teams from Hubei colleges and universities (Grant No. T2021026), the Young Top-notch Talent Cultivation Program of Hubei Province, the National Science Foundation (Grant Nos. AST-2107735 and AST-2219686), and NASA (Grant No. 80NSSC22K0668). Mr. Yongkai Zhu (Shanghai Jiao Tong University) provided useful comments on the manuscript.

Author contributions This paper was organized and structured by Wei Cui and Feng Yuan, and was primarily contributed by each author as follows: §1 (Wei Cui, Suoqing Ji, Feng Yuan), §2.1 (Suoqing Ji, Junjie Mao, Feng Yuan), §2.2 (Hui Li, Miao Li), §2.3 (Suoqing Ji, Jiangtao Li, Miao Li), §2.4 (Suoqing Ji), §2.5 (Jiangtao Li), §3.1 (Dandan Xu, Haiguang Xu), §3.2 (Dandan Xu), §3.3 (Zhongli Zhang, Haiguang Xu), §4.1 (Guiyun Liang, Wenhao Liu, Zhijie Qu, Hang Yang, Shuinai Zhang), §4.2 (Lei Sun, Ping Zhou, Yang Chen), §4.3 (Zhaosheng Li, Song Wang, Xiaojie Xu), §5.1 (Junjie Mao), §5.2 (Guiyun Liang, Junjie Mao), §5.3 (Junjie Mao, Ping Zhou, Shuinai Zhang), §6 (Wei Cui), and §7 (Wei Cui, Suoqing Ji). All authors critically reviewed and made contributions to the manuscript.

Conflict of interest The authors declare that they have no conflict of interest.

- 1 Martin J Rees and JP Ostriker. Cooling, dynamics and fragmentation of massive gas clouds: clues to the masses and radii of galaxies and clusters. *Monthly Notices of the Royal Astronomical Society*, 179(4):541–559, 1977.
- 2 Thorsten Naab and Jeremiah P. Ostriker. Theoretical Challenges in Galaxy Formation. *Annual Review of Astronomy and Astrophysics*, 55:59–109, 2017.
- 3 Claude-Andre Faucher-Giguere and S. Peng Oh. Key Physical Processes in the Circumgalactic Medium. *arXiv e-prints*, page arXiv:2301.10253, January 2023.
- 4 W. Cui, L. B. Chen, B. Gao, F. L. Guo, H. Jin, G. L. Wang, L. Wang, J. J. Wang, W. Wang, Z. S. Wang, Z. Wang, F. Yuan, and W. Zhang. *HUBS*: Hot Universe Baryon Surveyor. *Journal of Low Temperature Physics*, 199:502, 2020.
- 5 W. Cui, J. N. Bregman, M. P. Bruijn, L. B. Chen, Y. Chen, C. Cui, T. T. Fang, B. Gao, H. Gao, J. R. Gao, L. Gottardi, K. X. Gu, F. L. Guo, J. Guo, C. L. He, P. F. He, J. W. den Herder, Q. S. Huang, F. J. Li, J. T. Li, J. J. Li, L. Y. Li, T. P. Li, W. B. Li, J. T. Liang, Y. J. Liang, G. Y. Liang, Y. J. Liu, Z. Liu, Z. Y. Liu, F. Jaekel, L. Ji, W. Ji, H. Jin, X. Kang, Y. X. Ma, D. McCammon, H. J. Mo, K. Nagayoshi, K. Nelms, R. Qi, J. Quan, M. L. Ridder, Z. X. Shen, A. Simionescu,

- E. Taralli, Q. D. Wang, G. L. Wang, J. J. Wang, K. Wang, L. Wang, S. F. Wang, S. J. Wang, T. G. Wang, W. Wang, X. Q. Wang, Y. L. Wang, Y. R. Wang, Z. Wang, Z. S. Wang, N. Y. Wen, M. de Wit, S. F. Wu, D. Xu, D. D. Xu, H. G. Xu, X. J. Xu, R. X. Xu, Y. Q. Xue, S. Z. Yi, J. Yu, L. W. Yang, F. Yuan, S. Zhang, W. Zhang, Z. Zhang, Q. Zhong, Y. Zhou, and W. X. Zhu. HUBS: a dedicated hot circumgalactic medium explorer. In *Society of Photo-Optical Instrumentation Engineers (SPIE) Conference Series*, volume 11444 of *Society of Photo-Optical Instrumentation Engineers (SPIE) Conference Series*, page 114442S, December 2020.
- 6 Ya-Ping Li, Feng Yuan, Houjun Mo, Doosoo Yoon, Zhaoming Gan, Luis C. Ho, Bo Wang, Jeremiah P. Ostriker, and Luca Ciotti. Stellar and AGN Feedback in Isolated Early-type Galaxies: The Role in Regulating Star Formation and ISM Properties. *ApJ*, 866(1):70, October 2018.
- 7 Jason Tumlinson, Molly S. Peeples, and Jessica K. Werk. The Circumgalactic Medium. *ARA&A*, 55(1):389–432, August 2017.
- 8 Committee for a Decadal Survey on Astronomy and Astrophysics 2020 (Astro2020). Pathways to Discovery in Astronomy and Astrophysics for the 2020s. *Consensus Study Report. National Academies of Sciences, Engineering, and Medicine*, 2021.
- 9 Hagai Netzer. Revisiting the Unified Model of Active Galactic Nuclei. *ARA&A*, 53:365–408, August 2015.
- 10 John Magorrian, Scott Tremaine, Douglas Richstone, Ralf Bender, Gary Bower, Alan Dressler, S. M. Faber, Karl Gebhardt, Richard Green, Carl Grillmair, John Kormendy, and Tod Lauer. The Demography of Massive Dark Objects in Galaxy Centers. *AJ*, 115(6):2285–2305, June 1998.
- 11 Laura Ferrarese and David Merritt. A Fundamental Relation between Supermassive Black Holes and Their Host Galaxies. *ApJ*, 539(1):L9–L12, August 2000.
- 12 A. C. Fabian. Observational Evidence of Active Galactic Nuclei Feedback. *ARA&A*, 50:455–489, September 2012.
- 13 John Kormendy and Luis C. Ho. Coevolution (Or Not) of Supermassive Black Holes and Host Galaxies. *ARA&A*, 51(1):511–653, August 2013.
- 14 Sibasish Laha, Christopher S. Reynolds, James Reeves, Gerard Kriss, Matteo Guainazzi, Randall Smith, Sylvain Veilleux, and Daniel Proga. Ionized outflows from active galactic nuclei as the essential elements of feedback. *Nature Astronomy*, 5:13–24, January 2021.
- 15 D. Michael Crenshaw, Steven B. Kraemer, and Ian M. George. Mass Loss from the Nuclei of Active Galaxies. *ARA&A*, 41:117–167, January 2003.
- 16 E. Costantini, J. S. Kaastra, N. Arav, G. A. Kriss, K. C. Steenbrugge, J. R. Gabel, F. Verbunt, E. Behar, C. M. Gaskell, K. T. Korista, D. Proga, J. Kim Quijano, J. E. Scott, E. S. Klimek, and C. H. Hedrick. X-ray/ultraviolet observing campaign of the Markarian 279 active galactic nucleus outflow: a close look at the absorbing/emitting gas with Chandra-LETGS. *A&A*, 461(1):121–134, January 2007.
- 17 J. S. Kaastra, C. P. de Vries, K. C. Steenbrugge, R. G. Detmers, J. Ebrero, E. Behar, S. Bianchi, E. Costantini, G. A. Kriss, M. Mehdipour, S. Paltani, P. O. Petrucci, C. Pinto, and G. Ponti. Multiwavelength campaign on Mrk 509. II. Analysis of high-quality Reflection Grating Spectrometer spectra. *A&A*, 534:A37, October 2011.
- 18 Junjie Mao, J. S. Kaastra, M. Mehdipour, A. J. J. Raassen, Liyi Gu, and J. M. Miller. Density diagnostics of ionized outflows in active galactic nuclei. X-ray and UV absorption lines from metastable levels in Be-like to C-like ions. *A&A*, 607:A100, November 2017.
- 19 M. Mehdipour, J. S. Kaastra, E. Costantini, E. Behar, G. A. Kriss, S. Bianchi, G. Branduardi-Raymont, M. Cappi, J. Ebrero, L. Di Gesu, S. Kaspi, J. Mao, B. De Marco, R. Middei, U. Peretz, P. O. Petrucci, G. Ponti, and F. Ursini. Multi-wavelength campaign on NGC 7469. III. Spectral energy distribution and the AGN wind photoionisation modelling, plus detection of diffuse X-rays from the starburst with Chandra HETGS. *A&A*, 615:A72, July 2018.
- 20 Junjie Mao, M. Mehdipour, J. S. Kaastra, E. Costantini, C. Pinto, G. Branduardi-Raymont, E. Behar, U. Peretz, S. Bianchi, G. A. Kriss, G. Ponti, B. De Marco, P. O. Petrucci, L. Di Gesu, R. Middei, J. Ebrero, and N. Arav. Photoionized emission and absorption features in the high-resolution X-ray spectra of NGC 3783. *A&A*, 621:A99, January 2019.
- 21 Yijun Wang, Jelle Kaastra, Missagh Mehdipour, Junjie Mao, Elisa Costantini, Gerard A. Kriss, Ciro Pinto, Gabriele Ponti, Ehud Behar, Stefano Bianchi, Graziella Branduardi-Raymont, Barbara De Marco, Sam Grafton-Waters, Pierre-Olivier Petrucci, Jacobo Ebrero, Dominic James Walton, Shai Kaspi, Yongquan Xue, Stéphane Paltani, Laura di Gesu, and Zhicheng He. Transient obscuration event captured in NGC 3227. II. Warm absorbers and obscuration events in archival XMM-Newton and NuSTAR observations. *A&A*, 657:A77, January 2022.
- 22 J. N. Reeves, P. T. O'Brien, and M. J. Ward. A Massive X-Ray Outflow from the Quasar PDS 456. *ApJ*, 593(2):L65–L68, August 2003.
- 23 F. Tombesi, M. Cappi, J. N. Reeves, G. G. C. Palumbo, T. Yaqoob, V. Braitto, and M. Dadina. Evidence for ultra-fast outflows in radio-quiet AGNs. I. Detection and statistical incidence of Fe K-shell absorption lines. *A&A*, 521:A57, October 2010.
- 24 E. Nardini, J. N. Reeves, J. Gofford, F. A. Harrison, G. Risaliti, V. Braitto, M. T. Costa, G. A. Matzeu, D. J. Walton, E. Behar, S. E. Boggs, F. E. Christensen, W. W. Craig, C. J. Hailey, G. Matt, J. M. Miller, P. T. O'Brien, D. Stern, T. J. Turner, and M. J. Ward. Black hole feedback in the luminous quasar PDS 456. *Science*, 347(6224):860–863, February 2015.
- 25 F. Tombesi, M. Meléndez, S. Veilleux, J. N. Reeves, E. González-Alfonso, and C. S. Reynolds. Wind from the black-hole accretion disk driving a molecular outflow in an active galaxy. *Nature*, 519(7544):436–438, March 2015.
- 26 Michael L. Parker, Ciro Pinto, Andrew C. Fabian, Anne Lohfink, Douglas J. K. Buisson, William N. Alston, Erin Kara, Edward M. Cackett, Chia-Ying Chiang, Thomas Dauser, Barbara De Marco, Luigi C. Gallo, Javier Garcia, Fiona A. Harrison, Ashley L. King, Matthew J. Middleton, Jon M. Miller, Giovanni Miniutti, Christopher S. Reynolds, Phil Uttley, Ranjan Vasudevan, Dominic J. Walton, Daniel R. Wilkins, and Abderahmen Zoghbi. The response of relativistic outflowing gas to the inner accretion disk of a black hole. *Nature*, 543(7643):83–86, March 2017.
- 27 J. S. Kaastra, G. A. Kriss, M. Cappi, M. Mehdipour, P. O. Petrucci, K. C. Steenbrugge, N. Arav, E. Behar, S. Bianchi, R. Boissay, G. Branduardi-Raymont, C. Chamberlain, E. Costantini, J. C. Ely, J. Ebrero, L. Di Gesu, F. A. Harrison, S. Kaspi, J. Malzac, B. De Marco, G. Matt, K. Nandra, S. Paltani, R. Person, B. M. Peterson, C. Pinto, G. Ponti, F. Pozo Nuñez, A. De Rosa, H. Seta, F. Ursini, C. P. de Vries, D. J. Walton, and M. Whewell. A fast and long-lived outflow from the supermassive black hole in NGC 5548. *Science*, 345(6192):64–68, July 2014.
- 28 J. Ebrero, G. A. Kriss, J. S. Kaastra, and J. C. Ely. Discovery of a fast, broad, transient outflow in NGC 985. *A&A*, 586:A72, February 2016.
- 29 M. Mehdipour, J. S. Kaastra, G. A. Kriss, N. Arav, E. Behar, S. Bianchi, G. Branduardi-Raymont, M. Cappi, E. Costantini, J. Ebrero, L. Di Gesu, S. Kaspi, J. Mao, B. De Marco, G. Matt, S. Paltani, U. Peretz, B. M. Peterson, P. O. Petrucci, C. Pinto, G. Ponti, F. Ursini, C. P. de Vries, and D. J. Walton. Chasing obscuration in type-I AGN: discovery of an eclipsing clumpy wind at the outer broad-line region of NGC 3783. *A&A*, 607:A28, October 2017.
- 30 Anna Lia Longinotti, Gerard Kriss, Yair Krongold, Karla Z. Arellano-Cordova, S. Komossa, Luigi Gallo, Dirk Grupe, Smita Mathur, Michael L. Parker, Anil Pradhan, and Dan Wilkins. The XMM-Newton/HST View of the Obscuring Outflow in the Seyfert Galaxy Mrk 335 Observed at Extremely Low X-Ray Flux. *ApJ*, 875(2):150,

- April 2019.
- 31 Erin Kara, Missagh Mehdipour, Gerard A. Kriss, Edward M. Cackett, Nahum Arav, Aaron J. Barth, Doyee Byun, Michael S. Brotherton, Gisella De Rosa, Jonathan Gelbord, Juan V. Hernández Santisteban, Chen Hu, Jelle Kaastra, Hermine Landt, Yan-Rong Li, Jake A. Miller, John Montano, Ethan Partington, Jesús Aceituno, Jin-Ming Bai, Dongwei Bao, Misty C. Bentz, Thomas G. Brink, Doron Chelouche, Yong-Jie Chen, Encarni Romero Colmenero, Elena Dalla Bontà, Maryam Dehghanian, Pu Du, Rick Edelson, Gary J. Ferland, Laura Ferrarese, Carina Fian, Alexei V. Filippenko, Travis Fischer, Michael R. Goad, Diego H. González Buitrago, Varoujan Gorjian, Catherine J. Grier, Wei-Jian Guo, Patrick B. Hall, Luis C. Ho, Y. Homayouni, Keith Horne, Dragana Ilić, Bo-Wei Jiang, Michael D. Joner, Shai Kaspi, Christopher S. Kochanek, Kirk T. Korista, Daniel Kynoch, Sha-Sha Li, Jun-Rong Liu, Ian M. McHardy, Jacob N. McLane, Jake A. J. Mitchell, Hagai Netzer, Kianna A. Olson, Richard W. Pogge, Luka Č. Popović, Daniel Proga, Thaisa Storchi-Bergmann, Erika Strasburger, Tommaso Treu, Marianne Vestergaard, Jian-Min Wang, Martin J. Ward, Tim Waters, Peter R. Williams, Sen Yang, Zhu-Heng Yao, Theodora E. Zastrocky, Shuo Zhai, and Ying Zu. AGN STORM 2. I. First results: A Change in the Weather of Mrk 817. *ApJ*, 922(2):151, December 2021.
 - 32 Junjie Mao, G. A. Kriss, H. Landt, M. Mehdipour, J. S. Kaastra, J. M. Miller, D. Stern, L. C. Gallo, A. G. Gonzalez, J. J. Simon, S. G. Djorgovski, S. Anand, Mansi M. Kasliwal, and V. Karambelkar. Multi-wavelength Observations of the Obscuring Wind in the Radio-quiet Quasar MR 2251-178. *ApJ*, 940(1):41, November 2022.
 - 33 C. S. Reynolds. An X-ray spectral study of 24 type 1 active galactic nuclei. *MNRAS*, 286(3):513–537, April 1997.
 - 34 B. McKernan, T. Yaqoob, and C. S. Reynolds. A soft X-ray study of type I active galactic nuclei observed with Chandra high-energy transmission grating spectrometer. *MNRAS*, 379(4):1359–1372, August 2007.
 - 35 Sibasish Laha, Matteo Guainazzi, Gulab C. Dewangan, Susmita Chakravorty, and Ajit K. Kembhavi. Warm absorbers in X-rays (WAX), a comprehensive high-resolution grating spectral study of a sample of Seyfert galaxies - I. A global view and frequency of occurrence of warm absorbers. *MNRAS*, 441(3):2613–2643, July 2014.
 - 36 Ashley L. King, Jon M. Miller, and John Raymond. Warm Absorbers and Outflows in the Seyfert-1 Galaxy NGC 4051. *ApJ*, 746(1):2, February 2012.
 - 37 A. Ogorzalek, A. L. King, S. W. Allen, J. C. Raymond, and D. R. Wilkins. A deep, multi-epoch Chandra HETG study of the ionized outflow from NGC 4051. *MNRAS*, 516(4):5027–5051, November 2022.
 - 38 J. M. Miller, J. Raymond, C. S. Reynolds, A. C. Fabian, T. R. Kallman, and J. Homan. The Accretion Disk Wind in the Black Hole GRO J1655-40. *ApJ*, 680(2):1359–1377, June 2008.
 - 39 Ryota Tomaru, Chris Done, and Junjie Mao. What powers the wind from the black hole accretion disc in GRO J1655-40? *MNRAS*, 518(2):1789–1801, January 2023.
 - 40 J. S. Kaastra, A. J. J. Raassen, R. Mewe, N. Arav, E. Behar, E. Costantini, J. R. Gabel, G. A. Kriss, D. Proga, M. Sako, and K. C. Steenbrugge. X-ray/UV campaign on the Mrk 279 outflow: Density diagnostics in Active Galactic Nuclei using O V K-shell absorption lines. *A&A*, 428:57–66, December 2004.
 - 41 J. S. Kaastra, R. Mewe, D. A. Liedahl, S. Komossa, and A. C. Brinkman. X-ray absorption lines in the Seyfert I galaxy NGC 5548 discovered with Chandra-LETGS. *A&A*, 354:L83–L86, February 2000.
 - 42 Shai Kaspi, W. N. Brandt, Hagai Netzer, Rita Sambruna, George Chartas, Gordon P. Garmire, and John A. Nousek. Discovery of Narrow X-Ray Absorption Lines from NGC 3783 with the Chandra High Energy Transmission Grating Spectrometer. *ApJ*, 535(1):L17–L20, May 2000.
 - 43 J. S. Kaastra, R. G. Detmers, M. Mehdipour, N. Arav, E. Behar, S. Bianchi, G. Branduardi-Raymont, M. Cappi, E. Costantini, J. Ebrero, G. A. Kriss, S. Paltani, P. O. Petrucci, C. Pinto, G. Ponti, K. C. Steenbrugge, and C. P. de Vries. Multiwavelength campaign on Mrk 509. VIII. Location of the X-ray absorber. *A&A*, 539:A117, March 2012.
 - 44 C. V. Silva, P. Uttley, and E. Costantini. Timing the warm absorber in NGC 4051. *A&A*, 596:A79, December 2016.
 - 45 A. Juránová, E. Costantini, and P. Uttley. Spectral-timing of AGN ionized outflows with Athena. *MNRAS*, 510(3):4225–4235, March 2022.
 - 46 Daniele Rogantini, Missagh Mehdipour, Jelle Kaastra, Elisa Costantini, Anna Juránová, and Erin Kara. TPHO: A Time-dependent Photoionization Model for AGN Outflows. *ApJ*, 940(2):122, December 2022.
 - 47 Luigi C. Gallo, Adam G. Gonzalez, and Jon M. Miller. Eclipsing the X-Ray Emitting Region in the Active Galaxy NGC 6814. *ApJ*, 908(2):L33, February 2021.
 - 48 B. Luo, W. N. Brandt, Y. Q. Xue, B. Lehmer, D. M. Alexander, F. E. Bauer, F. Vito, G. Yang, A. R. Basu-Zych, A. Comastri, R. Gilli, Q. S. Gu, A. E. Hornschemeier, A. Koekemoer, T. Liu, V. Mainieri, M. Pao-lillo, P. Ranalli, P. Rosati, D. P. Schneider, O. Shemmer, I. Smail, M. Sun, P. Tozzi, C. Vignali, and J. X. Wang. The Chandra Deep Field-South Survey: 7 Ms Source Catalogs. *ApJS*, 228(1):2, January 2017.
 - 49 Y. Q. Xue. The Chandra deep fields: Lifting the veil on distant active galactic nuclei and X-ray emitting galaxies. *New Astron. Rev.*, 79:59–84, November 2017.
 - 50 F. Tombesi, M. Cappi, J. N. Reeves, R. S. Nemmen, V. Braito, M. Gaspari, and C. S. Reynolds. Unification of X-ray winds in Seyfert galaxies: from ultra-fast outflows to warm absorbers. *MNRAS*, 430(2):1102–1117, April 2013.
 - 51 F. Tombesi, F. Tazaki, R. F. Mushotzky, Y. Ueda, M. Cappi, J. Gofford, J. N. Reeves, and M. Guainazzi. Ultrafast outflows in radio-loud active galactic nuclei. *MNRAS*, 443(3):2154–2182, September 2014.
 - 52 K. A. Pounds, J. N. Reeves, A. R. King, K. L. Page, P. T. O'Brien, and M. J. L. Turner. A high-velocity ionized outflow and XUV photosphere in the narrow emission line quasar PG1211+143. *MNRAS*, 345(3):705–713, November 2003.
 - 53 A. Gupta, S. Mathur, Y. Krongold, and F. Nicastro. Discovery of Relativistic Outflow in the Seyfert Galaxy Ark 564. *ApJ*, 772(1):66, July 2013.
 - 54 A. L. Longinotti, Y. Krongold, M. Guainazzi, M. Giroletti, F. Panessa, E. Costantini, M. Santos-Lleo, and P. Rodríguez-Pascual. X-Ray High-resolution Spectroscopy Reveals Feedback in a Seyfert Galaxy from an Ultra-fast Wind with Complex Ionization and Velocity Structure. *ApJ*, 813(2):L39, November 2015.
 - 55 A. Gupta, S. Mathur, and Y. Krongold. Detection of High Velocity Outflows in the Seyfert 1 Galaxy Mrk 590. *ApJ*, 798(1):4, January 2015.
 - 56 J. N. Reeves, V. Braito, G. Chartas, F. Hamann, S. Laha, and E. Nardini. Resolving the Soft X-Ray Ultrafast Outflow in PDS 456. *ApJ*, 895(1):37, May 2020.
 - 57 G. A. Matzue, J. N. Reeves, V. Braito, E. Nardini, D. E. McLaughlin, A. P. Lobban, F. Tombesi, and M. T. Costa. Evidence for a radiatively driven disc-wind in PDS 456? *MNRAS*, 472(1):L15–L19, November 2017.
 - 58 Takuya Midooka, Misaki Mizumoto, and Ken Ebisawa. A novel “spectral-ratio model fitting” to resolve complicated AGN X-ray spectral variations. *arXiv e-prints*, page arXiv:2210.11746, October 2022.
 - 59 Huaqing Cheng, Weimin Yuan, He-Yang Liu, Alice A Breeveld, Chichuan Jin, and Bifang Liu. Modelling accretion disc emission with generalized temperature profile and its effect on agn spectral energy distribution. *Monthly Notices of the Royal Astronomical Society*,

- 487(3):3884–3903, 2019.
- 60 Oren Slone and Hagai Netzer. The effects of disc winds on the spectrum and black hole growth rate of active galactic nuclei. *MNRAS*, 426(1):656–664, October 2012.
- 61 Ya-Ping Li, Feng Yuan, and Xinyu Dai. Reconciling the quasar microlensing disc size problem with a wind model of active galactic nucleus. *MNRAS*, 483(2):2275–2281, February 2019.
- 62 Mouyuan Sun, Yongquan Xue, Jonathan R. Trump, and Wei-Min Gu. Winds can ‘blow up’ AGN accretion disc sizes. *MNRAS*, 482(2):2788–2794, January 2019.
- 63 Martin J. Rees. Tidal disruption of stars by black holes of 10^6 - 10^8 solar masses in nearby galaxies. *Nature*, 333(6173):523–528, June 1988.
- 64 James Guillochon, Haik Manukian, and Enrico Ramirez-Ruiz. PS1-10jh: The Disruption of a Main-sequence Star of Near-solar Composition. *ApJ*, 783(1):23, March 2014.
- 65 Lixin Dai, Jonathan C. McKinney, and M. Coleman Miller. Soft X-Ray Temperature Tidal Disruption Events from Stars on Deep Plunging Orbits. *ApJ*, 812(2):L39, October 2015.
- 66 Eric R. Coughlin and Mitchell C. Begelman. Hyperaccretion during Tidal Disruption Events: Weakly Bound Debris Envelopes and Jets. *ApJ*, 781(2):82, February 2014.
- 67 Yan-Fei Jiang, James M. Stone, and Shane W. Davis. A Global Three-dimensional Radiation Magneto-hydrodynamic Simulation of Super-Eddington Accretion Disks. *ApJ*, 796(2):106, December 2014.
- 68 Dacheng Lin, James Guillochon, S. Komossa, Enrico Ramirez-Ruiz, Jimmy A. Irwin, W. Peter Maksym, Dirk Grupe, Olivier Godet, Natalie A. Webb, Didier Barret, B. Ashley Zauderer, Pierre-Alain Duc, Eleazar R. Carrasco, and Stephen D. J. Gwyn. A likely decade-long sustained tidal disruption event. *Nature Astronomy*, 1:0033, February 2017.
- 69 E. Kara, L. Dai, C. S. Reynolds, and T. Kallman. Ultrafast outflow in tidal disruption event ASASSN-14li. *MNRAS*, 474(3):3593–3598, March 2018.
- 70 Jon M. Miller, Jelle S. Kaastra, M. Coleman Miller, Mark T. Reynolds, Gregory Brown, S. Bradley Cenko, Jeremy J. Drake, Suvi Gezari, James Guillochon, Kayhan Gultekin, Jimmy Irwin, Andrew Levan, Dipankar Maitra, W. Peter Maksym, Richard Mushotzky, Paul O’Brien, Frits Paerels, Jelle de Plaa, Enrico Ramirez-Ruiz, Tod Strohmayer, and Nial Tanvir. Flows of X-ray gas reveal the disruption of a star by a massive black hole. *Nature*, 526(7574):542–545, October 2015.
- 71 R. Saxton, S. Komossa, K. Auchettl, and P. G. Jonker. X-Ray Properties of TDEs. *Space Sci. Rev.*, 216(5):85, July 2020.
- 72 Feng Yuan and Ramesh Narayan. Hot Accretion Flows Around Black Holes. *Annual Review of Astronomy and Astrophysics*, 52(1):529–588, 2014.
- 73 Feng Yuan, DooSoo Yoon, Ya-Ping Li, Zhao-Ming Gan, Luis C. Ho, and Fulai Guo. Active Galactic Nucleus Feedback in an Elliptical Galaxy with the Most Updated AGN Physics. I. Low Angular Momentum Case. *The Astrophysical Journal*, 857(2):121, 2018.
- 74 O. Agertz, A. V. Kravtsov, S. N. Leitner, and N. Y. Gnedin. Toward a Complete Accounting of Energy and Momentum from Stellar Feedback in Galaxy Formation Simulations. *ApJ*, 770:25, June 2013.
- 75 Sam Geen, Joakim Rosdahl, Jeremy Blaizot, Julien Devriendt, and Adrienne Slyz. A detailed study of feedback from a massive star. *MNRAS*, 448(4):3248–3264, April 2015.
- 76 Michael Y. Grudić, Dávid Guszejnov, Philip F. Hopkins, Stella S. R. Offner, and Claude-André Faucher-Giguère. STARFORGE: Towards a comprehensive numerical model of star cluster formation and feedback. *MNRAS*, 506(2):2199–2231, September 2021.
- 77 Philip F. Hopkins, Michael Y. Grudić, Andrew Wetzel, Dušan Kereš, Claude-André Faucher-Giguère, Xiangcheng Ma, Norman Murray, and Nathan Butcher. Radiative stellar feedback in galaxy formation: Methods and physics. *MNRAS*, 491(3):3702–3729, January 2020.
- 78 Matthew C. Smith, Greg L. Bryan, Rachel S. Somerville, Chia-Yu Hu, Romain Teyssier, Blakesley Burkhart, and Lars Hernquist. Efficient early stellar feedback can suppress galactic outflows by reducing supernova clustering. *MNRAS*, 506(3):3882–3915, September 2021.
- 79 Junjie Mao, Jelle De Plaa, Jelle S. Kaastra, Ciro Pinto, Liyi Gu, François Mernier, Hong-Liang Yan, Yu-Ying Zhang, and Hiroki Akamatsu. Nitrogen abundance in the x-ray halos of clusters and groups of galaxies. *Astronomy & Astrophysics*, 621:A9, 2019.
- 80 Junjie Mao, Ping Zhou, Aurora Simionescu, Yuanyuan Su, Yasushi Fukazawa, Liyi Gu, Hiroki Akamatsu, Zhenlin Zhu, Jelle de Plaa, François Mernier, et al. Elemental abundances of the hot atmosphere of luminous infrared galaxy arp 299. *The Astrophysical Journal Letters*, 918(1):L17, 2021.
- 81 Hui Li, Mark Vogelsberger, Federico Marinacci, Laura V. Sales, and Paul Torrey. The effects of subgrid models on the properties of giant molecular clouds in galaxy formation simulations. *MNRAS*, 499(4):5862–5872, December 2020.
- 82 David K Strickland and Timothy M Heckman. Iron line and diffuse hard x-ray emission from the starburst galaxy m82. *The Astrophysical Journal*, 658(1):258, 2007.
- 83 A. J. Richings, G. Fabbiano, Junfeng Wang, and T. P. Roberts. The Hot Interstellar Medium of the Interacting Galaxy NGC 4490. *ApJ*, 723(2):1375–1392, November 2010.
- 84 J.-T. Li and Q. D. Wang. Chandra survey of nearby highly inclined disc galaxies - I. X-ray measurements of galactic coronae. *MNRAS*, 428(3):2085–2108, 2013.
- 85 Q. Wang and D. J. Helfand. An X-Ray Image of the Violent Interstellar Medium in 30 Doradus. *ApJ*, 370:541, April 1991.
- 86 Yingjie Cheng, Q. Daniel Wang, and Seunghwan Lim. X-ray spectroscopy of the starburst feedback in 30 Doradus. *MNRAS*, 504(2):1627–1643, June 2021.
- 87 Aditi Vijayan, Bocheng Zhu, Miao Li, Feng Yuan, and Luis C. Ho. X-ray Emission from the Interstellar and Circumgalactic Medium of Elliptical Galaxies based on MACER simulations. *arXiv e-prints*, page arXiv:2210.12886, October 2022.
- 88 Lachlan Lancaster, Eve C. Ostriker, Jeong-Gyu Kim, and Chang-Goo Kim. Efficiently Cooled Stellar Wind Bubbles in Turbulent Clouds. I. Fractal Theory and Application to Star-forming Clouds. *ApJ*, 914(2):89, June 2021.
- 89 Liyi Gu, Jelle Kaastra, and A. J. J. Raassen. Plasma code for astrophysical charge exchange emission at X-ray wavelengths. *A&A*, 588:A52, April 2016.
- 90 T. Montmerle and L. K. Townsley. Charge exchange in massive star-forming regions. *Astronomische Nachrichten*, 333(4):355, April 2012.
- 91 Ivanna Escala, Andrew Wetzel, Evan N. Kirby, Philip F. Hopkins, Xiangcheng Ma, Coral Wheeler, Dušan Kereš, Claude-André Faucher-Giguère, and Eliot Quataert. Modelling chemical abundance distributions for dwarf galaxies in the Local Group: the impact of turbulent metal diffusion. *MNRAS*, 474(2):2194–2211, February 2018.
- 92 Renyue Cen and Jeremiah P Ostriker. Where are the baryons? *The Astrophysical Journal*, 514(1):1, 1999.
- 93 Hideki Tanimura. Probing the large-scale structure of the universe with the sunyaev-zel’dovich effect. *Ph. D. Thesis*, 2017.
- 94 G Efstathiou. A model of supernova feedback in galaxy formation. *Monthly Notices of the Royal Astronomical Society*, 317(3):697–719, 2000.
- 95 M Ryan Joung, Greg L Bryan, and Mary E Putman. Gas condensation in the galactic halo. *The Astrophysical Journal*, 745(2):148, 2012.
- 96 Drummond Fielding, Eliot Quataert, Davide Martizzi, and Claude-André Faucher-Giguère. How supernovae launch galactic winds? *Monthly Notices of the Royal Astronomical Society: Letters*, 470(1):L39–L43, 2017.
- 97 Miao Li and Stephanie Tonnesen. How do supernovae impact the cir-

- cumgalactic medium? i. large-scale fountains around a milky way-like galaxy. *The Astrophysical Journal*, 898(2):148, 2020.
- 98 Kung-Yi Su, Philip F Hopkins, Christopher C Hayward, Claude-André Faucher-Giguère, Dušan Kereš, Xiangcheng Ma, Matthew E Orr, TK Chan, and Victor H Robles. Cosmic rays or turbulence can suppress cooling flows (where thermal heating or momentum injection fail). *Monthly Notices of the Royal Astronomical Society*, 491(1):1190–1212, 2020.
- 99 Weixiao Wang, De-Fu Bu, and Feng Yuan. Magnetically driven accretion disc winds: the role of gas thermodynamics and comparison to ultra-fast outflows. *Monthly Notices of the Royal Astronomical Society*, 513(4):5818–5828, 2022.
- 100 Hai Yang, Feng Yuan, Hui Li, Yosuke Mizuno, Fan Guo, Rusen Lu, Luis C Ho, and Jieshuang Wang. Modeling the inner part of m87 jet: confronting jet morphology with theory. *arXiv preprint arXiv:2206.05661*, 2022.
- 101 Rachel S Somerville and Romeel Davé. Physical models of galaxy formation in a cosmological framework. *Annual Review of Astronomy and Astrophysics*, 53:51–113, 2015.
- 102 Liang Wang, Aaron A Dutton, Gregory S Stinson, Andrea V Macciò, Camilla Penzo, Xi Kang, Ben W Keller, and James Wadsley. Nihao project-i. reproducing the inefficiency of galaxy formation across cosmic time with a large sample of cosmological hydrodynamical simulations. *Monthly Notices of the Royal Astronomical Society*, 454(1):83–94, 2015.
- 103 Édouard Tollet, Andrea Cattaneo, Andrea V Macciò, Aaron A Dutton, and Xi Kang. Nihao xix: how supernova feedback shapes the galaxy baryon cycle. *Monthly Notices of the Royal Astronomical Society*, 485(2):2511–2531, 2019.
- 104 Aditi Vijayan and Miao Li. X-ray spectra of circumgalactic medium around star-forming galaxies: connecting simulations to observations. *Monthly Notices of the Royal Astronomical Society*, 510(1):568–580, 2022.
- 105 Planck Collaboration. Planck intermediate results. XI. The gas content of dark matter halos: the Sunyaev-Zeldovich-stellar mass relation for locally brightest galaxies. *A&A*, 557:52, 2013.
- 106 J. K. Werk, J. X. Prochaska, J. Tumlinson, M. S. Peeples, T. M. Tripp, A. J. Fox, N. Lehner, C. Thom, J. M. O’Meara, A. B. Ford, R. Bordoloi, N. Katz, N. Tejos, B. D. Oppenheimer, R. Davé, and D. H. Weinberg. The COS-Halos Survey: Physical Conditions and Baryonic Mass in the Low-redshift Circumgalactic Medium. *ApJ*, 792(1):8, 2014.
- 107 J. Xavier Prochaska, Jessica K. Werk, Gábor Worseck, Todd M. Tripp, Jason Tumlinson, Joseph N. Burchett, Andrew J. Fox, Michele Fumagalli, Nicolas Lehner, Molly S. Peeples, and Nicolas Tejos. The COS-halos survey: Metallicities in the low-redshift circumgalactic medium. *The Astrophysical Journal*, 837(2):169, mar 2017.
- 108 D. Eckert, M. Jauzac, H. Shan, J.-P. Kneib, T. Erben, H. Israel, E. Jullo, M. Klein, R. Massey, J. Richard, and C. Tchernin. Warm-hot baryons comprise 5-10 per cent of filaments in the cosmic web. *Nature*, 528:105–107, 2015.
- 109 J.-T. Li, J. N. Bregman, Q. D. Wang, R. A. Crain, and M. E. Anderson. Baryon Budget of the Hot Circumgalactic Medium of Massive Spiral Galaxies. *ApJL*, 855(2):L24, 2018.
- 110 J. N. Bregman, M. E. Anderson, M. J. Miller, E. Hodges-Kluck, X. Dai, J.-T. Li, Y. Li, and Z. Qu. The Extended Distribution of Baryons around Galaxies. *ApJ*, 862(1):3, 2018.
- 111 J. N. Bregman, E. Hodges-Kluck, Z. Qu, C. Pratt, J.-T. Li, and Y. Yun. Hot Extended Galaxy Halos around Local L^* Galaxies from Sunyaev-Zeldovich Measurements. *ApJ*, 928(1):14, 2022.
- 112 Liang Wang, Aaron A. Dutton, Gregory S. Stinson, Andrea V. Macciò, Thales Gutcke, and Xi Kang. NIHAO VII: predictions for the galactic baryon budget in dwarf to Milky Way mass haloes. *MNRAS*, 466(4):4858–4867, April 2017.
- 113 J.-T. Li, J. N. Bregman, Q. D. Wang, R. A. Crain, M. E. Anderson, and S. Zhang. The Circum-Galactic Medium of Massive Spirals. II. Probing the Nature of Hot Gaseous Halo around the Most Massive Isolated Spiral Galaxies. *ApJS*, 233(2):20, 2017.
- 114 Z. Qu, R. Huang, J. N. Bregman, and J.-T. Li. An X-Ray- and SZ-bright Diffuse Source toward M31: A Local Hot Bridge. *ApJ*, 907(1):14, 2021.
- 115 A. Tamm, E. Tempel, P. Tenjes, O. Tihhonova, and T. Tuvikene. Stellar mass map and dark matter distribution in M 31. *A&A*, 546(1):A4, 2012.
- 116 P. Barmby, M. L. N. Ashby, L. Bianchi, C. W. Engelbracht, R. D. Gehrz, and et al. Dusty Waves on a Starry Sea: The Mid-Infrared View of M31. *ApJL*, 650(1):L45–L49, 2006.
- 117 N. Lehner, S. C. Berek, J. C. Howk, B. P. Wakker, J. Tumlinson, E. B. Jenkins, J. X. Prochaska, R. Augustin, S. Ji, C.-A. Faucher-Giguère, Z. Hafen, M. S. Peeples, K. A. Barger, M. A. Berg, R. Bordoloi, T. M. Brown, A. J. Fox, K. M. Gilbert, P. Guhathakurta, J. S. Kalirai, F. J. Lockman, J. M. O’Meara, D. J. Pisano, J. Ribaud, and J. K. Werk. Project AMIGA: The Circumgalactic Medium of Andromeda. *ApJ*, 900(1):9, 2020.
- 118 R. Braun and D. A. Thilker. The WSRT wide-field H I survey. II. Local Group features. *A&A*, 417:421–435, 2004.
- 119 E. Patel, G. Besla, and S. T. Sohn. Orbits of massive satellite galaxies - I. A close look at the Large Magellanic Cloud and a new orbital history for M33. *MNRAS*, 464(4):3825–3849, 2017.
- 120 J. C. Richardson, M. J. Irwin, A. W. McConnachie, N. F. Martin, A. L. Dotter, A. M. N. Ferguson, R. A. Ibata, S. C. Chapman, G. F. Lewis, N. R. Tanvir, and R. M. Rich. Project AMIGA: The Circumgalactic Medium of Andromeda. *ApJ*, 732(2):76, 2011.
- 121 S. M. Rao, G. Sardane, D. A. Turnshek, D. Thilker, R. Walterbos, D. Vanden Berk, and D. G. York. Probing the extended gaseous regions of M31 with quasar absorption lines. *MNRAS*, 432(2):866–885, 2013.
- 122 N. Lehner, J. C. Howk, and B. P. Wakker. Evidence for a Massive, Extended Circumgalactic Medium Around the Andromeda Galaxy. *ApJ*, 804(2):79, 2015.
- 123 D. K. Strickland, T. M. Heckman, E. J. M. Colbert, C. G. Hoopes, and K. A. Weaver. A High Spatial Resolution X-Ray and H α Study of Hot Gas in the Halos of Star-forming Disk Galaxies. I. Spatial and Spectral Properties of the Diffuse X-Ray Emission. *ApJS*, 151(2):193–236, 2004.
- 124 J.-T. Li and Q. D. Wang. Chandra survey of nearby highly inclined disc galaxies - II. Correlation analysis of galactic coronal properties. *MNRAS*, 435(4):3071–3084, 2013.
- 125 Q. D. Wang, J. Li, X. Jiang, and T. Fang. Chandra survey of nearby highly inclined disk galaxies - IV. New insights into the working of stellar feedback. *MNRAS*, 457(2):1385–1392, 2016.
- 126 A. J. Benson, R. G. Bower, C. S. Frenk, and S. D. M. White. Diffuse X-ray emission from late-type galaxy haloes. *MNRAS*, 314(3):557–565, 2000.
- 127 R. A. Crain, I. G. McCarthy, J. Schaye, T. Theuns, and C. S. Frenk. Enriching the hot circumgalactic medium. *MNRAS*, 432(4):3005–3024, 2013.
- 128 J.-T. Li, J. N. Bregman, Q. D. Wang, R. A. Crain, and M. E. Anderson. The Circum-Galactic Medium of MASSive Spirals I: Overview and a Case Study of NGC 5908. *ApJ*, 830(2):134, 2016.
- 129 J.-T. Li. An X-ray view of the hot circum-galactic medium. *Astronomische Nachrichten*, 341(2):177–183, 2020.
- 130 Yu-Ning Zhang, Chengzhe Li, Dandan Xu, and Wei Cui. Mock HUBS observations of hot gas with IllustrisTNG. *Experimental Astronomy*, 53(3):1053–1074, June 2022.
- 131 X. Dai, M. E. Anderson, J. N. Bregman, and J. M. Miller. XMM-Newton Detects a Hot Gaseous Halo in the Fastest Rotating Spiral Galaxy UGC 12591. *ApJ*, 755(2):107, 2012.
- 132 Á Bogdán, W. R. Forman, M. Vogelsberger, H. Bourdin, D. Sijacki, P. Mazzotta, R. P. Kraft, C. Jones, M. Gilfanov, E. Churazov, and

- L. P. David. Hot X-Ray Coronae around Massive Spiral Galaxies: A Unique Probe of Structure Formation Models. *ApJ*, 772(2):97, 2013.
- 133 Á Bogdán, M. Vogelsberger, R. P. Kraft, L. Hernquist, M. Gilfanov, P. Torrey, E. Churazov, S. Genel, W. R. Forman, S. S. Murray, A. Vikhlinin, C. Jones, and H. Böhringer. Hot Gaseous Coronae around Spiral Galaxies: Probing the Illustris Simulation. *ApJ*, 804(1):72, 2015.
- 134 M. E. Anderson, E. Churazov, and J. N. Bregman. A deep XMM-Newton study of the hot gaseous halo around NGC 1961. *MNRAS*, 455(1):227–243, 2016.
- 135 Z. Qu and J. N. Bregman. The Mass and Absorption Columns of Galactic Gaseous Halos. *ApJ*, 856(1):5, 2018.
- 136 M. Haverkorn. Magnetic Fields in the Milky Way. In A. Lazarian, E. M. de Gouveia Dal Pino, and C. Melioli, editors, *Magnetic Fields in Diffuse Media*, volume 407 of *Astrophysics and Space Science Library*, page 483, 2015.
- 137 JL Han. Observing interstellar and intergalactic magnetic fields. *Annual Review of Astronomy and Astrophysics*, 55(1):111–157, 2017.
- 138 J. Irwin, R. Beck, R. A. Benjamin, R.-J. Dettmar, J. English, G. Heald, R. N. Henriksen, M. Johnson, M. Krause, J.-T. Li, A. Miskolczi, S. C. Mora, E. J. Murphy, T. Oosterloo, T. A. Porter, R. J. Rand, D. J. Saikia, P. Schmidt, A. W. Strong, R. Walterbos, Q. D. Wang, and T. Wiegert. Continuum Halos in Nearby Galaxies: An EVLA Survey (CHANG-ES). I. Introduction to the Survey. *AJ*, 144(2):43, 2012.
- 139 M. Krause, J. Irwin, P. Schmidt, Y. Stein, A. Miskolczi, S. C. Mora-Partiarroyo, T. Wiegert, R. Beck, J. M. Stil, G. Heald, J.-T. Li, A. Damas-Segovia, C. J. Vargas, R. J. Rand, J. West, R. A. M. Walterbos, R.-J. Dettmar, J. English, and A. Woodfinden. CHANG-ES. XXII. Coherent magnetic fields in the halos of spiral galaxies. *A&A*, 639:112, 2020.
- 140 Jiang-Tao Li, Zhiyuan Li, Q Daniel Wang, Judith A Irwin, and Joern Rossa. Chandra observation of the edge-on spiral ngc 5775: probing the hot galactic disc/halo connection. *Monthly Notices of the Royal Astronomical Society*, 390(1):59–70, 2008.
- 141 Taotao Fang, James Bullock, and Michael Boylan-Kolchin. On the hot gas content of the milky way halo. *The Astrophysical Journal*, 762(1):20, 2012.
- 142 J. Irwin, R. Beck, R. A. Benjamin, R.-J. Dettmar, J. English, G. Heald, R. N. Henriksen, M. Johnson, M. Krause, J.-T. Li, A. Miskolczi, S. C. Mora, E. J. Murphy, T. Oosterloo, T. A. Porter, R. J. Rand, D. J. Saikia, P. Schmidt, A. W. Strong, R. Walterbos, Q. D. Wang, and T. Wiegert. Continuum Halos in Nearby Galaxies: An EVLA Survey (CHANG-ES). II. First Results on NGC 4631. *AJ*, 144(2):44, 2012.
- 143 S. C. Mora-Partiarroyo, M. Krause, A. Basu, R. Beck, T. Wiegert, J. Irwin, R. Henriksen, Y. Stein, C. J. Vargas, V. Heesen, R. A. M. Walterbos, R. J. Rand, G. Heald, J. Li, P. Kamienieski, and J. English. CHANG-ES. XV. Large-scale magnetic field reversals in the radio halo of NGC 4631. *A&A*, 632:11, 2019.
- 144 Y. Stein, R. J. Dettmar, J. Irwin, R. Beck, M. Weżgowiec, A. Miskolczi, M. Krause, V. Heesen, T. Wiegert, G. Heald, R. A. M. Walterbos, J. T. Li, and M. Soida. CHANG-ES. XIII. Transport processes and the magnetic fields of NGC 4666: indication of a reversing disk magnetic field. *A&A*, 623:33, 2019.
- 145 Freeke van de Voort, Rebekka Bieri, Rüdiger Pakmor, Facundo A Gómez, Robert J J Grand, and Federico Marinacci. The effect of magnetic fields on properties of the circumgalactic medium. *Monthly Notices of the Royal Astronomical Society*, 501(4):4888–4902, 2021.
- 146 Sam B. Ponnada, Georgia V. Panopoulou, Iryna S. Butsky, Philip F. Hopkins, Sarah R. Loebman, Cameron Hummels, Suoqing Ji, Andrew Wetzel, Claude-André Faucher-Giguère, and Christopher C. Hayward. Magnetic Fields on FIRE: Comparing B-fields in the multiphase ISM and CGM of Simulated L_{*} Galaxies to Observations. *arXiv*, 2022.
- 147 Suoqing Ji, S. Peng Oh, and Michael McCourt. The impact of magnetic fields on thermal instability. *Mon. Not. Roy. Astron. Soc.*, 476(1):852–867, 2018.
- 148 LJ Dursi and C Pfrommer. Draping of cluster magnetic fields over bullets and bubbles—morphology and dynamic effects. *The Astrophysical Journal*, 677(2):993, 2008.
- 149 Michael McCourt, Ryan M. O’Leary, Ann-Marie Madigan, and Eliot Quataert. Magnetized gas clouds can survive acceleration by a hot wind. *Monthly Notices of the Royal Astronomical Society*, 449:2–7, 2015.
- 150 Suoqing Ji, S Peng Oh, and Phillip Masterson. Simulations of radiative turbulent mixing layers. *Monthly Notices of the Royal Astronomical Society*, 487(1):737–754, may 2019.
- 151 Yanhui Yang and Suoqing Ji. Radiative turbulent mixing layers at high mach numbers. *Monthly Notices of the Royal Astronomical Society*, 520(2):2148–2162, 2023.
- 152 Ian J Parrish, Eliot Quataert, and Prateek Sharma. Anisotropic thermal conduction and the cooling flow problem in galaxy clusters. *The Astrophysical Journal*, 703(1):96, 2009.
- 153 Ellen G. Zweibel. The microphysics and macrophysics of cosmic rays. *Physics of Plasmas*, 20(5):055501, 2013.
- 154 Bruce T. Draine. *Physics of the Interstellar and Intergalactic Medium*. 2011.
- 155 M. Krause, J. Irwin, T. Wiegert, A. Miskolczi, A. Damas-Segovia, R. Beck, J.-T. Li, G. Heald, P. Müller, Y. Stein, R. J. Rand, V. Heesen, R. A. M. Walterbos, R.-J. Dettmar, C. J. Vargas, J. English, and E. J. Murphy. CHANG-ES. IX. Radio scale heights and scale lengths of a consistent sample of 13 spiral galaxies seen edge-on and their correlations. *A&A*, 611:72, 2018.
- 156 G. H. Heald, V. Heesen, S. S. Sridhar, R. Beck, D. J. Bomans, M. Brüggén, K. T. Chyży, A. Damas-Segovia, R. J. Dettmar, J. English, R. Henriksen, S. Ideguchi, J. Irwin, M. Krause, J. T. Li, E. J. Murphy, B. Nikiel-Wroczyński, J. Piotrowska, R. J. Rand, T. Shimwell, Y. Stein, C. J. Vargas, Q. D. Wang, R. J. van Weeren, and T. Wiegert. CHANG-ES XXIII: influence of a galactic wind in NGC 5775. *MNRAS*, 509(1):658–684, 2022.
- 157 M. Stein, V. Heesen, R. J. Dettmar, Y. Stein, M. Brüggén, R. Beck, B. Adebahr, T. Wiegert, C. J. Vargas, D. J. Bomans, J. Li, J. English, K. T. Chyzy, R. Paladino, F. S. Tabatabaei, and A. Strong. CHANG-ES XXVI: Insights into cosmic-ray transport from radio halos in edge-on galaxies. *arXiv e-prints*, page arXiv:2210.07709, October 2022.
- 158 Suoqing Ji, Dušan Kereš, TK Chan, Jonathan Stern, Cameron B Hummels, Philip F Hopkins, Eliot Quataert, and Claude-André Faucher-Giguère. Virial shocks are suppressed in cosmic ray-dominated galaxy haloes. *Monthly Notices of the Royal Astronomical Society*, 505(1):259–273, 2021.
- 159 Munier Salem, Greg L Bryan, and Lauren Corlies. Role of cosmic rays in the circumgalactic medium. *Monthly Notices of the Royal Astronomical Society*, 456(1):582–601, 2016.
- 160 Ryan Farber, Mateusz Ruszkowski, H-YK Yang, and EG Zweibel. Impact of cosmic-ray transport on galactic winds. *The Astrophysical Journal*, 856(2):112, 2018.
- 161 Iryna S Butsky and Thomas R Quinn. The role of cosmic-ray transport in shaping the simulated circumgalactic medium. *The Astrophysical Journal*, 868(2):108, 2018.
- 162 Suoqing Ji, TK Chan, Cameron B Hummels, Philip F Hopkins, Jonathan Stern, Dušan Kereš, Eliot Quataert, Claude-André Faucher-Giguère, and Norman Murray. Properties of the circumgalactic medium in cosmic ray-dominated galaxy haloes. *Monthly Notices of the Royal Astronomical Society*, 496(4):4221–4238, 2020.
- 163 Tobias Buck, Christoph Pfrommer, Rüdiger Pakmor, Robert JJ Grand, and Volker Springel. The effects of cosmic rays on the formation of milky way-mass galaxies in a cosmological context. *Monthly Notices of the Royal Astronomical Society*, 497(2):1712–1737, 2020.

- 164 G. Ponti, F. Hofmann, E. Churazov, M. R. Morris, F. Haberl, K. Nandra, R. Terrier, M. Clavel, and A. Goldwurm. An X-ray chimney extending hundreds of parsecs above and below the Galactic Centre. *Nature*, 567:347–350, 2019.
- 165 Q. D. Wang. Chandra large-scale mapping of the Galactic Centre: probing high-energy structures around the central molecular zone. *MNRAS*, 504(2):1609–1618, 2021.
- 166 H. Y. K. Yang, M. Ruzkowski, and E. G. Zweibel. Giant Gamma-ray Bubbles from Fermi-LAT: Active Galactic Nucleus Activity or Bipolar Galactic Wind? *Nature Astronomy*, 6:584–591, 2022.
- 167 M. Su, T. R. Slatyer, and D. P. Finkbeiner. Giant Gamma-ray Bubbles from Fermi-LAT: Active Galactic Nucleus Activity or Bipolar Galactic Wind? *ApJ*, 724(2):1044–1082, 2010.
- 168 P. Predehl, R. A. Sunyaev, W. Becker, H. Brunner, R. Brunen, A. Bykov, A. Cherepashchuk, N. Chugai, E. Churazov, V. Doroshenko, N. Eismont, M. Freyberg, M. Gilfanov, F. Haberl, I. Khabibullin, R. Krivonos, C. Maitra, P. Medvedev, A. Merloni, K. Nandra, V. Nazarov, M. Pavlinsky, G. Ponti, J. S. Sanders, M. Sasaki, S. Sazonov, A. W. Strong, and J. Wilms. Detection of large-scale X-ray bubbles in the Milky Way halo. *Nature*, 588:227–231, 2020.
- 169 D. P. Finkbeiner. Microwave Interstellar Medium Emission Observed by the Wilkinson Microwave Anisotropy Probe. *ApJ*, 614(1):186–193, 2004.
- 170 Planck Collaboration. Planck intermediate results. IX. Detection of the Galactic haze with Planck. *A&A*, 554:139, 2013.
- 171 I. J. Feain, T. J. Cornwell, R. D. Ekers, M. R. Calabretta, R. P. Norris, M. Johnston-Hollitt, J. Ott, E. Lindley, B. M. Gaensler, T. Murphy, E. Middelberg, S. Jiraskova, S. O’Sullivan, N. M. McClure-Griffiths, and J. Bland-Hawthorn. The Radio Continuum Structure of Centaurus A at 1.4 GHz. *ApJ*, 740(1):17, 2011.
- 172 S. G. Neff, J. A. Eilek, and F. N. Owen. The Complex North Transition Region of Centaurus A: A Galactic Wind. *ApJ*, 802(2):88, 2015.
- 173 G. L. H. Harris, M. Rejkuba, and W. E. Harris. The Distance to NGC 5128 (Centaurus A). *Publications of the Astronomical Society of Australia*, 27(4):457–462, 2010.
- 174 Hitomi Collaboration. The quiescent intracluster medium in the core of the Perseus cluster. *Nature*, 535:117–121, 2016.
- 175 S. Zhang, Q. D. Wang, L. Ji, R. K. Smith, A. R. Foster, and X. Zhou. Spectral Modeling of the Charge-exchange X-Ray Emission from M82. *ApJ*, 794(1):61, 2014.
- 176 L. A. Lopez, S. Mathur, D. D. Nguyen, T. A. Thompson, and G. M. Olivier. Temperature and Metallicity Gradients in the Hot Gas Outflows of M82. *ApJ*, 904(2):152, 2020.
- 177 M. S. Yun, P. T. P. Ho, and K. Y. Lo. A high-resolution image of atomic hydrogen in the M81 group of galaxies. *Nature*, 372:530–532, 1994.
- 178 C. G. Hoopes, T. M. Heckman, D. K. Strickland, M. Seibert, B. F. Madore, R. M. Rich, L. Bianchi, A. Gil de Paz, D. Burgarella, D. A. Thilker, P. G. Friedman, T. A. Barlow, Y.-I. Byun, J. Donas, K. Forster, P. N. Jelinsky, Y.-W. Lee, R. F. Malina, D. C. Martin, B. Milliard, P. F. Morrissey, S. G. Neff, D. Schiminovich, O. H. W. Siegmund, T. Small, A. S. Szalay, B. Y. Welsh, and T. K. Wyder. GALEX Observations of the Ultraviolet Halos of NGC 253 and M82. *ApJ*, 619(1):L99–L102, 2005.
- 179 D. K. Strickland and T. M. Heckman. Supernova Feedback Efficiency and Mass Loading in the Starburst and Galactic Superwind Exemplar M82. *ApJ*, 697(2):2030–2056, 2009.
- 180 C. Melioli, E. M. de Gouveia Dal Pino, and F. G. Geraissate. Evolution of M82-like starburst winds revisited: 3D radiative cooling hydrodynamical simulations. *MNRAS*, 430(4):3235–3248, 2013.
- 181 H. Tanimura, N. Aghanim, A. Kolodzig, M. Douspis, and N. Malavasi. First detection of stacked X-ray emission from cosmic web filaments. *A&A*, 643:L2, 2020.
- 182 H. Tanimura, N. Aghanim, M. Douspis, and N. Malavasi. X-ray emission from cosmic web filaments in SRG/eROSITA data. 2022.
- 183 Sen Wang, Dandan Xu, Shengdong Lu, Zheng Cai, Maosheng Xiang, Shude Mao, Volker Springel, and Lars Hernquist. From large-scale environment to CGM angular momentum to star-forming activities - I. Star-forming galaxies. *MNRAS*, 509(3):3148–3162, January 2022.
- 184 Yen-Ting Lin and Joseph J. Mohr. K-band Properties of Galaxy Clusters and Groups: Brightest Cluster Galaxies and Intracluster Light. *ApJ*, 617(2):879–895, December 2004.
- 185 S. Giodini, D. Pierini, A. Finoguenov, G. W. Pratt, H. Boehringer, A. Leauthaud, L. Guzzo, H. Aussel, M. Bolzonella, P. Capak, M. Elvis, G. Hasinger, O. Ilbert, J. S. Kartaltepe, A. M. Koekemoer, S. J. Lilly, R. Massey, H. J. McCracken, J. Rhodes, M. Salvato, D. B. Sanders, N. Z. Scoville, S. Sasaki, V. Smolcic, Y. Taniguchi, D. Thompson, and COSMOS Collaboration. Stellar and Total Baryon Mass Fractions in Groups and Clusters Since Redshift 1. *ApJ*, 703(1):982–993, September 2009.
- 186 Alexie Leauthaud, Jeremy Tinker, Kevin Bundy, Peter S. Behroozi, Richard Massey, Jason Rhodes, Matthew R. George, Jean-Paul Kneib, Andrew Benson, Risa H. Wechsler, Michael T. Busha, Peter Capak, Marina Cortés, Olivier Ilbert, Anton M. Koekemoer, Oliver Le Fèvre, Simon Lilly, Henry J. McCracken, Mara Salvato, Tim Schrabback, Nick Scoville, Tristan Smith, and James E. Taylor. New Constraints on the Evolution of the Stellar-to-dark Matter Connection: A Combined Analysis of Galaxy-Galaxy Lensing, Clustering, and Stellar Mass Functions from $z = 0.2$ to $z = 1$. *ApJ*, 744(2):159, January 2012.
- 187 Anthony H. Gonzalez, Suresh Sivanandam, Ann I. Zabludoff, and Dennis Zaritsky. Galaxy Cluster Baryon Fractions Revisited. *ApJ*, 778(1):14, November 2013.
- 188 D. Eckert, S. Etori, S. Molendi, F. Vazza, and S. Paltani. The X-ray/SZ view of the virial region. II. Gas mass fraction. *A&A*, 551:A23, March 2013.
- 189 Glenn G. Kacprzak, Christopher W. Churchill, Charles C. Steidel, and Michael T. Murphy. Halo Gas Cross Sections and Covering Fractions of Mg II Absorption Selected Galaxies. *AJ*, 135(3):922–927, March 2008.
- 190 Glenn G. Kacprzak, Christopher W. Churchill, and Nikole M. Nielsen. Tracing Outflows and Accretion: A Bimodal Azimuthal Dependence of Mg II Absorption. *ApJ*, 760(1):L7, November 2012.
- 191 Nikole M. Nielsen, Christopher W. Churchill, and Glenn G. Kacprzak. MAGIICAT II. General Characteristics of the Mg II Absorbing Circumgalactic Medium. *ApJ*, 776(2):115, October 2013.
- 192 J. Xavier Prochaska, Marie Wingyee Lau, and Joseph F. Hennawi. Quasars Probing Quasars. VII. The Pinnacle of the Cool Circumgalactic Medium Surrounds Massive $z \sim 2$ Galaxies. *ApJ*, 796(2):140, December 2014.
- 193 Michael Rauch, Jordi Miralda-Escudé, Wallace L. W. Sargent, Tom A. Barlow, David H. Weinberg, Lars Hernquist, Neal Katz, Renyue Cen, and Jeremiah P. Ostriker. The Opacity of the Ly α Forest and Implications for Ω_b and the Ionizing Background. *ApJ*, 489(1):7–20, November 1997.
- 194 Khee-Gan Lee, Joseph F. Hennawi, Casey Stark, J. Xavier Prochaska, Martin White, David J. Schlegel, Anna-Christina Eilers, Andreu Arinyo-i-Prats, Nao Suzuki, Rupert A. C. Croft, Karina I. Caputi, Paolo Cassata, Olivier Ilbert, Bianca Garilli, Anton M. Koekemoer, Vincent Le Brun, Olivier Le Fèvre, Dario Maccagni, Peter Nugent, Yoshiaki Taniguchi, Lidia A. M. Tasca, Laurence Tresse, Gianni Zamorani, and Elena Zucca. Ly α Forest Tomography from Background Galaxies: The First Megaparsec-resolution Large-scale Structure Map at $z \lesssim 2$. *ApJ*, 795(1):L12, November 2014.
- 195 M. Fukugita, C. J. Hogan, and P. J. E. Peebles. The Cosmic Baryon Budget. *ApJ*, 503(2):518–530, August 1998.
- 196 Fabrizio Nicastro, Smita Mathur, Martin Elvis, Jeremy Drake, Tao-tao Fang, Antonella Fruscione, Yair Krongold, Herman Marshall, Rik Williams, and Andreas Zezas. The mass of the missing baryons

- in the X-ray forest of the warm-hot intergalactic medium. *Nature*, 433(7025):495–498, February 2005.
- 197 Hyesung Kang, Dongsu Ryu, Renyue Cen, and Doojong Song. Shock-heated Gas in the Large-Scale Structure of the Universe. *ApJ*, 620(1):21–30, February 2005.
- 198 Renyue Cen and Jeremiah P. Ostriker. Where Are the Baryons? II. Feedback Effects. *ApJ*, 650(2):560–572, October 2006.
- 199 Romeel Davé and Benjamin D. Oppenheimer. The enrichment history of baryons in the Universe. *MNRAS*, 374(2):427–435, January 2007.
- 200 Fabrizio Nicastro, Smita Mathur, and Martin Elvis. Missing Baryons and the Warm-Hot Intergalactic Medium. *Science*, 319(5859):55, January 2008.
- 201 Romeel Davé, Benjamin D. Oppenheimer, Neal Katz, Juna A. Kollmeier, and David H. Weinberg. The intergalactic medium over the last 10 billion years - I. Ly α absorption and physical conditions. *MNRAS*, 408(4):2051–2070, November 2010.
- 202 M. Haider, D. Steinhauser, M. Vogelsberger, S. Genel, V. Springel, P. Torrey, and L. Hernquist. Large-scale mass distribution in the Illustris simulation. *MNRAS*, 457(3):3024–3035, April 2016.
- 203 Davide Martizzi, Mark Vogelsberger, Maria Celeste Artale, Markus Haider, Paul Torrey, Federico Marinacci, Dylan Nelson, Annalisa Pillepich, Rainer Weinberger, Lars Hernquist, Jill Naiman, and Volker Springel. Baryons in the Cosmic Web of IllustrisTNG - I: gas in knots, filaments, sheets, and voids. *MNRAS*, 486(3):3766–3787, July 2019.
- 204 Lara Arielle Phillips, Jeremiah P. Ostriker, and Renyue Cen. Is There Still Room for Warm/Hot Gas? Simulating the X-Ray Background Spectrum. *ApJ*, 554(1):L9–L12, June 2001.
- 205 Kohji Yoshikawa, Noriko Y. Yamasaki, Yasushi Suto, Takaya Ohashi, Kazuhisa Mitsuda, Yuzuru Tawara, and Akihiro Furuzawa. Detectability of the Warm/Hot Intergalactic Medium through Emission Lines of O VII and O VIII. *PASJ*, 55(5):879–890, October 2003.
- 206 Jelle Kaastra, Alexis Finoguenov, Fabrizio Nicastro, Enzo Branchini, Joop Schaye, Nico Cappelluti, Jukka Nevalainen, Xavier Barcons, Joel Bregman, Judith Croston, Klaus Dolag, Stefano Ettori, Massimiliano Galeazzi, Takaya Ohashi, Luigi Piro, Etienne Pointecouteau, Gabriel Pratt, Thomas Reiprich, Mauro Roncarelli, Jeremy Sanders, Yoh Takei, and Eugenio Ursino. The Hot and Energetic Universe: The missing baryons and the warm-hot intergalactic medium. *arXiv e-prints*, page arXiv:1306.2324, June 2013.
- 207 F. Nicastro, J. Kaastra, Y. Krongold, S. Borgani, E. Branchini, R. Cen, M. Dadina, C. W. Danforth, M. Elvis, F. Fiore, A. Gupta, S. Mathur, D. Mayya, F. Paerels, L. Piro, D. Rosa-Gonzalez, J. Schaye, J. M. Shull, J. Torres-Zafra, N. Wijers, and L. Zappacosta. Observations of the missing baryons in the warm-hot intergalactic medium. *Nature*, 558(7710):406–409, June 2018.
- 208 Kazuo Makishima, Hajime Ezawa, Yasushi Fukuzawa, Hirohiko Honda, Yasushi Ikebe, Tuneyoshi Kamae, Ken'ich Kikuchi, Kyoko Matsushita, Kazuhiro Nakazawa, Takaya Ohashi, Tadayuki Takahashi, Takayuki Tamura, and Haiguang Xu. X-Ray Probing of the Central Regions of Clusters of Galaxies. *PASJ*, 53(3):401–420, June 2001.
- 209 A. Vikhlinin, R. A. Burenin, H. Ebeling, W. R. Forman, A. Hornstrup, C. Jones, A. V. Kravtsov, S. S. Murray, D. Nagai, H. Quintana, and A. Voevodkin. Chandra Cluster Cosmology Project. II. Samples and X-Ray Data Reduction. *ApJ*, 692(2):1033–1059, February 2009.
- 210 M. Pierre, F. Pcaud, C. Adami, S. Alis, B. Altieri, N. Baran, C. Benoist, M. Birkinshaw, A. Bongiorno, M. N. Bremer, M. Brusa, A. Butler, P. Ciliegi, L. Chiappetti, N. Clerc, P. S. Corasaniti, J. Coupon, C. De Breuck, J. Democles, S. Desai, J. Delhaize, J. Devriendt, Y. Dubois, D. Eckert, A. Elyiv, S. Ettori, A. Evrard, L. Faccioli, A. Farahi, C. Ferrari, F. Finet, S. Fotopoulou, N. Fourmanoit, P. Gandhi, F. Gastaldello, R. Gastaud, I. Georgantopoulos, P. Giles, L. Guennou, V. Guglielmo, C. Horellou, K. Husband, M. Huynh, A. Iovino, M. Kilbinger, E. Koulouridis, S. Lavoie, A. M. C. Le Brun, J. P. Le Fevre, C. Lidman, M. Lieu, C. A. Lin, A. Mantz, B. J. Maughan, S. Maurogordato, I. G. McCarthy, S. McGee, J. B. Melin, O. Melnyk, F. Menanteau, M. Novak, S. Paltani, M. Plionis, B. M. Poggianti, D. Pomarede, E. Pompei, T. J. Ponman, M. E. Ramos-Ceja, P. Ranalli, D. Rapetti, S. Raychaudury, T. H. Reiprich, H. Rottgering, E. Rozo, E. Rykoff, T. Sadibekova, J. Santos, J. L. Sauvageot, C. Schimd, M. Sereno, G. P. Smith, V. Smolčić, S. Snowden, D. Spergel, S. Stanford, J. Surdej, P. Valageas, A. Valotti, I. Valtchanov, C. Vignali, J. Willis, and F. Ziparo. The XXL Survey. I. Scientific motivations - XMM-Newton observing plan - Follow-up observations and simulation programme. *A&A*, 592:A1, June 2016.
- 211 Katsuji Koyama, Hiroshi Tsunemi, Tadayasu Dotani, Mark W. Bautz, Kiyoshi Hayashida, Takeshi Go Tsuru, Hironori Matsumoto, Yoshiaki Ogawara, George R. Ricker, John Doty, Steven E. Kissel, Rick Foster, Hiroshi Nakajima, Hiroya Yamaguchi, Hideyuki Mori, Masaaki Sakano, Kenji Hamaguchi, Mamiko Nishiuchi, Emi Miyata, Ken'ichi Torii, Masaaki Namiki, Satoru Katsuda, Daisuke Matsuura, Tomofumi Miyauchi, Naohisa Anabuki, Noriaki Tawa, Masanobu Ozaki, Hiroshi Murakami, Yoshitomo Maeda, Yoshinori Ichikawa, Gregory Y. Prigozhin, Edward A. Boughan, Beverly Lamarr, Eric D. Miller, Barry E. Burke, James A. Gregory, Allen Pillsbury, Aya Bamba, Junko S. Hiraga, Atsushi Senda, Haruyoshi Katayama, Shunji Kitamoto, Masahiro Tsujimoto, Takayoshi Kohmura, Yohko Tsuboi, and Hisamitsu Awaki. X-Ray Imaging Spectrometer (XIS) on Board Suzaku. *PASJ*, 59:23–33, January 2007.
- 212 Liyi Gu, Haiguang Xu, Junhua Gu, Madoka Kawaharada, Kazuhiro Nakazawa, Zhenzhen Qin, Jingying Wang, Yu Wang, Zhongli Zhang, and Kazuo Makishima. Two-phase ICM in the Central Region of the Rich Cluster of Galaxies A1795: A Joint Chandra, XMM-Newton, and Suzaku View. *ApJ*, 749(2):186, April 2012.
- 213 David A. Buote. X-ray evidence for multiphase hot gas with nearly solar Fe abundances in the brightest groups of galaxies. *MNRAS*, 311(1):176–200, January 2000.
- 214 J. R. Peterson and A. C. Fabian. X-ray spectroscopy of cooling clusters. *Phys. Rep.*, 427(1):1–39, April 2006.
- 215 Federico Marinacci, Mark Vogelsberger, Rüdiger Pakmor, Paul Torrey, Volker Springel, Lars Hernquist, Dylan Nelson, Rainer Weinberger, Annalisa Pillepich, Jill Naiman, and Shy Genel. First results from the IllustrisTNG simulations: radio haloes and magnetic fields. *MNRAS*, 480(4):5113–5139, November 2018.
- 216 Jill P. Naiman, Annalisa Pillepich, Volker Springel, Enrico Ramirez-Ruiz, Paul Torrey, Mark Vogelsberger, Rüdiger Pakmor, Dylan Nelson, Federico Marinacci, Lars Hernquist, Rainer Weinberger, and Shy Genel. First results from the IllustrisTNG simulations: a tale of two elements - chemical evolution of magnesium and europium. *MNRAS*, 477(1):1206–1224, June 2018.
- 217 Volker Springel, Rüdiger Pakmor, Annalisa Pillepich, Rainer Weinberger, Dylan Nelson, Lars Hernquist, Mark Vogelsberger, Shy Genel, Paul Torrey, Federico Marinacci, and Jill Naiman. First results from the IllustrisTNG simulations: matter and galaxy clustering. *MNRAS*, 475(1):676–698, March 2018.
- 218 Annalisa Pillepich, Dylan Nelson, Lars Hernquist, Volker Springel, Rüdiger Pakmor, Paul Torrey, Rainer Weinberger, Shy Genel, Jill P. Naiman, Federico Marinacci, and Mark Vogelsberger. First results from the IllustrisTNG simulations: the stellar mass content of groups and clusters of galaxies. *MNRAS*, 475(1):648–675, March 2018.
- 219 Dylan Nelson, Annalisa Pillepich, Volker Springel, Rainer Weinberger, Lars Hernquist, Rüdiger Pakmor, Shy Genel, Paul Torrey, Mark Vogelsberger, Guinevere Kauffmann, Federico Marinacci, and Jill Naiman. First results from the IllustrisTNG simulations: the galaxy colour bimodality. *MNRAS*, 475(1):624–647, March 2018.
- 220 Sofia G. Gallego, Sebastiano Cantalupo, Simon Lilly, Raffaella Anna Marino, Gabriele Pezzulli, Joop Schaye, Lutz Wisotzki, Roland Bacon, Hanae Inami, Mohammad Akhlaghi, Sandro Tacchella, Johan

- Richard, Nicolas F. Bouche, Matthias Steinmetz, and Marcella Carollo. Stacking the Cosmic Web in fluorescent Ly α emission with MUSE. *MNRAS*, 475(3):3854–3869, April 2018.
- 221 Anna de Graaff, Yan-Chuan Cai, Catherine Heymans, and John A. Peacock. Probing the missing baryons with the Sunyaev-Zel'dovich effect from filaments. *A&A*, 624:A48, April 2019.
- 222 Hideki Tanimura, Gary Hinshaw, Ian G. McCarthy, Ludovic Van Waerbeke, Nabila Aghanim, Yin-Zhe Ma, Alexander Mead, Alireza Hojjati, and Tilman Tröster. A search for warm/hot gas filaments between pairs of SDSS Luminous Red Galaxies. *MNRAS*, 483(1):223–234, February 2019.
- 223 H. Tanimura, N. Aghanim, A. Kolodzig, M. Douspis, and N. Malavasi. First detection of stacked X-ray emission from cosmic web filaments. *A&A*, 643:L2, November 2020.
- 224 H. Tanimura, N. Aghanim, M. Douspis, and N. Malavasi. X-ray emission from cosmic web filaments in SRG/eROSITA data. *A&A*, 667:A161, November 2022.
- 225 Shadab Alam, Franco D. Albareti, Carlos Allende Prieto, F. Anders, Scott F. Anderson, Timothy Anderton, Brett H. Andrews, Eric Armengaud, Éric Aubourg, Stephen Bailey, Sarbani Basu, Julian E. Bautista, Rachael L. Beaton, Timothy C. Beers, Chad F. Bender, Andreas A. Berlind, Florian Beutler, Vaishali Bhardwaj, Jonathan C. Bird, Dmitry Bizyaev, Cullen H. Blake, Michael R. Blanton, Michael Blomqvist, John J. Bochanski, Adam S. Bolton, Jo Bovy, A. Shelden Bradley, W. N. Brandt, D. E. Brauer, J. Brinkmann, Peter J. Brown, Joel R. Brownstein, Angela Burden, Etienne Burtin, Nicolás G. Busca, Zheng Cai, Diego Capozzi, Aurelio Carnero Rosell, Michael A. Carr, Ricardo Carrera, K. C. Chambers, William James Chaplin, Yen-Chi Chen, Cristina Chiappini, S. Drew Chojnowski, Chia-Hsun Chuang, Nicolas Clerc, Johan Comparat, Kevin Covey, Rupert A. C. Croft, Antonio J. Cuesta, Katia Cunha, Luiz N. da Costa, Nicola Da Rio, James R. A. Davenport, Kyle S. Dawson, Nathan De Lee, Timothée Delubac, Rohit Deshpande, Saurav Dhital, Letícia Dutra-Ferreira, Tom Dwelly, Anne Ealet, Garrett L. Ebelke, Edward M. Edmondson, Daniel J. Eisenstein, Tristan Ellsworth, Yvonne Elsworth, Courtney R. Epstein, Michael Eracleous, Stephanie Escoffier, Massimiliano Esposito, Michael L. Evans, Xiaohui Fan, Emma Fernández-Alvar, Diane Feuillet, Nurten Filiz Ak, Hayley Finley, Alexis Finoguenov, Kevin Flaherty, Scott W. Fleming, Andreu Font-Ribera, Jonathan Foster, Peter M. Frinchaboy, J. G. Galbraith-Frew, Rafael A. García, D. A. García-Hernández, Ana E. García Pérez, Patrick Gaulme, Jian Ge, R. Génova-Santos, A. Georgakakis, Luan Ghezzi, Bruce A. Gillespie, Léo Girardi, Daniel Goddard, Satya Gontcho A. Gontcho, Jonay I. González Hernández, Eva K. Grebel, Paul J. Green, Jan Niklas Grieb, Nolan Grieves, James E. Gunn, Hong Guo, Paul Harding, Sten Hasselquist, Suzanne L. Hawley, Michael Hayden, Fred R. Hearty, Saskia Hekker, Shirley Ho, David W. Hogg, Kelly Holley-Bockelmann, Jon A. Holtzman, Klaus Honscheid, Daniel Huber, Joseph Huehnerhoff, Inese I. Ivans, Linhua Jiang, Jennifer A. Johnson, Karen Kinemuchi, David Kirkby, Francisco Kitaura, Mark A. Klaene, Gillian R. Knapp, Jean-Paul Kneib, Xavier P. Koenig, Charles R. Lam, Ting-Wen Lan, Dustin Lang, Pierre Laurent, Jean-Marc Le Goff, Alexie Leauthaud, Kheegang Lee, Young Sun Lee, Timothy C. Licquia, Jian Liu, Daniel C. Long, Martín López-Corredoira, Diego Lorenzo-Oliveira, Sara Lucatello, Britt Lundgren, Robert H. Lupton, III Mack, Claude E., Suvrath Mahadevan, Marcio A. G. Maia, Steven R. Majewski, Elena Malanushenko, Viktor Malanushenko, A. Machado, Marc Manera, Qingqing Mao, Claudia Maraston, Robert C. Marchwinski, Daniel Margala, Sarah L. Martell, Marie Martig, Karen L. Masters, Savita Mathur, Cameron K. McBride, Peregrine M. McGehee, Ian D. McGreer, Richard G. McMahon, Brice Ménard, Marie-Luise Menzel, Andrea Merloni, Szabolcs Mészáros, Adam A. Miller, Jordi Miralda-Escudé, Hironao Miyatake, Antonio D. Montero-Dorta, Surhud More, Eric Morganson, Xan Morice-Atkinson, Heather L. Morrison, Benoit Mosser, Demitri Muna, Adam D. Myers, Kirpal Nandra, Jeffrey A. Newman, Mark Neyrinck, Duy Cuong Nguyen, Robert C. Nichol, David L. Nidever, Pasquier Noterdaeme, Sebastián E. Nuza, Julia E. O'Connell, Robert W. O'Connell, Ross O'Connell, Riccardo L. C. Ogando, Matthew D. Olmstead, Audrey E. Oravetz, Daniel J. Oravetz, Keisuke Osumi, Russell Owen, Deborah L. Padgett, Nikhil Padmanabhan, Martin Paegert, Nathalie Palanque-Delabrouille, Kaike Pan, John K. Parejko, Isabelle Pâris, Changbom Park, Petchara Pattarakijwanich, M. Pellejero-Ibanez, Joshua Pepper, Will J. Percival, Ismael Pérez-Fournon, Ignasi Pérez-Ràfols, Patrick Petitjean, Matthew M. Pieri, Marc H. Pinsonneault, Gustavo F. Porto de Mello, Francisco Prada, Abhishek Prakash, Adrian M. Price-Whelan, Pavlos Protopapas, M. Jordan Raddick, Mubdi Rahman, Beth A. Reid, James Rich, Hans-Walter Rix, Annie C. Robin, Constance M. Rockosi, Thaise S. Rodrigues, Sergio Rodríguez-Torres, Natalie A. Roe, Ashley J. Ross, Nicholas P. Ross, Graziano Rossi, John J. Ruan, J. A. Rubiño-Martín, Eli S. Rykoff, Salvador Salazar-Albornoz, Mara Salvato, Lado Samushia, Ariel G. Sánchez, Basilio Santiago, Conor Sayres, Ricardo P. Schiavon, David J. Schlegel, Sarah J. Schmidt, Donald P. Schneider, Mathias Schultheis, Axel D. Schwöpe, C. G. Scóccola, Caroline Scott, Kris Sellgren, Hee-Jong Seo, Aldo Serenelli, Neville Shane, Yue Shen, Matthew Shetrone, Yiping Shu, V. Silva Aguirre, Thirupathi Sivarani, M. F. Skrutskie, Anže Slosar, Verne V. Smith, Flávia Sobreira, Diogo Souto, Keivan G. Stassun, Matthias Steinmetz, Dennis Stello, Michael A. Strauss, Alina Streblyanska, Nao Suzuki, Molly E. C. Swanson, Jonathan C. Tan, Jamie Tayar, Ryan C. Terrien, Aniruddha R. Thakar, Daniel Thomas, Neil Thomas, Benjamin A. Thompson, Jeremy L. Tinker, Rita Tojeiro, Nicholas W. Troup, Mariana Vargas-Magaña, Jose A. Vazquez, Licia Verde, Matteo Viel, Nicole P. Vogt, David A. Wake, Ji Wang, Benjamin A. Weaver, David H. Weinberg, Benjamin J. Weiner, Martin White, John C. Wilson, John P. Wisniewski, W. M. Wood-Vasey, Christophe Ye'che, Donald G. York, Nadia L. Zakamska, O. Zamora, Gail Zasowski, Idit Zehavi, Gong-Bo Zhao, Zheng Zheng, Xu Zhou, Zhimin Zhou, Hu Zou, and Guangtun Zhu. The Eleventh and Twelfth Data Releases of the Sloan Digital Sky Survey: Final Data from SDSS-III. *ApJS*, 219(1):12, July 2015.
- 226 A. S. G. Robotham, P. Norberg, S. P. Driver, I. K. Baldry, S. P. Bamford, A. M. Hopkins, J. Liske, J. Loveday, A. Merson, J. A. Peacock, S. Brough, E. Cameron, C. J. Conselice, S. M. Croom, C. S. Frenk, M. Gunawardhana, D. T. Hill, D. H. Jones, L. S. Kelvin, K. Kuijken, R. C. Nichol, H. R. Parkinson, K. A. Pimblett, S. Phillipps, C. C. Popescu, M. Prescott, R. G. Sharp, W. J. Sutherland, E. N. Taylor, D. Thomas, R. J. Tuffs, E. van Kampen, and D. Wijesinghe. Galaxy and Mass Assembly (GAMA): the GAMA galaxy group catalogue (G^3Cv1). *MNRAS*, 416(4):2640–2668, October 2011.
- 227 Matthew Colless, Gavin Dalton, Steve Maddox, Will Sutherland, Peder Norberg, Shaun Cole, Joss Bland-Hawthorn, Terry Bridges, Russell Cannon, Chris Collins, Warrick Couch, Nicholas Cross, Kathryn Deeley, Roberto De Propris, Simon P. Driver, George Efstathiou, Richard S. Ellis, Carlos S. Frenk, Karl Glazebrook, Carole Jackson, Ofer Lahav, Ian Lewis, Stuart Lumsden, Darren Madgwick, John A. Peacock, Bruce A. Peterson, Ian Price, Mark Seaborne, and Keith Taylor. The 2dF Galaxy Redshift Survey: spectra and redshifts. *MNRAS*, 328(4):1039–1063, December 2001.
- 228 Michael J. Drinkwater, Russell J. Jurek, Chris Blake, David Woods, Kevin A. Pimblett, Karl Glazebrook, Rob Sharp, Michael B. Pracy, Sarah Brough, Matthew Colless, Warrick J. Couch, Scott M. Croom, Tamara M. Davis, Duncan Forbes, Karl Forster, David G. Gilbank, Michael Gladders, Ben Jelliffe, Nick Jones, I. Hui Li, Barry Madore, D. Christopher Martin, Gregory B. Poole, Todd Small, Emily Wisnioski, Ted Wyder, and H. K. C. Yee. The WiggleZ Dark Energy Survey: survey design and first data release. *MNRAS*, 401(3):1429–1452, January 2010.
- 229 S. P. Driver, J. Liske, N. J. G. Cross, R. De Propris, and P. D. Allen.

- The Millennium Galaxy Catalogue: the space density and surface-brightness distribution(s) of galaxies. *MNRAS*, 360(1):81–103, June 2005.
- 230 Stefania Barsanti, Matthew Colless, Charlotte Welker, Sree Oh, Sarah Casura, Julia J. Bryant, Scott M. Croom, Francesco D'Eugenio, Jon S. Lawrence, Samuel N. Richards, and Jesse van de Sande. The SAMI Galaxy Survey: flipping of the spin-filament alignment correlates most strongly with growth of the bulge. *arXiv e-prints*, page arXiv:2208.10767, August 2022.
- 231 H. Böhringer, P. Schuecker, L. Guzzo, C. A. Collins, W. Voges, R. G. Cruddace, A. Ortiz-Gil, G. Chincarini, S. De Grandi, A. C. Edge, H. T. MacGillivray, D. M. Neumann, S. Schindler, and P. Shaver. The ROSAT-ESO Flux Limited X-ray (REFLEX) Galaxy cluster survey. V. The cluster catalogue. *A&A*, 425:367–383, October 2004.
- 232 J. A. Frieman, M. S. Turner, and D. Huterer. Dark energy and the accelerating universe. *ARA&A*, 46:385–432, September 2008.
- 233 C. Adami, P. Giles, E. Koulouridis, F. Pacaud, C. A. Caretta, M. Pierre, D. Eckert, M. E. Ramos-Ceja, F. Gastaldello, S. Fotopoulou, V. Guglielmo, C. Lidman, T. Sadibekova, A. Iovino, B. Maughan, L. Chiappetti, S. Alis, B. Altieri, I. Baldry, D. Bottini, M. Birkinshaw, M. Bremer, M. Brown, O. Cucciati, S. Driver, E. Elmer, S. Ettori, A. E. Evrard, L. Faccioli, B. Granett, M. Grootes, L. Guzzo, A. Hopkins, C. Horellou, J. P. Lefèvre, J. Liske, K. Malek, F. Marulli, S. Maurogordato, M. Owers, S. Paltani, B. Poggianti, M. Polletta, M. Plionis, A. Pollo, E. Pompei, T. Ponman, D. Rapetti, M. Ricci, A. Robotham, R. Tuffs, L. Tasca, I. Valtchanov, D. Vergani, G. Wagner, J. Willis, and XXL Consortium. The XXL Survey. XX. The 365 cluster catalogue. *A&A*, 620:A5, November 2018.
- 234 A. Liu, E. Bulbul, V. Ghirardini, T. Liu, M. Klein, N. Clerc, Y. Özsoy, M. E. Ramos-Ceja, F. Pacaud, J. Comparat, N. Okabe, Y. E. Bahar, V. Biffi, H. Brunner, M. Brüggen, J. Buchner, J. Ider Chitham, I. Chiu, K. Dolag, E. Gattuzi, J. Gonzalez, D. N. Hoang, G. Lamer, A. Merloni, K. Nandra, M. Oguri, N. Ota, P. Predehl, T. H. Reiprich, M. Salvato, T. Schrabback, J. S. Sanders, R. Seppi, and Q. Thibaud. The eROSITA Final Equatorial-Depth Survey (eFEDS). Catalog of galaxy clusters and groups. *A&A*, 661:A2, May 2022.
- 235 S. Ettori, K. Dolag, S. Borgani, and G. Murante. The baryon fraction in hydrodynamical simulations of galaxy clusters. *MNRAS*, 365(3):1021–1030, January 2006.
- 236 W. Voges, B. Aschenbach, Th. Boller, H. Bräuninger, U. Briel, W. Burkert, K. Dennerl, J. Englhauser, R. Gruber, F. Haberl, G. Hartner, G. Hasinger, M. Kürster, E. Pfeffermann, W. Pietsch, P. Predehl, C. Rosso, J. H. M. M. Schmitt, J. Trümper, and H. U. Zimmermann. The ROSAT all-sky survey bright source catalogue. *A&A*, 349:389–405, September 1999.
- 237 A. Mantz, S. W. Allen, D. Rapetti, and H. Ebeling. The observed growth of massive galaxy clusters - I. Statistical methods and cosmological constraints. *MNRAS*, 406(3):1759–1772, August 2010.
- 238 Adam B. Mantz, Anja von der Linden, Steven W. Allen, Douglas E. Applegate, Patrick L. Kelly, R. Glenn Morris, David A. Rapetti, Robert W. Schmidt, Saroj Adhikari, Mark T. Allen, Patricia R. Burchat, David L. Burke, Matteo Cataneo, David Donovan, Harald Ebeling, Sarah Shandera, and Adam Wright. Weighing the giants - IV. Cosmology and neutrino mass. *MNRAS*, 446(3):2205–2225, January 2015.
- 239 P. Predehl, R. Andritschke, V. Arefiev, V. Babyshkin, O. Batanov, W. Becker, H. Böhringer, A. Bogomolov, T. Boller, K. Borm, W. Bornemann, H. Bräuninger, M. Brüggen, H. Brunner, M. Brusa, E. Bulbul, M. Buntov, V. Burwitz, W. Burkert, N. Clerc, E. Churazov, D. Coutinho, T. Dauser, K. Dennerl, V. Doroshenko, J. Eder, V. Emberger, T. Eraerds, A. Finoguenov, M. Freyberg, P. Friedrich, S. Friedrich, M. Fürmetz, A. Georgakakis, M. Gilfanov, S. Granato, C. Grossberger, A. Gueguen, P. Gureev, F. Haberl, O. Hälker, G. Hartner, G. Hasinger, H. Huber, L. Ji, A. v. Kienlin, W. Kink, F. Korotkov, I. Kreykenbohm, G. Lamer, I. Lomakin, I. Lapshov, T. Liu, C. Maitra, N. Meidinger, B. Menz, A. Merloni, T. Mernik, B. Mican, J. Mohr, S. Müller, K. Nandra, V. Nazarov, F. Pacaud, M. Pavlinsky, E. Perinati, E. Pfeffermann, D. Pietschner, M. E. Ramos-Ceja, A. Rau, J. Reiffers, T. H. Reiprich, J. Robrade, M. Salvato, J. Sanders, A. Santangelo, M. Sasaki, H. Scheuerle, C. Schmid, J. Schmitt, A. Schwobe, A. Shirshakov, M. Steinmetz, I. Stewart, L. Strüder, R. Sunyaev, C. Tenzer, L. Tiedemann, J. Trümper, V. Voron, P. Weber, J. Wilms, and V. Yaroshenko. The eROSITA X-ray telescope on SRG. *A&A*, 647:A1, March 2021.
- 240 eROSITA Team. Statement on the status of the erosita instrument aboard spektr-rg (srg), 2022.
- 241 Annalisa Pillepich, Cristiano Porciani, and Thomas H. Reiprich. The X-ray cluster survey with eRosita: forecasts for cosmology, cluster physics and primordial non-Gaussianity. *MNRAS*, 422(1):44–69, May 2012.
- 242 I. Non Chiu, Matthias Klein, Joseph Mohr, and Sebastian Bocquet. Cosmological constraints from galaxy clusters and groups in the eROSITA final equatorial depth survey. *MNRAS*, 522(2):1601–1642, June 2023.
- 243 F. Pacaud, M. Pierre, J. B. Melin, C. Adami, A. E. Evrard, S. Galli, F. Gastaldello, B. J. Maughan, M. Sereno, S. Alis, B. Altieri, M. Birkinshaw, L. Chiappetti, L. Faccioli, P. A. Giles, C. Horellou, A. Iovino, E. Koulouridis, J. P. Le Fèvre, C. Lidman, M. Lieu, S. Maurogordato, L. Moscardini, M. Plionis, B. M. Poggianti, E. Pompei, T. Sadibekova, I. Valtchanov, and J. P. Willis. The XXL Survey. XXV. Cosmological analysis of the C1 cluster number counts. *A&A*, 620:A10, November 2018.
- 244 I. K. Baldry, J. Liske, M. J. I. Brown, A. S. G. Robotham, S. P. Driver, L. Dunne, M. Alpaslan, S. Brough, M. E. Cluver, E. Eardley, D. J. Farrow, C. Heymans, H. Hildebrandt, A. M. Hopkins, L. S. Kelvin, J. Loveday, A. J. Moffett, P. Norberg, M. S. Owers, E. N. Taylor, A. H. Wright, S. P. Bamford, J. Bland-Hawthorn, N. Bourne, M. N. Bremer, M. Colless, C. J. Conselice, S. M. Croom, L. J. M. Davies, C. Foster, M. W. Grootes, B. W. Holwerda, D. H. Jones, P. R. Kafle, K. Kuijken, M. A. Lara-Lopez, Á. R. López-Sánchez, M. J. Meyer, S. Phillipps, W. J. Sutherland, E. van Kampen, and S. M. Wilkins. Galaxy And Mass Assembly: the G02 field, Herschel-ATLAS target selection and data release 3. *MNRAS*, 474(3):3875–3888, March 2018.
- 245 B. Garilli, L. Guzzo, M. Scodreggio, M. Bolzonella, U. Abbas, C. Adami, S. Arnouts, J. Bel, D. Bottini, E. Branchini, A. Cappi, J. Coupon, O. Cucciati, I. Davidzon, G. De Lucia, S. de la Torre, P. Franzetti, A. Fritz, M. Fumana, B. R. Granett, O. Ilbert, A. Iovino, J. Krywult, V. Le Brun, O. Le Fèvre, D. Maccagni, K. Malek, F. Marulli, H. J. McCracken, L. Paioro, M. Polletta, A. Pollo, H. Schlegelhauser, L. A. M. Tasca, R. Tojeiro, D. Vergani, G. Zamorani, A. Zanichelli, A. Burden, C. Di Porto, A. Marchetti, C. Marinoni, Y. Mellier, L. Moscardini, R. C. Nichol, J. A. Peacock, W. J. Percival, S. Phleps, and M. Wolk. The VIMOS Public Extragalactic Survey (VIPERS). First Data Release of 57 204 spectroscopic measurements. *A&A*, 562:A23, February 2014.
- 246 M. Hilton, C. Sifón, S. Naess, M. Madhavacheril, M. Oguri, E. Rozo, E. Rykoff, T. M. C. Abbott, S. Adhikari, M. Aguena, S. Aiola, S. Allam, S. Amodeo, A. Amon, J. Annis, B. Ansarinejad, C. Aros-Bunster, J. E. Austermann, S. Avila, D. Bacon, N. Battaglia, J. A. Beall, D. T. Becker, G. M. Bernstein, E. Bertin, T. Bhandarkar, S. Bhargava, J. R. Bond, D. Brooks, D. L. Burke, E. Calabrese, M. Carrasco Kind, J. Carretero, S. K. Choi, A. Choi, C. Conselice, L. N. da Costa, M. Costanzi, D. Crichton, K. T. Crowley, R. Dünner, E. V. Denison, M. J. Devlin, S. R. Dicker, H. T. Diehl, J. P. Dietrich, P. Doel, S. M. Duff, A. J. Duivenvoorden, J. Dunkley, S. Everett, S. Ferraro, I. Ferrero, A. Ferté, B. Flaugher, J. Frieman, P. A. Gallardo, J. García-Bellido, E. Gaztanaga, D. W. Gerdes, P. Giles, J. E. Golec, M. B. Gralla, S. Grandis, D. Gruen, R. A. Gruendl, J. Gschwend, G. Gutierrez, D. Han, W. G. Hartley, M. Hasselfield, J. C. Hill, G. C. Hilton, A. D. Hincks, S. R. Hinton, S. P. P. Ho,

- K. Honscheid, B. Hoyle, J. Hubmayr, K. M. Huffenberger, J. P. Hughes, A. T. Jaelani, B. Jain, D. J. James, T. Jeltema, S. Kent, K. Knowles, B. J. Koopman, K. Kuehn, O. Lahav, M. Lima, Y. T. Lin, M. Lokken, S. I. Loubser, N. MacCrann, M. A. G. Maia, T. A. Marriage, J. Martin, J. McMahon, P. Melchior, F. Menanteau, R. Miquel, H. Miyatake, K. Moodley, R. Morgan, T. Mroczkowski, F. Nati, L. B. Newburgh, M. D. Niemack, A. J. Nishizawa, R. L. C. Ogando, J. Orłowski-Scherer, L. A. Page, A. Palmese, B. Partridge, F. Paz-Chinchón, P. Phakathi, A. A. Plazas, N. C. Robertson, A. K. Romer, A. Carnero Rosell, M. Salatino, E. Sanchez, E. Schaan, A. Schillaci, N. Sehgal, S. Serrano, T. Shin, S. M. Simon, M. Smith, M. Soares-Santos, D. N. Spergel, S. T. Staggs, E. R. Storer, E. Suchyta, M. E. C. Swanson, G. Tarle, D. Thomas, C. To, H. Trac, J. N. Ullom, L. R. Vale, J. Van Lanen, E. M. Vavagiakis, J. De Vicente, R. D. Wilkinson, E. J. Wollack, Z. Xu, and Y. Zhang. The Atacama Cosmology Telescope: A Catalog of ~ 4000 Sunyaev-Zel'dovich Galaxy Clusters. *ApJS*, 253(1):3, March 2021.
- 247 Z. L. Wen and J. L. Han. Clusters of galaxies up to $z = 1.5$ identified from photometric data of the Dark Energy Survey and unWISE. *MNRAS*, 513(3):3946–3959, July 2022.
- 248 Michael R. Blanton, Matthew A. Bershady, Bela Abolfathi, Franco D. Albareti, Carlos Allende Prieto, Andres Almeida, Javier Alonso-García, Friedrich Anders, Scott F. Anderson, Brett Andrews, Erik Aquino-Ortiz, Alfonso Aragón-Salamanca, Maria Argudo-Fernández, Eric Armengaud, Eric Aubourg, Vladimir Avila-Reese, Carles Badenes, Stephen Bailey, Kathleen A. Barger, Jorge Barrera-Ballesteros, Curtis Bartosz, Dominic Bates, Falk Baumgarten, Julian Bautista, Rachael Beaton, Timothy C. Beers, Francesco Belfiore, Chad F. Bender, Andreas A. Berlind, Mariangela Bernardi, Florian Beutler, Jonathan C. Bird, Dmitry Bizyaev, Guillermo A. Blanc, Michael Blomqvist, Adam S. Bolton, Médéric Boquien, Jura Borissova, Remco van den Bosch, Jo Bovy, William N. Brandt, Jonathan Brinkmann, Joel R. Brownstein, Kevin Bundy, Adam J. Burgasser, Etienne Burtin, Nicolás G. Busca, Michele Cappellari, Maria Leticia Delgado Carigi, Joleen K. Carlberg, Aurelio Carnero Rosell, Ricardo Carrera, Nancy J. Chanover, Brian Cherinka, Edmond Cheung, Yilen Gómez Maqueo Chew, Cristina Chiappini, Peter Doohyun Choi, Drew Chojnowski, Chia-Hsun Chuang, Haeun Chung, Rafael Fernando Cirolini, Nicolas Clerc, Roger E. Cohen, Johan Comparat, Luiz da Costa, Marie-Claude Cousinou, Kevin Covey, Jeffrey D. Crane, Rupert A. C. Croft, Irene Cruz-Gonzalez, Daniel Garrido Cuadra, Katia Cunha, Guillermo J. Damke, Jeremy Darling, Roger Davies, Kyle Dawson, Axel de la Macorra, Flavia Dell'Agli, Nathan De Lee, Timothée Delubac, Francesco Di Mille, Aleks Diamond-Stanic, Mariana Cano-Díaz, John Donor, Juan José Downes, Niv Drory, Hélión du Mas des Bourboux, Christopher J. Duckworth, Tom Dwelly, Jamie Dyer, Garrett Ebelke, Arthur D. Eigenbrot, Daniel J. Eisenstein, Eric Emsellem, Mike Eracleous, Stephanie Escoffier, Michael L. Evans, Xiaohui Fan, Emma Fernández-Alvar, J. G. Fernandez-Trincado, Diane K. Feuillet, Alexis Finoguenov, Scott W. Fleming, Andreu Font-Ribera, Alexander Fredrickson, Gordon Freisclad, Peter M. Frinchaboy, Carla E. Fuentes, Lluís Galbany, R. García-Díaz, D. A. García-Hernández, Patrick Gaulme, Doug Geisler, Joseph D. Gelfand, Héctor Gil-Marín, Bruce A. Gillespie, Daniel Goddard, Violeta Gonzalez-Perez, Kathleen Grabowski, Paul J. Green, Catherine J. Grier, James E. Gunn, Hong Guo, Julien Guy, Alex Hagen, ChangHoon Hahn, Matthew Hall, Paul Harding, Sten Hasselquist, Suzanne L. Hawley, Fred Hartly, Jonay I. Gonzalez Hernández, Shirley Ho, David W. Hogg, Kelly Holley-Bockelmann, Jon A. Holtzman, Parker H. Holzer, Joseph Huehnerhoff, Timothy A. Hutchinson, Ho Seong Hwang, Héctor J. Ibarra-Medel, Gabriele da Silva Ilha, Inese I. Ivans, Ke-Shawn Ivory, Kelly Jackson, Trey W. Jensen, Jennifer A. Johnson, Amy Jones, Henrik Jönsson, Eric Jullo, Vikrant Kamble, Karen Kinemuchi, David Kirkby, Francisco-Shu Kitaura, Mark Klaene, Gillian R. Knapp, Jean-Paul Kneib, Juna A. Kollmeier, Ivan Lacerna, Richard R. Lane, Dustin Lang, David R. Law, Daniel Lazarz, Youngbae Lee, Jean-Marc Le Goff, Fu-Heng Liang, Cheng Li, Hongyu Li, Jianhui Lian, Marcos Lima, Lihwai Lin, Yen-Ting Lin, Sara Bertran de Lis, Chao Liu, Miguel Angel C. de Icaza Lizaola, Dan Long, Sara Lucatello, Britt Lundgren, Nicholas K. MacDonald, Alice Deconto Machado, Chelsea L. MacLeod, Suvrath Mahadevan, Marcio Antonio Geimba Maia, Roberto Maiolino, Steven R. Majewski, Elena Malanushenko, Viktor Malanushenko, Arturo Machado, Shude Mao, Claudia Maraston, Rui Marques-Chaves, Thomas Masseron, Karen L. Masters, Cameron K. McBride, Richard M. McDermid, Brianne McGrath, Ian D. McGreer, Nicolás Medina Peña, Matthew Melendez, Andrea Merloni, Michael R. Merrifield, Szabolcs Meszaros, Andres Meza, Ivan Minchev, Dante Minniti, Takamitsu Miyaji, Surhud More, John Mulchaey, Francisco Müller-Sánchez, Demitri Muna, Ricardo R. Munoz, Adam D. Myers, Preethi Nair, Kirpal Nandra, Janaina Correa do Nascimento, Alenka Negrete, Melissa Ness, Jeffrey A. Newman, Robert C. Nichol, David L. Nidever, Christian Nitschelm, Pierros Ntelis, Julia E. O'Connell, Ryan J. Oelkers, Audrey Oravetz, Daniel Oravetz, Zach Pace, Nelson Padilla, Nathalie Palanque-Delabrouille, Pedro Alonso Palicio, Kaike Pan, John K. Parejko, Taniya Parikh, Isabelle Pâris, Changbom Park, Alim Y. Patten, Sebastien Peirani, Marcos Pellejero-Ibanez, Samantha Penny, Will J. Percival, Ismael Perez-Fourmon, Patrick Petitjean, Matthew M. Pieri, Marc Pinsonneault, Alice Pisani, Radosław Poleski, Francisco Prada, Abhishek Prakash, Anna Bárbara de Andrade Queiroz, M. Jordan Raddick, Anand Raichoor, Sandro Barboza Rembold, Hannah Richtstein, Rogemar A. Riffel, Rogério Riffel, Hans-Walter Rix, Annie C. Robin, Constance M. Rockosi, Sergio Rodríguez-Torres, A. Roman-Lopes, Carlos Román-Zúñiga, Margarita Rosado, Ashley J. Ross, Graziano Rossi, John Ruan, Rossana Ruggeri, Eli S. Rykoff, Salvador Salazar-Albornoz, Mara Salvato, Ariel G. Sánchez, D. S. Aguado, José R. Sánchez-Gallego, Felipe A. Santana, Basilio Xavier Santiago, Conor Sayres, Ricardo P. Schiavon, Jaderson da Silva Schimoia, Edward F. Schlafly, David J. Schlegel, Donald P. Schneider, Mathias Schultheis, William J. Schuster, Axel Schwobe, Hee-Jong Seo, Zhengyi Shao, Shiyin Shen, Matthew Shetrone, Michael Shull, Joshua D. Simon, Danielle Skinner, M. F. Skrutskie, Anže Slosar, Verne V. Smith, Jennifer S. Sobek, Flavia Sobreira, Garrett Somers, Diogo Souto, David V. Stark, Keivan Stassun, Fritz Stauffer, Matthias Steinmetz, Thaisa Storchi-Bergmann, Alina Streblyanska, Guy S. Stringfellow, Genaro Suárez, Jing Sun, Nao Suzuki, Laszlo Szigeti, Manuchehr Taghizadeh-Popp, Baitian Tang, Charling Tao, Jamie Tayar, Mita Tembe, Johanna Teske, Aniruddha R. Thakar, Daniel Thomas, Benjamin A. Thompson, Jeremy L. Tinker, Patricia Tissera, Rita Tojeiro, Hector Hernandez Toledo, Sylvain de la Torre, Christy Tremonti, Nicholas W. Troup, Octavio Valenzuela, Inma Martinez Valpuesta, Jaime Vargas-González, Mariana Vargas-Magaña, Jose Alberto Vazquez, Sandro Villanova, M. Vivek, Nicole Vogt, David Wake, Rene Walterbos, Yuting Wang, Benjamin Alan Weaver, Anne-Marie Weijmans, David H. Weinberg, Kyle B. Westfall, David G. Whelan, Vivienne Wild, John Wilson, W. M. Wood-Vasey, Dominika Wylezalek, Ting Xiao, Renbin Yan, Meng Yang, Jason E. Ybarra, Christophe Yèche, Nadia Zakamska, Olga Zamora, Pauline Zarrouk, Gail Zasowski, Kai Zhang, Gong-Bo Zhao, Zheng Zheng, Zheng Zheng, Xu Zhou, Zhi-Min Zhou, Guangtun B. Zhu, Manuela Zoccali, and Hu Zou. Sloan Digital Sky Survey IV: Mapping the Milky Way, Nearby Galaxies, and the Distant Universe. *AJ*, 154(1):28, July 2017.
- 249 Edward L. Wright, Peter R. M. Eisenhardt, Amy K. Mainzer, Michael E. Ressler, Roc M. Cutri, Thomas Jarrett, J. Davy Kirkpatrick, Deborah Padgett, Robert S. McMillan, Michael Skrutskie, S. A. Stanford, Martin Cohen, Russell G. Walker, John C. Mather, David Leisawitz, III Gautier, Thomas N., Ian McLean, Dominic Benford, Carol J. Lonsdale, Andrew Blain, Bryan Mendez, William R.

- Trace, Valerie Duval, Fengchuan Liu, Don Royer, Ingolf Heinrichsen, Joan Howard, Mark Shannon, Martha Kendall, Amy L. Walsh, Mark Larsen, Joel G. Cardon, Scott Schick, Mark Schwalm, Mohamed Abid, Beth Fabinsky, Larry Naes, and Chao-Wei Tsai. The Wide-field Infrared Survey Explorer (WISE): Mission Description and Initial On-orbit Performance. *AJ*, 140(6):1868–1881, December 2010.
- 250 Luciana Bianchi, Bernie Shiao, and David Thilker. Revised Catalog of GALEX Ultraviolet Sources. I. The All-Sky Survey: GUVcat_AIS. *ApJS*, 230(2):24, June 2017.
- 251 T. Erben, H. Hildebrandt, L. Miller, L. van Waerbeke, C. Heymans, H. Hoekstra, T. D. Kitching, Y. Mellier, J. Benjamin, C. Blake, C. Bonnett, O. Cordes, J. Coupon, L. Fu, R. Gavazzi, B. Gillis, E. Grocutt, S. D. J. Gwyn, K. Holmberg, M. J. Hudson, M. Kilbinger, K. Kuijken, M. Milkeraitis, B. T. P. Rowe, T. Schrabback, E. Semboloni, P. Simon, M. Smit, O. Toader, S. Vafaei, E. van Uitert, and M. Velander. CFHTLenS: the Canada-France-Hawaii Telescope Lensing Survey - imaging data and catalogue products. *MNRAS*, 433(3):2545–2563, August 2013.
- 252 A. B. Mantz, S. W. Allen, R. G. Morris, D. A. Rapetti, D. E. Applegate, P. L. Kelly, A. von der Linden, and R. W. Schmidt. Cosmology and astrophysics from relaxed galaxy clusters - II. Cosmological constraints. *MNRAS*, 440(3):2077–2098, May 2014.
- 253 Adam B Mantz, R Glenn Morris, Steven W Allen, Rebecca EA Canning, Lucie Baumont, Bradford Benson, Lindsey E Bleem, Steven R Ehlert, Benjamin Floyd, Ricardo Herbonnet, et al. Cosmological constraints from gas mass fractions of massive, relaxed galaxy clusters. *Monthly Notices of the Royal Astronomical Society*, 510(1):131–145, 2022.
- 254 Riccardo Giacconi, Herbert Gursky, Frank R. Paolini, and Bruno B. Rossi. Evidence for x Rays From Sources Outside the Solar System. *Phys. Rev. Lett.*, 9(11):439–443, December 1962.
- 255 C. S. Bowyer, G. B. Field, and J. E. Mack. Detection of an Anisotropic Soft X-ray Background Flux. *Nature*, 217(5123):32–34, January 1968.
- 256 A. N. Bunner, P. C. Coleman, W. L. Kraushaar, D. McCammon, T. M. Palmieri, A. Shilepsky, and M. Ulmer. Soft X-Ray Background Flux. *Nature*, 223(5212):1222–1226, September 1969.
- 257 Ray Weymann. Possible Thermal Histories of Intergalactic Gas. *ApJ*, 147:887, March 1967.
- 258 R. C. Henry, G. Fritz, J. F. Meekins, H. Friedman, and E. T. Byram. Possible Detection of a Dense Intergalactic Plasma. *ApJ*, 153:L11, July 1968.
- 259 W. T. Sanders, Richard J. Edgar, W. L. Kraushaar, D. McCammon, and J. P. Morgenthaler. Spectra of the 1/4 keV X-Ray Diffuse Background from the Diffuse X-Ray Spectrometer Experiment. *ApJ*, 554(2):694–709, June 2001.
- 260 M. Hurwitz, T. P. Sasseen, and M. M. Sirk. Observations of Diffuse Extreme-Ultraviolet Emission with the Cosmic Hot Interstellar Plasma Spectrometer (CHIPS). *ApJ*, 623(2):911–916, April 2005.
- 261 Massimiliano Galeazzi, Meng Chiao, Michael R. Collier, Thomas Cravens, Dimitra Koutroumpa, Kip D. Kuntz, Susan Lepri, Dan McCammon, Frederick S. Porter, Krishna Prasai, Ina Robertson, Steve Snowden, and Youaraj Uprety. DXL: a sounding rocket mission for the study of solar wind charge exchange and local hot bubble X-ray emission. *Experimental Astronomy*, 32(2):83–99, November 2011.
- 262 M. Galeazzi, M. Chiao, M. R. Collier, T. Cravens, D. Koutroumpa, K. D. Kuntz, R. Lallement, S. T. Lepri, D. McCammon, K. Morgan, F. S. Porter, I. P. Robertson, S. L. Snowden, N. E. Thomas, Y. Uprety, E. Ursino, and B. M. Walsh. The origin of the local 1/4-keV X-ray flux in both charge exchange and a hot bubble. *Nature*, 512(7513):171–173, August 2014.
- 263 P. Kaaret, A. Zajczyk, D. M. LaRocca, R. Ringuette, J. Bluem, W. Fuelberth, H. Gulick, K. Jahoda, T. E. Johnson, D. L. Kirchner, D. Koutroumpa, K. D. Kuntz, R. McCurdy, D. M. Miles, W. T. Robinson, and E. M. Silich. HaloSat: A CubeSat to Study the Hot Galactic Halo. *ApJ*, 884(2):162, October 2019.
- 264 R. Lallement. On the contribution of charge-exchange induced X-ray emission in the ISM and ICM. *A&A*, 422:391–400, August 2004.
- 265 D. Koutroumpa, R. Lallement, J. C. Raymond, and V. Kharchenko. The Solar Wind Charge-Transfer X-Ray Emission in the 1/4 keV Energy Range: Inferences on Local Bubble Hot Gas at Low Z . *ApJ*, 696(2):1517–1525, May 2009.
- 266 Ina P. Robertson, Kip D. Kuntz, Michael R. Collier, Thomas E. Cravens, and Steven L. Snowden. The Heliospheric Contribution to the Soft X-ray Background Emission. In Randall K. Smith, Steven L. Snowden, and K. D. Kuntz, editors, *The Local Bubble and Beyond II*, volume 1156 of *American Institute of Physics Conference Series*, pages 52–61, August 2009.
- 267 Francesco Haardt and Piero Madau. Radiative Transfer in a Clumpy Universe. IV. New Synthesis Models of the Cosmic UV/X-Ray Background. *ApJ*, 746(2):125, February 2012.
- 268 Vikram Khaire and Raghunathan Srikanand. New synthesis models of consistent extragalactic background light over cosmic time. *MNRAS*, 484(3):4174–4199, April 2019.
- 269 Claude-André Faucher-Giguère. A cosmic UV/X-ray background model update. *MNRAS*, 493(2):1614–1632, April 2020.
- 270 S. L. Snowden, R. Egger, M. J. Freyberg, D. McCammon, P. P. Plucinsky, W. T. Sanders, J. H. M. M. Schmitt, J. Trümper, and W. Voges. ROSAT Survey Diffuse X-Ray Background Maps. II. *ApJ*, 485(1):125–135, August 1997.
- 271 W. T. Sanders, W. L. Kraushaar, J. A. Nousek, and P. M. Fried. Soft diffuse X-rays in the southern galactic hemisphere. *ApJ*, 217:L87–L91, October 1977.
- 272 Donald P. Cox and Ronald J. Reynolds. The local interstellar medium. *ARA&A*, 25:303–344, January 1987.
- 273 S. L. Snowden, C. Heiles, D. Koutroumpa, K. D. Kuntz, R. Lallement, D. McCammon, and J. E. G. Peek. Revisiting the Local Leo Cold Cloud and Revised Constraints on the Local Hot Bubble. *ApJ*, 806(1):119, June 2015.
- 274 S. L. Snowden, D. Koutroumpa, K. D. Kuntz, R. Lallement, and L. Puspitarini. The North Galactic Pole Rift and the Local Hot Bubble. *ApJ*, 806(1):120, June 2015.
- 275 W. Liu, M. Chiao, M. R. Collier, T. Cravens, M. Galeazzi, D. Koutroumpa, K. D. Kuntz, R. Lallement, S. T. Lepri, D. McCammon, K. Morgan, F. S. Porter, S. L. Snowden, N. E. Thomas, Y. Uprety, E. Ursino, and B. M. Walsh. The Structure of the Local Hot Bubble. *ApJ*, 834(1):33, January 2017.
- 276 Catherine Zucker, Alyssa A. Goodman, João Alves, Shmuel Bialy, Michael Foley, Joshua S. Speagle, Josefa Großschedl, Douglas P. Finkbeiner, Andreas Burkert, Diana Khimey, and Cameren Swiggum. Star formation near the Sun is driven by expansion of the Local Bubble. *Nature*, 601(7893):334–337, January 2022.
- 277 Dallas Wulf, Megan E. Eckart, Massimiliano Galeazzi, Felix Jaeckel, Richard L. Kelley, Caroline A. Kilbourne, Kelsey M. Morgan, F. Scott Porter, Dan McCammon, and Andrew E. Szymkowiak. A High Spectral Resolution Study of the Soft X-Ray Background with the X-Ray Quantum Calorimeter. *ApJ*, 884(2):120, October 2019.
- 278 Y. Uprety, M. Chiao, M. R. Collier, T. Cravens, M. Galeazzi, D. Koutroumpa, K. D. Kuntz, R. Lallement, S. T. Lepri, W. Liu, D. McCammon, K. Morgan, F. S. Porter, K. Prasai, S. L. Snowden, N. E. Thomas, E. Ursino, and B. M. Walsh. Solar Wind Charge Exchange Contribution to the ROSAT All Sky Survey Maps. *ApJ*, 829(2):83, October 2016.
- 279 Edward B. Jenkins. Pressure and Ionization Balances in the Circum-Heliospheric Interstellar Medium and the Local Bubble. *Space Sci. Rev.*, 143(1-4):205–216, March 2009.
- 280 Jr. Spitzer, Lyman. On a Possible Interstellar Galactic Corona. *ApJ*, 124:20, July 1956.
- 281 J. Truemper. The ROSAT mission. *Advances in Space Research*, 2(4):241–249, January 1982.

- 282 S. L. Snowden, M. J. Freyberg, P. P. Plucinsky, J. H. M. M. Schmitt, J. Truemper, W. Voges, R. J. Edgar, D. McCammon, and W. T. Sanders. First Maps of the Soft X-Ray Diffuse Background from the ROSAT XRT/PSPC All-Sky Survey. *ApJ*, 454:643, December 1995.
- 283 D. McCammon, R. Almy, E. Apodaca, W. Bergmann Tiest, W. Cui, S. Deiker, M. Galeazzi, M. Juda, A. Lesser, T. Mihara, J. P. Morgenthaler, W. T. Sanders, J. Zhang, E. Figueroa-Feliciano, R. L. Kelley, S. H. Moseley, R. F. Mushotzky, F. S. Porter, C. K. Stahle, and A. E. Szymkowiak. A High Spectral Resolution Observation of the Soft X-Ray Diffuse Background with Thermal Detectors. *ApJ*, 576(1):188–203, September 2002.
- 284 A. E. Hornschemeier, W. N. Brandt, G. P. Garmire, D. P. Schneider, S. S. Broos, L. K. Townsley, M. W. Bautz, D. N. Burrows, G. Chartas, E. D. Feigelson, R. Griffiths, D. Lumb, J. A. Nousek, and W. L. W. Sargent. X-Ray Sources in the Hubble Deep Field Detected by Chandra. *ApJ*, 541(1):49–53, September 2000.
- 285 D. Henley and R. Shelton. An XMM-Newton Survey of the Soft X-Ray Background. II. An All-Sky Catalog of Diffuse O VII and O VIII Emission Intensities. *ApJS*, 202:14, October 2012.
- 286 A. Gupta, S. Mathur, Y. Krongold, F. Nicastro, and M. Galeazzi. A Huge Reservoir of Ionized Gas around the Milky Way: Accounting for the Missing Mass? *ApJ*, 756:L8, September 2012.
- 287 M. J. Miller and J. N. Bregman. The Structure of the Milky Way's Hot Gas Halo. *ApJ*, 770:118, June 2013.
- 288 Sanskriti Das, Smita Mathur, Fabrizio Nicastro, and Yair Krongold. Discovery of a Very Hot Phase of the Milky Way Circumgalactic Medium with Non-solar Abundance Ratios. *ApJ*, 882(2):L23, September 2019.
- 289 P. Predehl, R. A. Sunyaev, W. Becker, H. Brunner, R. Burtenin, A. Bykov, A. Cherepashchuk, N. Chugai, E. Churazov, V. Doroshenko, N. Eismont, M. Freyberg, M. Gilfanov, F. Haberl, I. Khabibullin, R. Krivonos, C. Maitra, P. Medvedev, A. Merloni, K. Nandra, V. Nazarov, M. Pavlinsky, G. Ponti, J. S. Sanders, M. Sasaki, S. Sazonov, A. W. Strong, and J. Wilms. Detection of large-scale X-ray bubbles in the Milky Way halo. *Nature*, 588(7837):227–231, January 2020.
- 290 Sanskriti Das, Smita Mathur, Anjali Gupta, and Yair Krongold. The Hot Circumgalactic Medium of the Milky Way: Evidence for Super-virial, Virial, and Subvirial Temperatures; Nonsolar Chemical Composition; and Nonthermal Line Broadening. *ApJ*, 918(2):83, September 2021.
- 291 Sanskriti Das, Smita Mathur, Anjali Gupta, Fabrizio Nicastro, and Yair Krongold. Multiple Temperature Components of the Hot Circumgalactic Medium of the Milky Way. *ApJ*, 887(2):257, December 2019.
- 292 Jesse Bluem, Philip Kaaret, K. D. Kuntz, Keith M. Jahoda, Dimitra Koutroumpa, Edmund J. Hodges-Kluck, Chase A. Fuller, Daniel M. LaRocca, and Anna Zajczyk. Widespread Detection of Two Components in the Hot Circumgalactic Medium of the Milky Way. *ApJ*, 936(1):72, September 2022.
- 293 A. Moretti, S. Campana, D. Lazzati, and G. Tagliaferri. The Resolved Fraction of the Cosmic X-Ray Background. *ApJ*, 588(2):696–703, May 2003.
- 294 M. A. Worsley, A. C. Fabian, F. E. Bauer, D. M. Alexander, G. Hasinger, S. Mateos, H. Brunner, W. N. Brandt, and D. P. Schneider. The unresolved hard X-ray background: the missing source population implied by the Chandra and XMM-Newton deep fields. *MNRAS*, 357(4):1281–1287, March 2005.
- 295 Ryan C. Hickox and Maxim Markevitch. Absolute Measurement of the Unresolved Cosmic X-Ray Background in the 0.5–8 keV Band with Chandra. *ApJ*, 645(1):95–114, July 2006.
- 296 B. D. Lehmer, Y. Q. Xue, W. N. Brandt, D. M. Alexander, F. E. Bauer, M. Brusa, A. Comastri, R. Gilli, A. E. Hornschemeier, B. Luo, M. Paolillo, A. Ptak, O. Shemmer, D. P. Schneider, P. Tozzi, and C. Vignali. The 4 Ms Chandra Deep Field-South Number Counts Apportioned by Source Class: Pervasive Active Galactic Nuclei and the Ascent of Normal Galaxies. *ApJ*, 752(1):46, June 2012.
- 297 Y. Q. Xue, S. X. Wang, W. N. Brandt, B. Luo, D. M. Alexander, F. E. Bauer, A. Comastri, A. C. Fabian, R. Gilli, B. D. Lehmer, D. P. Schneider, C. Vignali, and M. Young. Tracking down the Source Population Responsible for the Unresolved Cosmic 6–8 keV Background. *ApJ*, 758(2):129, October 2012.
- 298 S. Mineo, M. Gilfanov, and R. Sunyaev. X-ray emission from star-forming galaxies - II. Hot interstellar medium. *MNRAS*, 426(3):1870–1883, November 2012.
- 299 Renyue Cen and Jeremiah P. Ostriker. Where Are the Baryons? *ApJ*, 514(1):1–6, March 1999.
- 300 E. Treister, C. Megan Urry, and Shanil Virani. The Space Density of Compton-Thick Active Galactic Nucleus and the X-Ray Background. *ApJ*, 696(1):110–120, May 2009.
- 301 T. E. Cravens. Comet Hyakutake x-ray source: Charge transfer of solar wind heavy ions. *Geophys. Res. Lett.*, 24(1):105–108, January 1997.
- 302 S. L. Snowden, D. McCammon, D. N. Burrows, and J. A. Mendenhall. Analysis Procedures for ROSAT XRT/PSPC Observations of Extended Objects and the Diffuse Background. *ApJ*, 424:714, April 1994.
- 303 I. P. Robertson and T. E. Cravens. X-ray emission from the terrestrial magnetosheath. *Geophys. Res. Lett.*, 30(8):1439, April 2003.
- 304 D. Koutroumpa, R. Lallement, V. Kharchenko, A. Dalgarno, R. Pepino, V. Izmodenov, and E. Quémerais. Charge-transfer induced EUV and soft X-ray emissions in the heliosphere. *A&A*, 460(1):289–300, December 2006.
- 305 D. Koutroumpa, F. Acero, R. Lallement, J. Ballet, and V. Kharchenko. OVII and OVIII line emission in the diffuse soft X-ray background: heliospheric and galactic contributions. *A&A*, 475(3):901–914, December 2007.
- 306 D. Bodewits, D. J. Christian, M. Torney, M. Dryer, C. M. Lisse, K. Dennerl, T. H. Zurbuchen, S. J. Wolk, A. G. G. M. Tielens, and R. Hoekstra. Spectral analysis of the Chandra comet survey. *A&A*, 469(3):1183–1195, July 2007.
- 307 D. Koutroumpa, M. R. Collier, K. D. Kuntz, R. Lallement, and S. L. Snowden. Solar Wind Charge Exchange Emission from the Helium Focusing Cone: Model to Data Comparison. *ApJ*, 697(2):1214–1225, June 2009.
- 308 S. L. Snowden, M. R. Collier, T. Cravens, K. D. Kuntz, S. T. Lepri, I. Robertson, and L. Tomas. Observation of solar wind charge exchange emission from exospheric material in and outside Earth's magnetosheath 2008 september 25. *ApJ*, 691(2):372–381, January 2009.
- 309 R. Ringuette, D. Koutroumpa, K. D. Kuntz, P. Kaaret, K. Jahoda, D. LaRocca, M. Kounkel, J. Richardson, A. Zajczyk, and J. Bluem. HaloSat Observations of Heliospheric Solar Wind Charge Exchange. *ApJ*, 918(2):41, September 2021.
- 310 Rosine Lallement. Some Observations Related to the Origin and Evolution of the Local Bubble/Local ISM. *Space Sci. Rev.*, 143(1–4):427–436, March 2009.
- 311 T. R. Sun, C. Wang, H. K. Connor, A. M. Jorgensen, and S. Sembay. Deriving the magnetopause position for the soft X-ray image by using the tangent fitting approach. *J. Geophys. Res.: Spac. Phys.*, 125:e2020JA028169, September 2020.
- 312 J. H. M. M. Schmitt, S. L. Snowden, B. Aschenbach, G. Hasinger, E. Pfeffermann, P. Predehl, and J. Truemper. A soft x-ray image of the Moon. *Nature*, 349(1):583–587, February 1991.
- 313 B. J. Wargelin, M. Markevitch, M. Juda, V. Kharchenko, R. Edgar, and A. Dalgarno. Chandra observation of the "dark" Moon and geocoronal solar wind charge transfer. *ApJ*, 607:596–610, May 2004.
- 314 Jacco Vink. Supernova remnants: the X-ray perspective. *A&ARv*, 20:49, December 2012.

- 315 K. Maeda, F. K. Röpke, M. Fink, W. Hillebrandt, C. Travaglio, and F. K. Thielemann. Nucleosynthesis in Two-Dimensional Delayed Detonation Models of Type Ia Supernova Explosions. *ApJ*, 712(1):624–638, March 2010.
- 316 Ivo R. Seitenzahl, Franco Ciaraldi-Schoolmann, Friedrich K. Röpke, Michael Fink, Wolfgang Hillebrandt, Markus Kromer, Rüdiger Pakmor, Ashley J. Ruiter, Stuart A. Sim, and Stefan Taubenberger. Three-dimensional delayed-detonation models with nucleosynthesis for Type Ia supernovae. *MNRAS*, 429(2):1156–1172, February 2013.
- 317 Ken'ichi Nomoto, Nozomu Tominaga, Hideyuki Umeda, Chiaki Kobayashi, and Keiichi Maeda. Nucleosynthesis yields of core-collapse supernovae and hypernovae, and galactic chemical evolution. *Nuclear Phys. A*, 777:424–458, October 2006.
- 318 Tuguldur Sukhbold, T. Ertl, S. E. Woosley, Justin M. Brown, and H. T. Janka. Core-collapse Supernovae from 9 to 120 Solar Masses Based on Neutrino-powered Explosions. *ApJ*, 821(1):38, April 2016.
- 319 Ping Zhou and Jacco Vink. Asymmetric Type-Ia supernova origin of W49B as revealed from spatially resolved X-ray spectroscopic study. *A&A*, 615:A150, July 2018.
- 320 J. Vink, J. S. Kaastra, and J. A. M. Bleeker. A new mass estimate and puzzling abundances of SNR Cassiopeia A. *A&A*, 307:L41–L44, March 1996.
- 321 Stephen P. Reynolds, Kazimierz J. Borkowski, Una Hwang, John P. Hughes, Carles Badenes, J. M. Laming, and J. M. Blondin. A Deep Chandra Observation of Kepler's Supernova Remnant: A Type Ia Event with Circumstellar Interaction. *ApJ*, 668(2):L135–L138, October 2007.
- 322 Lei Sun and Yang Chen. Spatially Resolved X-Ray Spectroscopy of Kepler's Supernova Remnant: Distinct Properties of the Circumstellar Medium and the Ejecta. *ApJ*, 872(1):45, February 2019.
- 323 Jiang-Tao Li, Anne Decourchelle, Marco Miceli, Jacco Vink, and Fabrizio Bocchino. XMM-Newton large program on SN1006 - I. Methods and initial results of spatially resolved spectroscopy. *MNRAS*, 453(4):3953–3974, November 2015.
- 324 Lei Sun, Jacco Vink, Yang Chen, Ping Zhou, Dmitry Prokhorov, Gerd Pühlhofer, and Denys Malyshev. The Post-impact Evolution of the X-Ray-emitting Gas in SNR 1987A as Viewed by XMM-Newton. *ApJ*, 916(1):41, July 2021.
- 325 Masahiro T. Kawasaki, Masanobu Ozaki, Fumiaki Nagase, Kuniaki Masai, Manabu Ishida, and Robert Petre. ASCA Observations of the Supernova Remnant IC 443: Thermal Structure and Detection of Overionized Plasma. *ApJ*, 572(2):897–905, June 2002.
- 326 H. Yamaguchi, M. Ozawa, K. Koyama, K. Masai, J. S. Hiraga, M. Ozaki, and D. Yonetoku. Discovery of Strong Radiative Recombination Continua from the Supernova Remnant IC 443 with Suzaku. *ApJ*, 705(1):L6–L9, November 2009.
- 327 Takao Ohnishi, Katsuji Koyama, Takeshi Go Tsuru, Kuniaki Masai, Hiroya Yamaguchi, and Midori Ozawa. X-Ray Spectrum of a Peculiar Supernova Remnant, G359.1-0.5. *PASJ*, 63:527, June 2011.
- 328 Makoto Sawada and Katsuji Koyama. X-Ray Observations of the Supernova Remnant W28 with Suzaku. I. Spectral Study of the Recombining Plasma. *PASJ*, 64:81, August 2012.
- 329 Hiroyuki Uchida, Katsuji Koyama, Hiroya Yamaguchi, Makoto Sawada, Takao Ohnishi, Takeshi Go Tsuru, Takaaki Tanaka, Satoshi Yoshiike, and Yasuo Fukui. Recombining Plasma and Hard X-Ray Filament in the Mixed-Morphology Supernova Remnant W 44. *PASJ*, 64:141, December 2012.
- 330 Lei Sun and Yang Chen. An XMM-Newton X-Ray View of Supernova Remnant W49B: Revisiting Its Recombining Plasmas and Progenitor Type. *ApJ*, 893(2):90, April 2020.
- 331 Shigeo Yamauchi, Masayoshi Nobukawa, and Katsuji Koyama. A systematic comparison of ionization temperatures between ionizing and recombining plasmas in supernova remnants. *PASJ*, 73(3):728–734, June 2021.
- 332 Hiroshi Itoh and Kuniaki Masai. The effect of a circumstellar medium on the X-ray emission of young remnants of type II supernovae. *MNRAS*, 236:885–899, February 1989.
- 333 Xin Zhou, Marco Miceli, Fabrizio Bocchino, Salvatore Orlando, and Yang Chen. Unveiling the spatial structure of the overionized plasma in the supernova remnant W49B. *MNRAS*, 415(1):244–250, July 2011.
- 334 Gao-Yuan Zhang, Jonathan D. Slavin, Adam Foster, Randall K. Smith, John A. Zuhone, Ping Zhou, and Yang Chen. Nonequilibrium Ionization in Mixed-morphology Supernova Remnants. *ApJ*, 875(2):81, April 2019.
- 335 Sjors Broersen and Jacco Vink. A Chandra X-ray study of the mixed-morphology supernova remnant 3C 400.2. *MNRAS*, 446(4):3885–3894, February 2015.
- 336 Miho Katsuragawa, Shinya Nakashima, Hideaki Matsumura, Takaaki Tanaka, Hiroyuki Uchida, Shiu-Hang Lee, Yasunobu Uchiyama, Masanori Arakawa, and Tadayuki Takahashi. Suzaku X-ray observations of the mixed-morphology supernova remnant CTB 1. *PASJ*, 70(6):110, December 2018.
- 337 R. A. Chevalier, R. P. Kirshner, and J. C. Raymond. The optical emission from a fast shock wave with application to supernova remnants. *ApJ*, 235:186–195, January 1980.
- 338 Parviz Ghavamian, John Raymond, R. Chris Smith, and Patrick Hartigan. Balmer-dominated Spectra of Nonradiative Shocks in the Cygnus Loop, RCW 86, and Tycho Supernova Remnants. *ApJ*, 547(2):995–1009, February 2001.
- 339 Satoru Katsuda, Hiroshi Tsunemi, Koji Mori, Hiroyuki Uchida, Hiroko Kosugi, Masashi Kimura, Hiroshi Nakajima, Satoru Takakura, Robert Petre, John W. Hewitt, and Hiroya Yamaguchi. Possible Charge-exchange X-ray Emission in the Cygnus Loop Detected with Suzaku. *ApJ*, 730(1):24, March 2011.
- 340 Shawn R. Roberts and Q. Daniel Wang. X-ray emission from charge exchange in the Cygnus Loop SNR. *MNRAS*, 449(2):1340–1346, May 2015.
- 341 H. Uchida, S. Katsuda, H. Tsunemi, K. Mori, L. Gu, R. S. Cumbee, R. Petre, and T. Tanaka. High Forbidden-to-resonance Line Ratio of O VII Discovered from the Cygnus Loop. *ApJ*, 871(2):234, February 2019.
- 342 Satoru Katsuda, Hiroshi Tsunemi, Koji Mori, Hiroyuki Uchida, Robert Petre, Shin'ya Yamada, Hiroki Akamatsu, Saori Konami, and Toru Tamagawa. High-resolution X-Ray Spectroscopy of the Galactic Supernova Remnant Puppis A with XMM-Newton/RGS. *ApJ*, 756(1):49, September 2012.
- 343 Yukiko Tanaka, Hiroyuki Uchida, Takaaki Tanaka, Yuki Amano, Yosuke Koshihara, Takeshi Go Tsuru, Hidetoshi Sano, and Yasuo Fukui. Charge Exchange X-Ray Emission Detected in Multiple Shells of Supernova Remnant G296.1-0.5. *ApJ*, 933(1):101, July 2022.
- 344 A. P. Rasmussen, E. Behar, S. M. Kahn, J. W. den Herder, and K. van der Heyden. The X-ray spectrum of the supernova remnant JAS-TROBJ₁E 0102.2-7219. *A&A*, 365:L231–L236, January 2001.
- 345 Hitomi Suzuki, Hiroya Yamaguchi, Manabu Ishida, Hiroyuki Uchida, Paul P. Plucinsky, Adam R. Foster, and Eric D. Miller. Plasma Diagnostics of the Supernova Remnant N132D using Deep XMM-Newton Observations with the Reflection Grating Spectrometer. *ApJ*, 900(1):39, September 2020.
- 346 Yosuke Koshihara, Hiroyuki Uchida, Takaaki Tanaka, Yuki Amano, Hidetoshi Sano, and Takeshi Go Tsuru. High-resolution X-ray study of supernova remnant J0453.6-6829 with unusually high forbidden-to-resonance ratio. *PASJ*, 74(4):757–766, August 2022.
- 347 J. S. Kaastra and R. Mewe. Optical depth effects in the X-ray emission from supernova remnants. *A&A*, 302:L13, October 1995.
- 348 N. A. Levenson, James R. Graham, Luke D. Keller, and Matthew J. Richter. Panoramic Views of the Cygnus Loop. *ApJS*, 118(2):541–561, October 1998.

- 349 William P. Blair, Ravi Sankrit, and John C. Raymond. Hubble Space Telescope Imaging of the Primary Shock Front in the Cygnus Loop Supernova Remnant. *AJ*, 129(5):2268–2280, May 2005.
- 350 H. Xu, S. M. Kahn, J. R. Peterson, E. Behar, F. B. S. Paerels, R. F. Mushotzky, J. G. Jernigan, A. C. Brinkman, and K. Makishima. High-Resolution Observations of the Elliptical Galaxy NGC 4636 with the Reflection Grating Spectrometer on Board XMM-Newton. *ApJ*, 579(2):600–606, November 2002.
- 351 Yang Chen, Q. Daniel Wang, Gao-Yuan Zhang, Shuinai Zhang, and Li Ji. Resonant Scattering Effect on the Soft X-Ray Line Emission from the Hot Interstellar Medium. I. Galactic Bulges. *ApJ*, 861(2):138, July 2018.
- 352 Hitomi Collaboration, Felix Aharonian, Hiroki Akamatsu, Fumie Akimoto, Steven W. Allen, Lorella Angelini, Marc Audard, Hisamitsu Awaki, Magnus Axelsson, Aya Bamba, Marshall W. Bautz, Roger Blandford, Laura W. Brenneman, Gregory V. Brown, Esra Bulbul, Edward M. Cackett, Maria Chernyakova, Meng P. Chiao, Paolo S. Coppi, Elisa Costantini, Jelle de Plaa, Cor P. de Vries, Jan-Willem den Herder, Chris Done, Tadayasu Dotani, Ken Ebisawa, Megan E. Eckart, Teruaki Enoto, Yuichiro Ezoe, Andrew C. Fabian, Carlo Ferrigno, Adam R. Foster, Ryuichi Fujimoto, Yasushi Fukazawa, Maki Furukawa, Akihiro Furuzawa, Massimiliano Galeazzi, Luigi C. Gallo, Poshak Gandhi, Margherita Giustini, Andrea Goldwurm, Liyi Gu, Matteo Guainazzi, Yoshito Haba, Kouichi Hagino, Kenji Hamaguchi, Ilana M. Harrus, Isamu Hatsukade, Katsuhiro Hayashi, Takayuki Hayashi, Kiyoshi Hayashida, Junko S. Hiraga, Ann Hornschemeier, Akio Hoshino, John P. Hughes, Yuto Ichinohe, Ryo Iizuka, Hajime Inoue, Yoshiyuki Inoue, Manabu Ishida, Kumi Ishikawa, Yoshitaka Ishisaki, Masachika Iwai, Jelle Kaastra, Tim Kallman, Tsuneyoshi Kamae, Jun Kataoka, Satoru Katsuda, Nobuyuki Kawai, Richard L. Kelley, Caroline A. Kilbourne, Takao Kitaguchi, Shunji Kitamoto, Tetsu Kitayama, Takayoshi Kohmura, Motohide Kokubun, Katsuji Koyama, Shu Koyama, Peter Kretschmar, Hans A. Krimm, Aya Kubota, Hideyo Kunieda, Philippe Laurent, Shiu-Hang Lee, Maurice A. Leutenegger, Olivier O. Limousin, Michael Loewenstein, Knox S. Long, David Lumb, Greg Madejski, Yoshitomo Maeda, Daniel Maier, Kazuo Makishima, Maxim Markevitch, Hironori Matsumoto, Kyoko Matsushita, Dan McCammon, Brian R. McNamara, Missagh Mehdipour, Eric D. Miller, Jon M. Miller, Shin Mineshige, Kazuhisa Mitsuda, Ikuyuki Mitsuishi, Takuya Miyazawa, Tsunefumi Mizuno, Hideyuki Mori, Koji Mori, Koji Mukai, Hiroshi Murakami, Richard F. Mushotzky, Takao Nakagawa, Hiroshi Nakajima, Takeshi Nakamori, Shinya Nakashima, Kazuhiro Nakazawa, Kumiko K. Nobukawa, Masayoshi Nobukawa, Hirofumi Noda, Hirokazu Odaka, Anna Ogorzalek, Takaya Ohashi, Masanori Ohno, Takashi Okajima, Naomi Ota, Masanobu Ozaki, Frits Paerels, Stéphane Paltani, Robert Petre, Ciro Pinto, Frederick S. Porter, Katja Pottschmidt, Christopher S. Reynolds, Samar Safi-Harb, Shinya Saito, Kazuhiro Sakai, Toru Sasaki, Goro Sato, Kosuke Sato, Rie Sato, Makoto Sawada, Norbert Schartel, Peter J. Serlemitsos, Hiromi Seta, Megumi Shidatsu, Aurora Simionescu, Randall K. Smith, Yang Soong, Łukasz Stawarz, Yasuharu Sugawara, Satoshi Sugita, Andrew Szymkowiak, Hiroyasu Tajima, Hiromitsu Takahashi, Tadayuki Takahashi, Shin'ichiro Takeda, Yoh Takei, Toru Tamagawa, Takayuki Tamura, Takaaki Tanaka, Yasuo Tanaka, Yasuyuki T. Tanaka, Makoto S. Tashiro, Yuzuru Tawara, Yukikatsu Terada, Yuichi Terashima, Francesco Tombesi, Hiroshi Tomida, Yohko Tsuboi, Masahiro Tsujimoto, Hiroshi Tsunemi, Takeshi Go Tsuru, Hiroyuki Uchida, Hideki Uchiyama, Yasunobu Uchiyama, Shutaro Ueda, Yoshihiro Ueda, Shin'ichiro Uno, C. Megan Urry, Eugenio Ursino, Shin Watanabe, Norbert Werner, Dan R. Wilkins, Brian J. Williams, Shinya Yamada, Hiroya Yamaguchi, Kazutaka Yamaoka, Noriko Y. Yamasaki, Makoto Yamauchi, Shigeo Yamauchi, Tahir Yaqoob, Yoichi Yatsu, Daisuke Yonetoku, Irina Zhuravleva, and Abderahmen Zoghbi. Measurements of resonant scattering in the Perseus Cluster core with Hitomi SXS. *PASJ*, 70(2):10, March 2018.
- 353 Yuki Amano, Hiroyuki Uchida, Takaaki Tanaka, Liyi Gu, and Takeshi Go Tsuru. Evidence for Resonance Scattering in the X-Ray Grating Spectrum of the Supernova Remnant N49. *ApJ*, 897(1):12, July 2020.
- 354 James M. Lattimer and Madappa Prakash. Neutron star observations: Prognosis for equation of state constraints. *Phys. Rep.*, 442(1-6):109–165, April 2007.
- 355 Andrew W. Steiner, James M. Lattimer, and Edward F. Brown. The Neutron Star Mass-Radius Relation and the Equation of State of Dense Matter. *ApJ*, 765(1):L5, March 2013.
- 356 Lai Xiaoyu and Xu Renxin. Strangeon and Strangeon Star. In *Journal of Physics Conference Series*, volume 861 of *Journal of Physics Conference Series*, page 012027, June 2017.
- 357 Feryal Özel and Paulo Freire. Masses, Radii, and the Equation of State of Neutron Stars. *ARA&A*, 54:401–440, September 2016.
- 358 P. B. Demorest, T. Pennucci, S. M. Ransom, M. S. E. Roberts, and J. W. T. Hessels. A two-solar-mass neutron star measured using Shapiro delay. *Nature*, 467(7319):1081–1083, October 2010.
- 359 Shuang-Nan Zhang, Jinyuan Liao, and Yangsen Yao. Measuring the black hole masses in accreting X-ray binaries by detecting the Doppler orbital motion of their accretion disc wind absorption lines. *MNRAS*, 421(4):3550–3556, April 2012.
- 360 Gabriele Ponti, Stefano Bianchi, Teo Muñoz-Darias, and Kirpal Nandra. Measuring masses in low mass X-ray binaries via X-ray spectroscopy: the case of MXB 1659-298. *MNRAS*, 481(1):L94–L99, November 2018.
- 361 A. A. Nucita, S. Stefanelli, F. De Paolis, N. Masetti, G. Ingrassia, M. Del Santo, and L. Manni. The puzzling symbiotic X-ray system 4U1700+24. *A&A*, 562:A55, February 2014.
- 362 Ren-Xin Xu. A solution to the puzzling symbiotic X-ray system 4U 1700+24. *Research in Astronomy and Astrophysics*, 14(6):617–624, June 2014.
- 363 Duncan K. Galloway and Laurens Keek. Thermonuclear X-ray Bursts. In Tomaso M. Belloni, Mariano Méndez, and Chengmin Zhang, editors, *Astrophysics and Space Science Library*, volume 461 of *Astrophysics and Space Science Library*, pages 209–262, January 2021.
- 364 Andrew Cumming and Lars Bildsten. Carbon Flashes in the Heavy-Element Ocean on Accreting Neutron Stars. *ApJ*, 559(2):L127–L130, October 2001.
- 365 J. Cottam, F. Paerels, and M. Mendez. Gravitationally redshifted absorption lines in the X-ray burst spectra of a neutron star. *Nature*, 420(6911):51–54, November 2002.
- 366 Duncan K. Galloway, Jinrong Lin, Deepto Chakrabarty, and Jacob M. Hartman. Discovery of a 552 Hz Burst Oscillation in the Low-Mass X-Ray Binary EXO 0748-676. *ApJ*, 711(2):L148–L151, March 2010.
- 367 J. J. M. in 't Zand, T. Bagnoli, C. D'Angelo, A. Patruno, D. K. Galloway, M. B. M. van der Klis, A. L. Watts, and H. L. Marshall. Chandra spectroscopy of Rapid Burster type-I X-ray bursts. *arXiv e-prints*, page arXiv:1703.07221, March 2017.
- 368 T. Rauch, V. Suleimanov, and K. Werner. Absorption features in the spectra of X-ray bursting neutron stars. *A&A*, 490(3):1127–1134, November 2008.
- 369 Frank Haberl. The magnificent seven: magnetic fields and surface temperature distributions. *Ap&SS*, 308(1-4):181–190, April 2007.
- 370 V. Burwitz, V. E. Zavlin, R. Neuhäuser, P. Predehl, J. Trümper, and A. C. Brinkman. The Chandra LETGS high resolution X-ray spectrum of the isolated neutron star RX J1856.5-3754. *A&A*, 379:L35–L38, November 2001.
- 371 W. C. G. Ho, D. L. Kaplan, P. Chang, M. van Adelsberg, A. Y. Potekhin, and G. Chabrier. Magnetic Hydrogen Atmosphere Models and the Neutron Star RX J1856.5-3754. In *American Astronomical Society Meeting Abstracts*, volume 207 of *American Astronomical*

- Society Meeting Abstracts*, page 198.03, December 2005.
- 372 Weiyang Wang, Jiguang Lu, Hao Tong, Mingyu Ge, Zhaosheng Li, Yunpeng Men, and Renxin Xu. The Optical/UV Excess of X-Ray-dim Isolated Neutron Stars. I. Bremsstrahlung Emission from a Strageon Star Atmosphere. *ApJ*, 837(1):81, March 2017.
- 373 Victoria M. Kaspi. Recent progress on anomalous X-ray pulsars. *Ap&SS*, 308(1-4):1–11, April 2007.
- 374 Sandro Mereghetti. Pulsars and Magnetars. *Brazilian Journal of Physics*, 43(5-6):356–368, December 2013.
- 375 Andrea Tiengo, Paolo Esposito, Sandro Mereghetti, Roberto Turolla, Luciano Nobili, Fabio Gastaldello, Diego Götz, Gian Luca Israel, Nanda Rea, Luigi Stella, Silvia Zane, and Giovanni F. Bignami. A variable absorption feature in the X-ray spectrum of a magnetar. *Nature*, 500(7462):312–314, August 2013.
- 376 S. Sazonov, M. Revnivtsev, M. Gilfanov, E. Churazov, and R. Sunyaev. X-ray luminosity function of faint point sources in the Milky Way. *A&A*, 450(1):117–128, April 2006.
- 377 K. Mukai, A. Kinkhabwala, J. R. Peterson, S. M. Kahn, and F. Paerels. Two types of x-ray spectra in cataclysmic variables. *The Astrophysical Journal*, 586(1):L77–L80, mar 2003.
- 378 Dirk Pandel, France A. Cordova, Keith O. Mason, and William C. Priedhorsky. X-ray observations of the boundary layer in dwarf novae at low accretion rates. *The Astrophysical Journal*, 626(1):396–410, jun 2005.
- 379 Manuel Güdel and Yaël Nazé. X-ray spectroscopy of stars. *A&ARv*, 17(3):309–408, September 2009.
- 380 Kensuke Masui, Kazuhisa Mitsuda, Noriko Y. Yamasaki, Yoh Takei, Shunsuke Kimura, Tomotaka Yoshino, and Dan McCammon. The Nature of Unresolved Soft X-Ray Emission from the Galactic Disk. *PASJ*, 61:S115, January 2009.
- 381 Paola Testa, Jeremy J. Drake, and Giovanni Peres. The Density of Coronal Plasma in Active Stellar Coronae. *ApJ*, 617(1):508–530, December 2004.
- 382 C. P. Johnstone and M. Güdel. The coronal temperatures of low-mass main-sequence stars. *A&A*, 578:A129, June 2015.
- 383 N. Pizzolato, A. Maggio, G. Micela, S. Sciortino, and P. Ventura. The stellar activity-rotation relationship revisited: Dependence of saturated and non-saturated X-ray emission regimes on stellar mass for late-type dwarfs. *A&A*, 397:147–157, January 2003.
- 384 Nicholas J. Wright, Jeremy J. Drake, Eric E. Mamajek, and Gregory W. Henry. The Stellar-activity-Rotation Relationship and the Evolution of Stellar Dynamos. *ApJ*, 743(1):48, December 2011.
- 385 Manuel Güdel. X-ray astronomy of stellar coronae. *A&ARv*, 12(2-3):71–237, September 2004.
- 386 R. Nordon and E. Behar. Abundance variations and first ionization potential trends during large stellar flares. *A&A*, 482(2):639–651, May 2008.
- 387 A. Reiners, M. Schüssler, and V. M. Passegger. Generalized Investigation of the Rotation-Activity Relation: Favoring Rotation Period instead of Rossby Number. *ApJ*, 794(2):144, October 2014.
- 388 M. Mittag, J. H. M. M. Schmitt, and K. P. Schröder. Revisiting the connection between magnetic activity, rotation period, and convective turnover time for main-sequence stars. *A&A*, 618:A48, October 2018.
- 389 Natalie R. Hinkel, Eric E. Mamajek, Margaret C. Turnbull, Ella Osby, Evgenya L. Shkolnik, Graeme H. Smith, Alexis Klimasewski, Garrett Somers, and Steven J. Desch. A Catalog of Stellar Unified Properties (CATSUP) for 951 FGK-Stars within 30 pc. *ApJ*, 848(1):34, October 2017.
- 390 M. Güdel, M. Audard, F. Reale, S. L. Skinner, and J. L. Linsky. Flares from small to large: X-ray spectroscopy of Proxima Centauri with XMM-Newton. *A&A*, 416:713–732, March 2004.
- 391 C. Liefke, B. Fuhrmeister, and J. H. M. M. Schmitt. Multiwavelength observations of a giant flare on CN Leonis. III. Temporal evolution of coronal properties. *A&A*, 514:A94, May 2010.
- 392 Frederik B. S. Paerels and Steven M. Kahn. High-Resolution X-Ray Spectroscopy with CHANDRA and XMM-NEWTON. *ARA&A*, 41:291–342, January 2003.
- 393 D. Porquet, J. Dubau, and N. Grosso. He-like Ions as Practical Astrophysical Plasma Diagnostics: From Stellar Coronae to Active Galactic Nuclei. *Space Sci. Rev.*, 157(1-4):103–134, December 2010.
- 394 Sylvain Veilleux, Gerald Cecil, and Joss Bland-Hawthorn. Galactic Winds. *ARA&A*, 43(1):769–826, September 2005.
- 395 Jacco Vink. Supernova remnants: the X-ray perspective. *A&ARv*, 20:49, December 2012.
- 396 N. Werner, B. R. McNamara, E. Churazov, and E. Scannapieco. Hot Atmospheres, Cold Gas, AGN Feedback and the Evolution of Early Type Galaxies: A Topical Perspective. *Space Sci. Rev.*, 215(1):5, January 2019.
- 397 A. C. Brinkman, C. J. T. Gunsing, J. S. Kaastra, R. L. J. van der Meer, R. Mewe, F. Paerels, A. J. J. Raassen, J. J. van Rooijen, H. Bräuninger, W. Burkert, V. Burwitz, G. Hartner, P. Predehl, J. U. Ness, J. H. M. M. Schmitt, J. J. Drake, O. Johnson, M. Juda, V. Kashyap, S. S. Murray, D. Pease, P. Ratzlaff, and B. J. Wargelin. First Light Measurements of Capella with the Low-Energy Transmission Grating Spectrometer aboard the Chandra X-Ray Observatory. *ApJ*, 530(2):L111–L114, February 2000.
- 398 J. W. den Herder, A. C. Brinkman, S. M. Kahn, G. Branduardi-Raymont, K. Thomsen, H. Aarts, M. Audard, J. V. Bixler, A. J. den Boggende, J. Cottam, T. Decker, L. Dubbeldam, C. Erd, H. Goulooze, M. Güdel, P. Guttridge, C. J. Hailey, K. Al Janabi, J. S. Kaastra, P. A. J. de Korte, B. J. van Leeuwen, C. Mauche, A. J. McCalden, R. Mewe, A. Naber, F. B. Paerels, J. R. Peterson, A. P. Rasmussen, K. Rees, I. Sakelliou, M. Sako, J. Spodek, M. Stern, T. Tamura, J. Tandy, C. P. de Vries, S. Welch, and A. Zehnder. The Reflection Grating Spectrometer on board XMM-Newton. *A&A*, 365:L7–L17, January 2001.
- 399 Claude R. Canizares, John E. Davis, Daniel Dewey, Kathryn A. Flanagan, Eugene B. Galton, David P. Huenemoerder, Kazunori Ishibashi, Thomas H. Markert, Herman L. Marshall, Michael McGuirk, Mark L. Schattenburg, Norbert S. Schulz, Henry I. Smith, and Michael Wise. The Chandra High-Energy Transmission Grating: Design, Fabrication, Ground Calibration, and 5 Years in Flight. *PASP*, 117(836):1144–1171, October 2005.
- 400 J. S. Kaastra, F. B. S. Paerels, F. Durret, S. Schindler, and P. Richter. Thermal Radiation Processes. *Space Sci. Rev.*, 134(1-4):155–190, February 2008.
- 401 Junjie Mao and Jelle Kaastra. Parameterization of the level-resolved radiative recombination rate coefficients for the SPEX code. *A&A*, 587:A84, March 2016.
- 402 Randall K. Smith, Nancy S. Brickhouse, Duane A. Liedahl, and John C. Raymond. Collisional Plasma Models with APEC/APED: Emission-Line Diagnostics of Hydrogen-like and Helium-like Ions. *ApJ*, 556(2):L91–L95, August 2001.
- 403 A. R. Foster, L. Ji, R. K. Smith, and N. S. Brickhouse. Updated Atomic Data and Calculations for X-Ray Spectroscopy. *ApJ*, 756(2):128, September 2012.
- 404 R. K. Smith, A. R. Foster, and N. S. Brickhouse. Approximating the X-ray spectrum emitted from astrophysical charge exchange. *Astronomische Nachrichten*, 333(4):301, April 2012.
- 405 Randall K. Smith and John P. Hughes. Ionization Equilibrium Timescales in Collisional Plasmas. *ApJ*, 718(1):583–585, July 2010.
- 406 K. P. Dere, E. Landi, H. E. Mason, B. C. Monsignori Fossi, and P. R. Young. CHIANTI - an atomic database for emission lines. *A&AS*, 125:149–173, October 1997.
- 407 G. Del Zanna, K. P. Dere, P. R. Young, and E. Landi. CHIANTI—An Atomic Database for Emission Lines. XVI. Version 10, Further Extensions. *ApJ*, 909(1):38, March 2021.
- 408 G. J. Ferland, K. T. Korista, D. A. Verner, J. W. Ferguson, J. B. Kingdon, and E. M. Verner. CLOUDY 90: Numerical Simulation of Plas-

- mas and Their Spectra. *PASP*, 110(749):761–778, July 1998.
- 409 G. J. Ferland, M. Chatzikos, F. Guzmán, M. L. Lykins, P. A. M. van Hoof, R. J. R. Williams, N. P. Abel, N. R. Badnell, F. P. Keenan, R. L. Porter, and P. C. Stancil. The 2017 Release Cloudy. *Rev. Mex. Astron. Astrofis.*, 53:385–438, October 2017.
- 410 J. S. Kaastra, R. Mewe, and H. Nieuwenhuijzen. SPEX: a new code for spectral analysis of X & UV spectra. In *UV and X-ray Spectroscopy of Astrophysical and Laboratory Plasmas*, pages 411–414, January 1996.
- 411 J. S. Kaastra, A. J. J. Raassen, J. de Plaa, and Liyi Gu. SPEX X-ray spectral fitting package. Zenodo, December 2020.
- 412 G. Y. Liang, F. Li, F. L. Wang, Y. Wu, J. Y. Zhong, and G. Zhao. X-Ray and EUV Spectroscopy of Various Astrophysical and Laboratory Plasmas: Collisional, Photoionization and Charge-exchange Plasmas. *ApJ*, 783(2):124, March 2014.
- 413 G. Y. Liang, F. Li, F. L. Wang, Y. Wu, J. Y. Zhong, and G. Zhao. A simulation package—SASAL for x-ray and EUV spectroscopy of Astrophysical and Laboratory Plasmas. *Research in Astronomy and Astrophysics*, 14(10):1352, October 2014.
- 414 T. Kallman and M. Bautista. Photoionization and High-Density Gas. *ApJS*, 133(1):221–253, March 2001.
- 415 Claudio Mendoza, Manuel A. Bautista, Jérôme Deprince, Javier A. García, Efraín Gatuzz, Thomas W. Gorczyca, Timothy R. Kallman, Patrick Palmeri, Pascal Quinet, and Michael C. Witthoef. The XSTAR Atomic Database. *Atoms*, 9(1):12, February 2021.
- 416 J. Mao, F. Mernier, J. S. Kaastra, L. Gu, M. Mehdipour, and J. de Plaa. The impact of improved plasma diagnostics on modeling the X-ray Universe. *Journal of Instrumentation*, 14(7):C07012, July 2019.
- 417 Junjie Mao, G. Del Zanna, Liyi Gu, C. Y. Zhang, and N. R. Badnell. R-matrix Electron-impact Excitation Data for the H- and He-like Ions with $Z = 6-30$. *ApJS*, 263(2):35, December 2022.
- 418 N. R. Badnell, G. Del Zanna, L. Fernández-Menchero, A. S. Giunta, G. Y. Liang, H. E. Mason, and P. J. Storey. Atomic processes for astrophysical plasmas. *Journal of Physics B Atomic Molecular Physics*, 49(9):094001, May 2016.
- 419 Gabriele Betancourt-Martinez, Hiroki Akamatsu, Didier Barret, Manuel Bautista, Sven Bernitt, Stefano Bianchi, Dennis Bodewits, Nancy Brickhouse, Gregory V. Brown, Elisa Costantini, Marcello Coreno, José R. Crespo López-Urrutia, Renata Cumbee, Megan Eckart, Gary Ferland, Fabrizio Fiore, Michael Fogle, Adam Foster, Javier Garcia, Tom Gorczyca, Victoria Grinberg, Nicolas Grosso, Liyi Gu, Ming Feng Gu, Matteo Guainazzi, Natalie Hell, Jan-Willem den Herder, Jelle Kaastra, Timothy Kallman, Julia Lee, Maurice Leutenegger, Joan Marler, Dan McCammon, Shinya Nakashima, Fabrizio Nicastro, Frits Paerels, François Pajot, Etienne Pointecouteau, Delphine Porquet, F. Scott Porter, Daniel Wolf Savin, Makoto Sawada, Chintan Shah, Aurora Simionescu, Monica de Simone, Chad Sosolik, Phillip Stancil, René Steinbrügge, and Hiroya Yamaguchi. Unlocking the Capabilities of Future High-Resolution X-ray Spectroscopy Missions Through Laboratory Astrophysics. *BAAS*, 51(3):337, May 2019.
- 420 Randall Smith, Michael Hahn, John Raymond, T. Kallman, C. P. Balance, Vanessa Polito, Giulio Del Zanna, Liyi Gu, Natalie Hell, Renata Cumbee, Gabriele Betancourt-Martinez, Elisa Costantini, and Lia Corrales. Roadmap on cosmic EUV and x-ray spectroscopy. *Journal of Physics B Atomic Molecular Physics*, 53(9):092001, May 2020.
- 421 Hitomi Collaboration, Felix Aharonian, Hiroki Akamatsu, Fumie Akimoto, Steven W. Allen, Naohisa Anabuki, Lorella Angelini, Keith Arnaud, Marc Audard, Hisamitsu Awaki, Magnus Axelsson, Aya Bamba, Marshall Bautz, Roger Blandford, Laura Brenneman, Gregory V. Brown, Esra Bulbul, Edward Cackett, Maria Chernyakova, Meng Chiao, Paolo Coppi, Elisa Costantini, Jelle de Plaa, Jan-Willem den Herder, Chris Done, Tadayasu Dotani, Ken Ebisawa, Megan Eckart, Teruaki Enoto, Yuichiro Ezoe, Andrew C. Fabian, Carlo Ferrigno, Adam R. Foster, Ryuichi Fujimoto, Yasushi Fukazawa, Akihiro Furuzawa, Massimiliano Galeazzi, Luigi C. Gallo, Poshak Gandhi, Margherita Giustini, Andrea Goldwurm, Liyi Gu, Matteo Guainazzi, Yoshito Haba, Kouichi Hagino, Kenji Hamaguchi, Ilana M. Harrus, Isamu Hatsukade, Katsuhiro Hayashi, Takayuki Hayashi, Kiyoshi Hayashida, Natalie Hell, Junko S. Hiraga, Ann Hornschemeier, Akio Hoshino, John P. Hughes, Yuto Ichidrew C. Fabian, Carlo Ferrigno, Adam Foster, Ryuichi Fujimoto, Yasushi Fukazawa, Akihiro Furuzawa, Massimiliano Galeazzi, Luigi Gallo, Poshak Gandhi, Margherita Giustini, Andrea Goldwurm, Liyi Gu, Matteo Guainazzi, Yoshito Haba, Kouichi Hagino, Kenji Hamaguchi, Ilana Harrus, Isamu Hatsukade, Katsuhiro Hayashi, Takayuki Hayashi, Kiyoshi Hayashida, Junko Hiraga, Ann Hornschemeier, Akio Hoshino, John Hughes, Ryo Iizuka, Hajime Inoue, Yoshiyuki Inoue, Kazunori Ishibashi, Manabu Ishida, Kumi Ishikawa, Yoshitaka Ishisaki, Masayuki Itoh, Naoko Iyomoto, Jelle Kaastra, Timothy Kallman, Tuneyoshi Kamae, Erin Kara, Jun Kataoka, Satoru Katsuda, Junichiro Katsuta, Madoka Kawaharada, Nobuyuki Kawai, Richard Kelley, Dmitry Khangulyan, Caroline Kilbourne, Ashley King, Takao Kitaguchi, Shunji Kitamoto, Tetsu Kitayama, Takayoshi Kohmura, Motohide Kokubun, Shu Koyama, Katsuji Koyama, Peter Kretschmar, Hans Krimm, Aya Kubota, Hideyo Kunieda, Philippe Laurent, François Lebrun, Shiu-Hang Lee, Maurice Leutenegger, Olivier Limousin, Michael Loewenstein, Knox S. Long, David Lumb, Grzegorz Madejski, Yoshitomo Maeda, Daniel Maier, Kazuo Makishima, Maxim Markevitch, Hironori Matsumoto, Kyoko Matsushita, Dan McCammon, Brian McNamara, Missagh Mehdipour, Eric Miller, Jon Miller, Shin Mineshige, Kazuhisa Mitsuda, Ikuyuki Mitsuishi, Takuya Miyazawa, Tsunefumi Mizuno, Hideyuki Mori, Koji Mori, Harvey Moseley, Koji Mukai, Hiroshi Murakami, Toshio Murakami, Richard Mushotzky, Ryo Nagino, Takao Nakagawa, Hiroshi Nakajima, Takeshi Nakamori, Toshio Nakano, Shinya Nakashima, Kazuhiro Nakazawa, Masayoshi Nobukawa, Hirofumi Noda, Masaharu Nomachi, Steve O’Dell, Hirokazu Odaka, Takaya Ohashi, Masanori Ohno, Takashi Okajima, Naomi Ota, Masanobu Ozaki, Frits Paerels, Stephane Paltani, Arvind Parmar, Robert Petre, Ciro Pinto, Martin Pohl, F. Scott Porter, Katja Pottschmidt, Brian Ramsey, Christopher Reynolds, Helen Russell, Samar Safi-Harb, Shinya Saito, Kazuhiro Sakai, Hiroaki Sameshima, Goro Sato, Kosuke Sato, Rie Sato, Makoto Sawada, Norbert Schartel, Peter Serlemitsos, Hiromi Seta, Megumi Shidatsu, Aurora Simionescu, Randall Smith, Yang Soong, Lukasz Stawarz, Yasuharu Sugawara, Satoshi Sugita, Andrew Szymkowiak, Hiroyasu Tajima, Hiromitsu Takahashi, Tadayuki Takahashi, Shin’Ichiro Takeda, Yoh Takei, Toru Tamagawa, Keisuke Tamura, Takayuki Tamura, Takaaki Tanaka, Yasuo Tanaka, Yasuyuki Tanaka, Makoto Tashiro, Yuzuru Tawara, Yukikatsu Terada, Yuichi Terashima, Francesco Tombesi, Hiroshi Tomida, Yohko Tsuboi, Masahiro Tsujimoto, Hiroshi Tsunemi, Takeshi Tsuru, Hiroyuki Uchida, Hideki Uchiyama, Yasunobu Uchiyama, Shutaro Ueda, Yoshihiro Ueda, Shiro Ueno, Shin’Ichiro Uno, Meg Urry, Eugenio Ursino, Cor de Vries, Shin Watanabe, Norbert Werner, Daniel Wik, Dan Wilkins, Brian Williams, Shinya Yamada, Hiroya Yamaguchi, Kazutaka Yamaoka, Noriko Y. Yamasaki, Makoto Yamauchi, Shigeo Yamauchi, Tahir Yaqoob, Yoichi Yatsu, Daisuke Yonetoku, Atsumasa Yoshida, Takayuki Yuasa, Irina Zhuravleva, and Abderahmen Zoghbi. The quiescent intracluster medium in the core of the Perseus cluster. *Nature*, 535(7610):117–121, July 2016.
- 422 Hitomi Collaboration, Felix Aharonian, Hiroki Akamatsu, Fumie Akimoto, Steven W. Allen, Lorella Angelini, Marc Audard, Hisamitsu Awaki, Magnus Axelsson, Aya Bamba, Marshall W. Bautz, Roger Blandford, Laura W. Brenneman, Gregory V. Brown, Esra Bulbul, Edward M. Cackett, Maria Chernyakova, Meng P. Chiao, Paolo S. Coppi, Elisa Costantini, Jelle de Plaa, Cor P. de Vries, Jan-Willem den Herder, Chris Done, Tadayasu Dotani, Ken Ebisawa, Megan E. Eckart, Teruaki Enoto, Yuichiro Ezoe, Andrew C. Fabian, Carlo Ferrigno, Adam R. Foster, Ryuichi Fujimoto, Yasushi Fukazawa, Akihiro Furuzawa, Massimiliano Galeazzi, Luigi C. Gallo, Poshak Gandhi, Margherita Giustini, Andrea Goldwurm, Liyi Gu, Matteo Guainazzi, Yoshito Haba, Kouichi Hagino, Kenji Hamaguchi, Ilana M. Harrus, Isamu Hatsukade, Katsuhiro Hayashi, Takayuki Hayashi, Kiyoshi Hayashida, Natalie Hell, Junko S. Hiraga, Ann Hornschemeier, Akio Hoshino, John P. Hughes, Yuto Ichi-

- nohe, Ryo Iizuka, Hajime Inoue, Yoshiyuki Inoue, Manabu Ishida, Kumi Ishikawa, Yoshitaka Ishisaki, Masachika Iwai, Jelle Kaastra, Tim Kallman, Tsuneyoshi Kamae, Jun Kataoka, Satoru Katsuda, Nobuyuki Kawai, Richard L. Kelley, Caroline A. Kilbourne, Takao Kitaguchi, Shunji Kitamoto, Tetsu Kitayama, Takayoshi Kohmura, Motohide Kokubun, Katsuji Koyama, Shu Koyama, Peter Kretschmar, Hans A. Krimm, Aya Kubota, Hideyo Kunieda, Philippe Laurent, Shiu-Hang Lee, Maurice A. Leutenegger, Olivier Limousin, Michael Loewenstein, Knox S. Long, David Lumb, Greg Madejski, Yoshitomo Maeda, Daniel Maier, Kazuo Makishima, Maxim Markevitch, Hironori Matsumoto, Kyoko Matsushita, Dan McCammon, Brian R. McNamara, Missagh Mehdipour, Eric D. Miller, Jon M. Miller, Shin Mineshige, Kazuhisa Mitsuda, Ikuyuki Mitsuishi, Takuya Miyazawa, Tsunefumi Mizuno, Hideyuki Mori, Koji Mori, Koji Mukai, Hiroshi Murakami, Richard F. Mushotzky, Takao Nakagawa, Hiroshi Nakajima, Takeshi Nakamori, Shinya Nakashima, Kazuhiro Nakazawa, Kumiko K. Nobukawa, Masayoshi Nobukawa, Hirofumi Noda, Hirokazu Odaka, Takaya Ohashi, Masanori Ohno, Takashi Okajima, Naomi Ota, Masanobu Ozaki, Frits Paerels, Stéphane Paltani, Robert Petre, Ciro Pinto, Frederick S. Porter, Katja Pottschmidt, Christopher S. Reynolds, Samar Safi-Harb, Shinya Saito, Kazuhiro Sakai, Toru Sasaki, Goro Sato, Kosuke Sato, Rie Sato, Makoto Sawada, Norbert Schartel, Peter J. Serlemitsos, Hiromi Seta, Megumi Shidatsu, Aurora Simionescu, Randall K. Smith, Yang Soong, Łukasz Stawarz, Yasuharu Sugawara, Satoshi Sugita, Andrew Szymkowiak, Hiroyasu Tajima, Hiromitsu Takahashi, Tadayuki Takahashi, Shin'ichiro Takeda, Yoh Takei, Toru Tamagawa, Takayuki Tamura, Takaaki Tanaka, Yasuo Tanaka, Yasuyuki T. Tanaka, Makoto S. Tashiro, Yuzuru Tawara, Yukikatsu Terada, Yuichi Terashima, Francesco Tombesi, Hiroshi Tomida, Yohko Tsuboi, Masahiro Tsujimoto, Hiroshi Tsunemi, Takeshi Go Tsuru, Hiroyuki Uchida, Hideki Uchiyama, Yasunobu Uchiyama, Shutaro Ueda, Yoshihiro Ueda, Shin'ichiro Uno, C. Megan Urry, Eugenio Ursino, Shin Watanabe, Norbert Werner, Dan R. Wilkins, Brian J. Williams, Shinya Yamada, Hiroya Yamaguchi, Kazutaka Yamaoka, Noriko Y. Yamasaki, Makoto Yamauchi, Shigeo Yamauchi, Tahir Yaqoob, Yoichi Yatsu, Daisuke Yonetoku, Irina Zhuravleva, Abderahmen Zoghbi, and A. J. J. Raassen. Atomic data and spectral modeling constraints from high-resolution X-ray observations of the Perseus cluster with Hitomi. *PASJ*, 70(2):12, March 2018.
- 423 Esra Bulbul, Maxim Markevitch, Adam Foster, Randall K. Smith, Michael Loewenstein, and Scott W. Randall. Detection of an Unidentified Emission Line in the Stacked X-Ray Spectrum of Galaxy Clusters. *ApJ*, 789(1):13, July 2014.
- 424 A. Boyarsky, O. Ruchayskiy, D. Iakubovskiy, and J. Franse. Unidentified Line in X-Ray Spectra of the Andromeda Galaxy and Perseus Galaxy Cluster. *Phys. Rev. Lett.*, 113(25):251301, December 2014.
- 425 L. Gu, J. Kaastra, A. J. J. Raassen, P. D. Mullen, R. S. Cumbee, D. Lyons, and P. C. Stancil. A novel scenario for the possible X-ray line feature at ~ 3.5 keV. Charge exchange with bare sulfur ions. *A&A*, 584:L11, December 2015.
- 426 Liyi Gu, Jelle Kaastra, and A. J. J. Raassen. Plasma code for astrophysical charge exchange emission at X-ray wavelengths. *A&A*, 588:A52, April 2016.
- 427 Chintan Shah, Stepan Dobrodey, Sven Bernitt, René Steinbrügge, José R. Crespo López-Urrutia, Liyi Gu, and Jelle Kaastra. Laboratory Measurements Compellingly Support a Charge-exchange Mechanism for the 'Dark Matter' ~ 3.5 keV X-Ray Line. *ApJ*, 833(1):52, December 2016.
- 428 Esra Bulbul, Adam Foster, Gregory V. Brown, Mark W. Bautz, Peter Beiersdorfer, Natalie Hell, Caroline Kilbourne, Ralph Kraft, Richard Kelley, Maurice A. Leutenegger, Eric D. Miller, F. Scott Porter, and Randall K. Smith. Laboratory Measurements of X-Ray Emission from Highly Charged Argon Ions. *ApJ*, 870(1):21, January 2019.
- 429 Junjie Mao, Jelle S. Kaastra, Matteo Guainazzi, Rosario González-Riestra, Maria Santos-Lleó, Peter Kretschmar, Victoria Grinberg, Eleni Kalfountzou, Aitor Ibarra, Gabi Matzeu, Michael Parker, and Pedro Rodríguez-Pascual. CIELO-RGS: a catalog of soft X-ray ionized emission lines. *A&A*, 625:A122, May 2019.
- 430 G. Branduardi-Raymont, A. Bhardwaj, R. F. Elsner, G. R. Gladstone, G. Ramsay, P. Rodriguez, R. Soria, Jr. Waite, J. H., and T. E. Cravens. A study of Jupiter's aurorae with XMM-Newton. *A&A*, 463(2):761–774, February 2007.
- 431 Shuinai Zhang, Q. Daniel Wang, Li Ji, Randall K. Smith, Adam R. Foster, and Xin Zhou. Spectral Modeling of the Charge-exchange X-Ray Emission from M82. *ApJ*, 794(1):61, October 2014.
- 432 P. Chakraborty, G. J. Ferland, M. Chatzikos, F. Guzmán, and Y. Su. X-Ray Spectroscopy in the Microcalorimeter Era. I. Effects of Fe XXIV Resonant Auger Destruction on Fe XXV $K\alpha$ Spectra. *ApJ*, 901(1):68, September 2020.
- 433 P. Chakraborty, G. J. Ferland, M. Chatzikos, F. Guzmán, and Y. Su. X-Ray Spectroscopy in the Microcalorimeter Era. II. A New Diagnostic on Column Density from the Case A to B Transition in H- and He-like Iron. *ApJ*, 901(1):69, September 2020.
- 434 P. Chakraborty, G. J. Ferland, M. Chatzikos, F. Guzmán, and Y. Su. X-Ray Spectroscopy in the Microcalorimeter Era. III. Line Formation under Case A, Case B, Case C, and Case D in H- and He-like Iron for a Photoionized Cloud. *ApJ*, 912(1):26, May 2021.
- 435 Priyanka Chakraborty, Gary J. Ferland, Marios Chatzikos, Andrew C. Fabian, Stefano Bianchi, Francisco Guzmán, and Yuanyuan Su. X-Ray Spectroscopy in the Microcalorimeter Era 4: Optical Depth Effects on the Soft X-Rays Studied with CLOUDY. *ApJ*, 935(2):70, August 2022.
- 436 K. J. H. Phillips, A. K. Bhatia, H. E. Mason, and D. M. Zarro. High Coronal Electron Densities in a Solar Flare from Fe XXI and Fe XXII X-Ray Line Measurements. *ApJ*, 466:549, July 1996.
- 437 E. Behar, A. P. Rasmussen, R. G. Griffiths, K. Dennerl, M. Audard, B. Aschenbach, and A. C. Brinkman. High-resolution X-ray spectroscopy and imaging of supernova remnant N132D. *A&A*, 365:L242–L247, January 2001.
- 438 H. Xu, S. M. Kahn, J. R. Peterson, E. Behar, F. B. S. Paerels, R. F. Mushotzky, J. G. Jernigan, A. C. Brinkman, and K. Makishima. High-Resolution Observations of the Elliptical Galaxy NGC 4636 with the Reflection Grating Spectrometer on Board XMM-Newton. *ApJ*, 579(2):600–606, November 2002.
- 439 J. de Plaa, I. Zhuravleva, N. Werner, J. S. Kaastra, E. Churazov, R. K. Smith, A. J. J. Raassen, and Y. G. Grange. Estimating turbulent velocities in the elliptical galaxies NGC 5044 and NGC 5813. *A&A*, 539:A34, March 2012.
- 440 C. Pinto, A. C. Fabian, A. Ogorzalek, I. Zhuravleva, N. Werner, J. Sanders, Y. Y. Zhang, Liyi Gu, J. de Plaa, J. Ahoranta, A. Finoguenov, R. Johnstone, and R. E. A. Canning. Insights into the location and dynamics of the coolest X-ray emitting gas in clusters of galaxies. *MNRAS*, 461(2):2077–2084, September 2016.
- 441 A. Ogorzalek, I. Zhuravleva, S. W. Allen, C. Pinto, N. Werner, A. B. Mantz, R. E. A. Canning, A. C. Fabian, J. S. Kaastra, and J. de Plaa. Improved measurements of turbulence in the hot gaseous atmospheres of nearby giant elliptical galaxies. *MNRAS*, 472(2):1659–1676, December 2017.
- 442 G. V. Brown, P. Beiersdorfer, D. A. Liedahl, K. Widmann, and S. M. Kahn. Laboratory Measurements and Modeling of the Fe XVII X-Ray Spectrum. *ApJ*, 502(2):1015–1026, August 1998.
- 443 Guo Xin Chen and Anil K. Pradhan. Influence of Resonances on Spectral Formation of X-Ray Lines in Fe XVII. *Phys. Rev. Lett.*, 89(1):013202, June 2002.
- 444 P. Beiersdorfer, E. Behar, K. R. Boyce, G. V. Brown, H. Chen, K. C. Gendreau, M. F. Gu, J. Gygas, S. M. Kahn, R. L. Kelley, F. S. Porter, C. K. Stahle, and A. E. Szymkowiak. Laboratory Measurements of the Relative Intensity of the $3s\text{-}i2p$ and $3d\text{-}i2p$ Transitions in Fe XVII. *ApJ*, 576(2):L169–L172, September 2002.

- 445 P. Beiersdorfer, M. Bitter, S. von Goeler, and K. W. Hill. Laboratory Measurements of the Fe XVII 2p-3s and 2p-3d Transitions and Comparison with Solar and Astrophysical Observations. *ApJ*, 610(1):616–623, July 2004.
- 446 G. V. Brown, P. Beiersdorfer, H. Chen, J. H. Scofield, K. R. Boyce, R. L. Kelley, C. A. Kilbourne, F. S. Porter, M. F. Gu, S. M. Kahn, and A. E. Szymkowiak. Energy-Dependent Excitation Cross Section Measurements of the Diagnostic Lines of Fe XVII. *Phys. Rev. Lett.*, 96(25):253201, June 2006.
- 447 G. Y. Liang and N. R. Badnell. R-matrix electron-impact excitation data for the Ne-like iso-electronic sequence. *A&A*, 518:A64, July 2010.
- 448 G. Del Zanna. Benchmarking atomic data for astrophysics: Fe XVII X-ray lines. *A&A*, 536:A59, December 2011.
- 449 S. Bernitt, G. V. Brown, J. K. Rudolph, R. Steinbrügge, A. Graf, M. Leutenegger, S. W. Epp, S. Eberle, K. Kubiček, V. Mäkel, M. C. Simon, E. Träbert, E. W. Magee, C. Beilmann, N. Hell, S. Schippers, A. Müller, S. M. Kahn, A. Surzhykov, Z. Harman, C. H. Keitel, J. Clementson, F. S. Porter, W. Schlotter, J. J. Turner, J. Ullrich, P. Beiersdorfer, and J. R. Crespo López-Urrutia. An unexpectedly low oscillator strength as the origin of the Fe XVII emission problem. *Nature*, 492(7428):225–228, December 2012.
- 450 Liyi Gu, A. J. J. Raassen, Junjie Mao, Jelle de Plaa, Chintan Shah, Ciro Pinto, Norbert Werner, Aurora Simionescu, François Mernier, and Jelle S. Kaastra. X-ray spectra of the Fe-L complex. *A&A*, 627:A51, July 2019.
- 451 Liyi Gu, Chintan Shah, Junjie Mao, Ton Raassen, Jelle de Plaa, Ciro Pinto, Hiroki Akamatsu, Norbert Werner, Aurora Simionescu, François Mernier, Makoto Sawada, Pranav Mohanty, Pedro Amaro, Ming Feng Gu, F. Scott Porter, José R. Crespo López-Urrutia, and Jelle S. Kaastra. X-ray spectra of the Fe-L complex. II. Atomic data constraints from the EBIT experiment and X-ray grating observations of Capella. *A&A*, 641:A93, September 2020.
- 452 M. Ozawa, K. Koyama, H. Yamaguchi, K. Masai, and T. Tamagawa. Suzaku Discovery of the Strong Radiative Recombination Continuum of Iron from the Supernova Remnant W49B. *ApJ*, 706(1):L71–L75, November 2009.
- 453 H. Yamaguchi, M. Ozawa, K. Koyama, K. Masai, J. S. Hiraga, M. Ozaki, and D. Yonetoku. Discovery of Strong Radiative Recombination Continua from the Supernova Remnant IC 443 with Suzaku. *ApJ*, 705(1):L6–L9, November 2009.
- 454 Frits Paerels, Jean Cottam, Masao Sako, Duane A. Liedahl, A. C. Brinkman, R. L. J. van der Meer, J. S. Kaastra, and P. Predehl. High-Resolution Spectroscopy of the X-Ray-photoionized Wind in Cygnus X-3 with the Chandra High-Energy Transmission Grating Spectrometer. *ApJ*, 533(2):L135–L138, April 2000.
- 455 Ali Kinkhabwala, Masao Sako, Ehud Behar, Steven M. Kahn, Frits Paerels, Albert C. Brinkman, Jelle S. Kaastra, Ming Feng Gu, and Duane A. Liedahl. XMM-Newton Reflection Grating Spectrometer Observations of Discrete Soft X-Ray Emission Features from NGC 1068. *ApJ*, 575(2):732–746, August 2002.
- 456 Junjie Mao, J. S. Kaastra, M. Mehdipour, Liyi Gu, E. Costantini, G. A. Kriss, S. Bianchi, G. Branduardi-Raymont, E. Behar, L. Di Gesu, G. Ponti, P. O. Petrucci, and J. Ebrero. Anatomy of the AGN in NGC 5548. IX. Photoionized emission features in the soft X-ray spectra. *A&A*, 612:A18, April 2018.
- 457 J. S. Kaastra, A. M. Bykov, and N. Werner. Non-Maxwellian electron distributions in clusters of galaxies. *A&A*, 503(2):373–378, August 2009.
- 458 P. Bryans, E. Landi, and D. W. Savin. A New Approach to Analyzing Solar Coronal Spectra and Updated Collisional Ionization Equilibrium Calculations. II. Updated Ionization Rate Coefficients. *ApJ*, 691(2):1540–1559, February 2009.
- 459 I. Urdampilleta, J. S. Kaastra, and M. Mehdipour. X-ray emission from thin plasmas. Collisional ionization for atoms and ions of H to Zn. *A&A*, 601:A85, May 2017.
- 460 R. P. Dufresne and G. Del Zanna. Modelling ion populations in astrophysical plasmas: carbon in the solar transition region. *A&A*, 626:A123, June 2019.
- 461 R. P. Dufresne, G. Del Zanna, and N. R. Badnell. Effects of density on the oxygen ionization equilibrium in collisional plasmas. *MNRAS*, 497(2):1443–1456, September 2020.
- 462 J. W. Xu, C. X. Xu, R. T. Zhang, X. L. Zhu, W. T. Feng, L. Gu, G. Y. Liang, D. L. Guo, L. Gao, D. M. Zhao, S. F. Zhang, M. G. Su, and X. Ma. Measurement of n-resolved state-selective charge exchange in Ne^{8,9+} collision with He and H₂. *ApJS*, 253:13, March 2021.
- 463 L. Y. Gu, C. Shah, and R. T. Zhang. Uncertainties in atomic data for modeling astrophysical charge exchange plasmas. *Sensors*, 22, January 2022.
- 464 Steven Diehl and Thomas S. Statler. Adaptive binning of X-ray data with weighted Voronoi tessellations. *MNRAS*, 368(2):497–510, May 2006.
- 465 J. R. Peterson, P. J. Marshall, and K. Andersson. Smoothed Particle Inference: A Kilo-Parametric Method for X-Ray Galaxy Cluster Modeling. *ApJ*, 655(1):109–127, January 2007.
- 466 Makoto S. Tashiro. XRISM: X-ray imaging and spectroscopy mission. *International Journal of Modern Physics D*, 31(2):2230001, January 2022.
- 467 D. McCammon, R. Almy, E. Apodaca, W. Bergmann Tiest, W. Cui, S. Deiker, M. Galeazzi, M. Juda, A. Lesser, T. Mihara, J. P. Morgenthaler, W. T. Sanders, J. Zhang, E. Figueroa-Feliciano, R. L. Kelley, S. H. Moseley, R. F. Mushotzky, F. S. Porter, C. K. Stahle, and A. E. Szymkowiak. A high spectral resolution observation of the soft x-ray diffuse background with thermal detectors. *The Astrophysical Journal*, 576(1):188–203, sep 2002.
- 468 Philippe Peill, Didier Barret, Vincent Albuys, Jan-Willem den Herder, Luigi Piro, Massimo Cappi, Juhani Huovelin, Richard Kelley, J. Miguel Mas-Hesse, Kazuhisa Mitsuda, Stéphane Paltani, Gregor Rauw, Agata Rozanska, Jiri Svoboda, and Joern Wilms. The X-ray Integral Field Unit instrument: science, design, performances and status. In *Proc. SPIE 11444, Space Telescopes and Instrumentation 2020: Ultraviolet to Gamma Ray*, volume 11444, page 114440V, 2020.